Development of soft nanocarriers from novel amphiphilic hyaluronic acid derivatives towards drug delivery

Eenschooten, Corinne Diane

Publication date:
2008

Document Version
Publisher's PDF, also known as Version of record

Technical University of Denmark

Development of soft nanocarriers from novel amphiphilic hyaluronic acid derivatives towards drug delivery

Corinne Eenschooten

2008

DTU Chemical Engineering
Department of Chemical and Biochemical Engineering

Technical University of Denmark

Development of soft nanocarriers from novel amphiphilic hyaluronic acid derivatives towards drug delivery

Corinne Eenschooten
2008

DTU Chemical Engineering
Department of Chemical and Biochemical Engineering

2008 ISBN-13: 978-87-91435-84-6
Printed by J&R Frydenberg A/S, Copenhagen, Denmark

Development of soft nanocarriers from novel amphiphilic hyaluronic acid derivatives towards drug delivery

Corinne Eenschooten

English abstract

Drug delivery is an important pharmaceutical research area currently facing limitations such as drug insolubility and instability in biological media, poor bioavailability and unspecific targeting. As a consequence, high doses are used to achieve a therapeutic effect which increases the risk for toxicity in patients and health costs. The design of advanced drug delivery systems addressing these challenges has therefore become more and more crucial. Hyaluronic acid (HA) is a natural linear glycosaminoglycan ubiquitous and identical in all mammals. Due to its native intrinsic biocompatibility, resorbability and biological functions, and the possibility for an easy chemical functionalisation, HA constitutes an excellent starting material for the design of advanced biomaterials. The objective of this project was to develop HA-based nanocarriers towards the encapsulation and delivery of hydrophobic drugs.

However, due to its high hydrophilicity, HA exhibits physicochemical properties incompatible with the spontaneous and stable formation of segregated structures in aqueous solutions. Therefore, HA was first rendered amphiphilic by the covalent binding of hydrophobic groups onto its backbone. After a preliminary investigation of two different modification methods, the proprietary technology eventually selected was based on the grafting of octenyl succinic anhydride and was optimised so as to develop a reproducible and robust process for the synthesis of functionalised polymers. Fundamental properties such as the structure, degree of hydrophobicity, substitution pattern as well as intra- and intermolecular interactions of a selection of derivatives were then studied. Submicronic multiphasic physically cross-linked nanogel particles capable of solubilising a model hydrophobic substance were prepared by spontaneous self-association and characterized with regard to their morphology, size and surface charge. A multivesicular model was finally put forward to explain their internal structure.

In conclusion, a molecular method based on controlled self-association was developed towards the formation of HA soft nanostructures. These represent novel and promising biomaterial templates for the fabrication of stable and multifunctional HA-based nanogel particles and could be valuable to the industry since their underlying production methods are aqueous and easily upscalable.

Dansk abstrakt

Fordeling af lægemidler er et vigtigt farmaceutisk forskningsområde, der i øjeblikket står overfor begrænsninger som lægemidlets uopløselighed og instabilitet i biologiske miljøer, ringe tilgængelighed og uspecifik levering. Som en konsekvens heraf, anvendes høje doser for at opnå en terapeutisk virkning, hvilket forøger risikoen for toksicitet i patienter og sundhedsudgifter. Design af avancerede systemer til fordeling af lægemidler, der tager udgangspunkt i disse udfordringer, er derfor blevet mere og mere afgørende. Hyaluronsyre (HA) er en naturlig lineær glycosaminoglycan, der er tilstede og identisk i alle pattedyr. HA udgør et fortrinligt udgangsstof i designet af avancerede biomaterialer på grund af dets naturlige biokompatibilitet, resorption, biologiske funktioner og muligheden for simpel kemisk funktionalisering. Formålet for projektet var at udvikle HA-baserede nanobærere til indkapsling og levering af hydrofobiske stoffer.

HA er meget hydrofilt og besidder fysisk-kemiske egenskaber, der er uforenelige med en spontan og stabil dannelse af isolerede strukturer i vandige opløsninger. HA blev derfor først gjort amfifilt ved kovalent binding af hydrofobiske grupper på dets rygrad. Efter en forberedende undersøgelse af to forskellige derivatiserings-metoder, den endelige valgte patenterede teknologi var baseret på bindingen af octenyl succinic anhydride og blev optimeret for at udvikle en reproducerbar og robust proces til syntese af funktionaliserede polymerer. Grundlæggende egenskaber som struktur, grad af hydrofobicitet, substitutionsmønster samt intra- og intermolekulær vekselvirkning blev herefter undersøgt for et udvalg af derivater. Submikroniske multifasiske fysisk krydsforbundne nanogelpartikler, der kan opløse et hydrofobiskt modelstof, blev dannet ved spontan selvsamling og karakteriseret ud fra deres morfologi, størrelse og overfladeladning. En multivesikulær model blev til sidst opstillet for at forklare deres indre struktur.

Afslutningsvist blev der udviklet en molekylær metode til dannelsen af bløde HA nanostrukturer baseret på kontrolleret selvsamling. Disse repræsenterer nye og lovende biomaterialeskabeloner til fremstilling af stabile og multifunktionelle HA-baserede nanogelpartikler og kunne være værdifulde for industrien, eftersom deres produktionsmetoder er vandige og let opskalerbare.

Preface

The present manuscript is a summary of the work I, Corinne Eenschooten, carried out in the period May 2005-July 2008 towards the achievement of the Industrial Philosophy Doctorate (Industrial Ph.D.) degree. This double diploma is granted by Danish universities and the Danish Ministry of Science, Technology and Innovation (VTU) to Ph.D. students having undertaken their research project in the industry. The Danish industrial Ph.D. programme has indeed for purpose to educate scientists with an insight in the commercial aspects of *Research and Development* (R&D), increase the R&D and innovative capacity in private companies and build networks disseminating knowledge between universities and private companies.

This project was a collaboration between the Technical University of Denmark (DTU), Department of Chemical and Biochemical Engineering, Center for Phase Equilibria and Separation Processes (IVC-SEP, Building 229, 2800 Lyngby, Denmark), Novozymes Biopolymer A/S (NZBP, Krogshøjvej 36, 2880 Bagsværd, Denmark) and the University of Geneva, University of Lausanne (UGL), School of Pharmaceutical Sciences, Department of Pharmaceutics and Biopharmaceutics (DPBP, 30 quai Ernest-Ansermet, 1211 Geneva 4, Switzerland) which acted as a third party.
Most of the work was achieved at IVC-SEP and NZBP. The rest was conducted at DPBP within the frame of two study trips in the periods July-August 2006 and March-June 2007.
The project was co-funded by the Danish Ministry of Science, Technology and Innovation (Grant number: 07-001687) and Novozymes Biopolymer A/S, the employer.

The project supervisors were, from IVC-SEP, Doctor Georgios M. Kontogeorgis and IVC-SEP director Professor Erling H. Stenby, from NZBP, Doctors Fanny Longin and Khadija Schwach-Abdellaoui, Science Manager and Senior R&D Manager, respectively and, from DPBP, Doctor Florence Delie and President of the School of Pharmaceutical Sciences (UGL) Professor Robert Gurny.

The overall purpose of the project was to design and implement a method for the preparation of hyaluronic acid-based nanocarriers towards drug delivery.
The dissertation consists of five chapters. A general introduction (Chapter I) opens the thesis and is followed by a review on a subject related to the project area (Chapter II). The experimental work is described in the following two chapters (Chapter III and Chapter IV). The thesis continues with a conclusion (Chapter V) which summarises the work, puts it into perspectives and suggests future research directions. The manuscript ends with appendices containing a record of the educational activities completed during the Ph.D. programme.

Chapter II, Chapter III, B and Chapter IV are written in a recognisable paper format and will after a few adjustments be submitted to scientific journals by the time of the Ph.D. defence or immediately after.
The experimental work presented in Chapter III, sections A and B was entirely performed by me while that of section C was partly accomplished by Sara Sparre Kofoed. Sara was a master student at the Technical University of Denmark, Department of Chemistry (DC) who carried out her master's thesis in collaboration with NZBP in the period September 2007-February 2008 under Associate Professor Charlotte Held Gotfredsen's and my own supervision. In Chapter IV, Andrea Vaccaro (UGL, Department of Inorganic Analytical and Applied Chemistry, DIAAC) completed the light scattering experiments and participated to the simulation work. The compilation and writing of all the material in this thesis is the result of my own efforts.

During my education, I had the opportunity to evolve in a multidisciplinary environment and to become acquainted with exceptionally knowledgeable and inspiring people whom I would like to express my gratitude to.
I address my first acknowledgements to my supervisors Dr. Georgios M. Kontogeorgis, Prof. Erling H. Stenby, Dr. Fanny Longin, Dr. Khadija Schwach-Abdellaoui, Dr. Florence Delie and Prof. Robert Gurny.
I wish to thank Dr. Georgios M. Kontogeorgis and Prof. Erling H. Stenby (IVC-SEP) for their support and encouragements at an earlier stage in the process of finding a

Ph.D. project and an industrial partner, their following-up on the course of my studies and active participation to our scientific discussions.
I address Dr. Georgios M. Kontogeorgis (IVC-SEP) my greatest recognition for having given me a durable taste for colloid and surface chemistry and entrusted me with the mission to teach this topic twice by his side.
To Dr. Fanny Longin (NZBP), I express all my thankfulness and acknowledge her for her large availability and dynamism. I have learned a lot from her about polysaccharide chemistry and modification and surely, these years would have had another flavour without her optimism and positivism.
My gratitude also goes to Dr. Khadija Schwach-Abdellaoui (NZBP) who gave me the fantastic opportunity to work in an emerging and fascinating area of research and who benevolently saw to my educational and personal development.
I owe a lot to Dr. Florence Delie for kindly accompanying me during my external stay at DPBP, contributing to make my study trips fruitful and enriching experiences and sharing her expertise about polymeric nanoparticulate systems.
Prof. Robert Gurny who generously welcomed me at DPBP and recommended me to various disciplinary experts to help me come forward with my project also deserves strong acknowledgements.

I am grateful to my present and former colleagues at DTU, NZBP and UGL for their contribution to a productive and pleasant working environment.
I particularly wish to thank Dr. Kristoffer Tømmeraas and Dr. Birgitte Mølholm Malle (NZBP) for sharing their knowledge in polysaccharide chemistry, modification and industrial applications, Sara Sparre Kofoed (DC) for letting me experience my fledgling teaching skills and for the quality of the work she performed, Dr. Charlotte Held Gotfredsen (DC) for co-supervising Sara's project and having Sara and myself benefited from her expertise in nuclear magnetic resonance spectroscopy (NMR) and both of them for pursuing NMR experiments even after the term of Sara's project.
I am obliged to Dr. Christoph Bauer (UGL, National Centre of Competence in Research, Frontiers in Genetics, Bioimaging Platform) for having acquired the first transmission electron microscopy (TEM) micrographs and trained me in TEM with great patience.

Dr. Andrea Vaccaro and Prof. Michal Borkovec (DIAAC) who shared their insight in colloid chemistry and made ingenious propositions to explain aggregation phenomena have also earned my infinite credit.
My gratitude finally goes to the administrative staff at IVC-SEP (Anne Louise Biede and Patricia Wagner), NZBP (Nadia Ehlers Nielsen), Novozymes A/S (Asta Wielandt Pedersen) and DPBP (Myrtha Copin and Florence von Ow) for their help in numerous occasions and to Patent Attorney Peter Würtz Lindum (Novozymes A/S) for carrying through the patent applications and mediating my disclosure of information.

I am especially appreciative of VTU and DTU for their constantly evolving and improving educational structures and their following-up on industrial Ph.D. students. I also salute the quality of the complementary learning and networking activities organised by VTU along the industrial Ph.D. programme.

My kindest thoughts are directed to my family, my mother and father (Martine Aubert and Richard Eenschooten) and my friends in France (Thibault Roques, Éric Piel and Laurène Champalle) and in Denmark (Sylvain Verdier, Mette Fuglsang Larsen and Michelangelo Dall'Ora) who always supported and encouraged me.

I finally gratefully acknowledge the Danish Ministry of Science, Technology and Innovation (Grant number: 07-001687) and Novozymes Biopolymer A/S for funding.

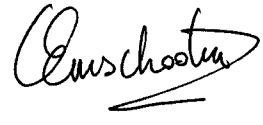

Corinne Eenschooten
Lyngby, July 2008

Table of content

English abstract iv
Dansk abstrakt v
Preface vi
Table of content x
List of abbreviations xvi
List of figures xxii
List of tables xxiv
List of equations xxv

CHAPTER I
Introduction 1
I. Hyaluronic acid 3
I.1. Origin and molecular structure 3
I.2. Industrial manufacture 4
I.3. Structures in aqueous solutions 5
I.4. Biological functions in the skin 9
I.5. Applications 13
II. Hyaluronic acid-mediated dermal drug delivery 14
II.1. First generation systems 15
II.2. Second generation systems 15
III. Hyaluronic acid-based colloidal particles 16
III.1. Microparticles 16
III.2. Nanoparticles 18
IV. Hydrophobically modified hyaluronic acid 23
V. The Ph.D. project 25
V.1. Objectives and challenges 25
V.2. Experimental approach 27
V.3. Thesis structure 28
References 29

CHAPTER II
Review 37
Towards an understanding of the mechanisms underlying polymeric nanoparticle-mediated (trans)dermal drug delivery 39
Abstract 39
I. Introduction 40
II. Technical advances in assessing skin penetration pathways 44
II.1. Skin penetration pathways 44
II.2. Microscopic imaging 47
II.2.1. Confocal laser scanning microscopy 47
II.2.2. Multiphoton laser scanning microscopy 48
II.3. Skin penetration quantification 49
II.3.1. The skin sandwich model 49
II.3.2. Differential stripping 52
III. Mechanisms underlying polymeric nanoparticle-mediated drug delivery 53
III.1. Redistribution and accumulation of polymeric nanoparticles in the skin 53
III.2. Possible mechanisms underlying polymeric nanoparticle skin penetration 56
III.2.1. Influence of nanoparticle size 58
III.2.2. Influence of nanoparticle surface charge 59
III.2.3. Influence of nanoparticle shape 60
III.3. Hypothesis with regards to how polymeric nanoparticles enhance percutaneous penetration and/or sustain drug release 61
IV. Future challenges in polymeric nanoparticle-mediated (trans)dermal drug delivery 63
IV.1. Nanoparticle design 63
IV.2. Nanoparticle performance assessment 64
IV.2.1. Fate 64
IV.2.2. Skin penetration 65
IV.3. Nanoparticle risk assessment 66
V. Conclusion 68
References 69

CHAPTER III
Preparation and structural characterisation of amphiphilic hyaluronic acid derivatives 79

A. Investigation of novel modification methods for the preparation of amphiphilic hyaluronic acid derivatives 81
Abstract 81
I. Introduction 81
II. Materials and methods 83
II.1. Materials 83
II.2. Methods 83
II.2.1. Preparation of low molecular weight hyaluronic acid 83
II.2.2. Preparation of aryl/alkyl vinyl sulfone-modified hyaluronic acid 85
II.2.3. Preparation of alkenyl succinic anhydride-modified hyaluronic acid 87
II.2.4. Characterisation techniques 90
III. Results and discussion 92
III.1. Characterisation of aryl/alkyl vinyl sulfone-modified hyaluronic acid 92
III.2. Characterisation of alkenyl succinic anhydride-modified hyaluronic acid 99
III.3. Comparison between the two preparation methods 103
IV. Conclusion 106
References 107

B. Optimisation of the preparation of octenyl succinic anhydride-modified hyaluronic acid 109
Foreword 109
References 113
Preparation and structural characterisation of novel and versatile amphiphilic octenyl succinic anhydride-modified hyaluronic acid 114
Abstract 114
I. Introduction 115
II. Materials and methods 117
II.1. Materials 117
II.2. Methods 117

II.2.1. Preparation of low molecular weight hyaluronic acid 117
II.2.2. Preparation of octenyl succinic anhydride-modified hyaluronic acid 118
II.2.3. Characterisation methods 119
III. Results and discussion 119
III.1. Characterisation of octenyl succinic anhydride-modified hyaluronic acid 119
III.2. Influence of the reaction conditions on the degree of substitution of octenyl succinic anhydride-modified hyaluronic acid 123
IV. Conclusion 128
References 129

C. Additional characterisation of octenyl succinic anhydride-modified hyaluronic acid – Substitution pattern, molecular weight and conformation in aqueous media 132
Abstract 132
I. Introduction 132
II. Materials and methods 134
II.1. Materials 134
II.2. Methods 135
III. Results and discussion 136
III.1. Structural study 136
III.1.1. Molecular level 137
III.1.2. Macromolecular level 142
III.2. Molecular weight and conformation study 144
IV. Conclusion 149
References 150

CHAPTER IV
Physicochemical characterisation of amphiphilic hyaluronic acid derivatives 153
Novel self-associative multi-phase nanostructured soft carriers based on amphiphilic hyaluronic acid derivatives 155
Abstract 155
I. Introduction 156
II. Materials and methods 157

II.1. Materials 157
II.2. Methods 158
II.2.1. Critical aggregation concentration of the OSA-HA derivatives 158
II.2.2. Morphology of the OSA-HA polymeric micelles 159
II.2.3. Size distribution of the OSA-HA polymeric micelles 159
II.2.4. Zeta potential of the OSA-HA polymeric micelles 161
III. Results and discussion 161
III.1. Critical aggregation concentration of the OSA-HA derivatives 161
III.2. Morphology of the OSA-HA polymeric micelles 165
III.3. Size distribution of the OSA-HA polymeric micelles 166
III.4. Zeta potential of the OSA-HA polymeric micelles 171
III.5. Molecular structure of the OSA-HA polymeric micelles 171
IV. Conclusion 176
References 177

CHAPTER V
Conclusion and future work 179
I. Summary 181
II. Future work 182

Appendices 185
Educational activities 187
I. Training 187
I.1. Courses 187
I.2. Conferences 188
I.3. External study trips 188
II. Dissemination of knowledge 189
II.1. Publications 189
II.1.1. Posters 189
II.1.2. Oral presentations 190
II.1.3. Manuscript contributions 191
II.1.4. Patents 192
II.1.5. Articles in preparation 192

II.2. Teaching 192
II.2.1. Assistantship in master's courses 192
II.2.2. Co-supervision 193

List of abbreviations

ADH	Adipic acid dihydrazide
AlkS	Alkenyl succinate
AlkSA	Alkenyl succinic anhydride
ar	Aromatic
Ar/AlVS	Aryl/alkyl vinyl sulfone
Ar/AlVS-HA	Aryl/alkyl vinyl sulfone-modified hyaluronic acid
Arlacel® A	Mannide monostearate
as	Asymmetric
A_2	Osmotic second virial coefficient
B	*Bacillus*
bd	Bending
BS	*Bacillus Subtilis*
c	Polymer concentration
CA	Carboxylic acid
CAC	Critical aggregation concentration
CLSM	Confocal laser scanning microscopy
C(X)	Concentration of the entity X
d	Doublet
DC	Department of Chemistry
DDSA	Dodecyl succinic anhydride
d_H	Hydrodynamic diameter
d_i	Diameter of the micelle class i
DIAAC	Department of Inorganic Analytical and Applied Chemistry
DLS	Dynamic light scattering
DMF	*N*,*N*-dimethylformamide
DMSO	Dimethyl sulfoxide
DPBP	Department of Pharmaceutics and Biopharmaceutics
DQF-COSY	Double quantum filtered–correlation spectroscopy
DS	Degree of substitution
DTU	Technical University of Denmark
DVS	Divinyl sulfone

D_2O	Deuterated water
ECM	Extracellular matrix
EDC	1-ethyl-3-[3-dimethyl amino] propyl carbodiimide
EVS	Ethyl vinyl sulfone
EVS-HA	Ethyl vinyl sulfone-modified hyaluronic acid
f_i	Probability density of the micelle class i
FITC	Fluorescein 5-isothiocyanate
f–log-normal	log-normal distribution
f–Schulz	Schulz distribution
FT-IR	Fourier transform infrared spectroscopy
G	Glucuronic acid
GAG	Glycosaminoglycan
gHMBC	Gradient heteronuclear multiple bond correlation
gHSQC	Gradient heteronuclear single quantum correlation
HA	Hyaluronic acid
HA-C_{12}	Dodecyl bromide-modified hyaluronic acid
HA-C_{18}	Octadecyl bromide-modified hyaluronic acid
HAu	Hyaluronic acid unit
HAX	~X,000-Da hyaluronic acid
HLB	Hydrophilic/lipophilic balance
hmHA	Hydrophobically modified hyaluronic acid
HPAEC	High performance anion-exchange chromatography
HPLC	High performance liquid chromatography
HYAFF®	Fidia's trademark for hydrophobically modified HA obtained by reacting HA and alkyliodides in dimethyl sulfoxide, using the tetrabutylammonium salt of hyaluronic acid
H2BC	Heteronuclear 2-bond correlation
H_3PO_4	Phosphoric acid
IVC-SEP	Center for Phase Equilibria and Separation Processes
K	Constant defined in Chapter III, C, Equation III.C.2
KBr	Potassium bromide
KCl	Potassium chloride
KH_2PO_4	Potassium dihydrogen phosphate

LPGC	Low pressure gas chromatography
LS	Light scattering
LSM	Laser scanning microscopy
l(X)	Length of the entity X
-m	Methyl
m	Multiplet
MALDI-TOF-MS	Matrix-assisted laser desorption/ionisation–time-of-flight–mass spectrometry
MALLS	Multi-angle laser light scattering
MHKS	Mark-Houwink-Kunh-Sakurada
MP	Microparticle
MPLSM	Multiphoton laser scanning microscopy
MR	Molar ratio
MV	Model validity
MW	Molecular weight
MWCO	Molecular weight cut-off
MW_W	Weight-averaged molecular weight
MW(X)	Molecular weight of the entity X
n	Refractive index of a given polymer solution
N	Acetylglucosamine
N_A	Avogadro's number
NaCl	Sodium chloride
$NaHCO_3$	Sodium bicarbonate
NaOAc	Sodium acetate
NaOH	Sodium hydroxide
Na_2HPO_4	Disodium hydrogen phosphate
NHSS	Sodium *N*-hydroxysulfosuccinimide
NMR	Nuclear magnetic resonance spectroscopy
NOESY	Nuclear Overhauser enhancement spectroscopy
NP	Nanoparticle
N(X)	Number of the entity X
NZBP	Novozymes Biopolymer A/S
n_0	Refractive index of a given solution medium

ODH	Oxalic acid dihydrazide
ODSA	Octadecenyl succinic anhydride
ODSA-HA	Octadecenyl succinic anhydride-modified hyaluronic acid
ODSA-HA30 (A)	Octadecenyl succinic anhydride-modified hyaluronic acid prepared from 30,000 Da hyaluronic acid with the combination of molar equivalents A
oop	Out-of-plane
OS	Octenyl succinate
OSA	Octenyl succinic anhydride
OSA-HA	Octenyl succinic anhydride-modified hyaluronic acid
OSA-HAu	Octenyl succinic anhydride-modified hyaluronic acid unit
OSA-HAX	Octenyl succinic anhydride-modified hyaluronic acid with a degree of substitution equal to X % per disaccharide unit
OSA-HA30 (A)	Octenyl succinic anhydride-modified hyaluronic acid prepared from 30,000 Da hyaluronic acid with the combination of molar equivalents A
o/w	Oil-in-water
P	Function defined in Chapter III, C, Equation III.C.3
PBS	Phosphate buffer saline
PEG	Poly(ethylene glycol)
PG	Proteoglycan
PH	Polyhydrazide
P-HA20	Palmitoyl chloride-modified hyaluronic acid prepared from 20,000-Da hyaluronic acid
P-HA2000	Palmitoyl chloride-modified hyaluronic acid prepared from 2,000,000-Da hyaluronic acid
Ph.D.	Philosophy doctorate
PLGA	poly(lactide-co-glycolide)
PLS	Partial least square
PVS	Phenyl vinyl sulfone
PVS-HA	Phenyl vinyl sulfone-modified hyaluronic acid
PVS-HAX (A)	Phenyl vinyl sulfone prepared from X,000-Da hyaluronic acid with the combination of molar equivalents A

q	Modulus of the scattering vector
Q2	Prediction coefficient
R	Excess Rayleigh ratio
R&D	Research and development
RC	Reproducibility coefficient
RE	Reaction efficiency
RGD	Rayleigh-Gans-Debye
R_H	Hydrodynamic radius
RHAMM	Receptor for HA-mediated mobility
ROS	Reactive oxygen species
R_{rms}	Root mean square radius
R(X)	Radius of the entity X
R2	Regression coefficient
s	Singlet
S	*Streptococcus*
SC	Stratum corneum
SEC-MALLS	Size exclusion chromatography–multi-angle laser light scattering
Span 80	Sorbitan monostearate
Span 85	Sorbitan tristearate
st	Stretch
sy	Symmetric
t	Triplet (in nuclear magnetic resonance spectroscopy) or time
T	Temperature
TEM	Transmission electron microscopy
THF	Tetrahydrofurane
TLC	Thin layer chromatography
TOCSY	Total correlation spectroscopy
u	Function of a variable
UGL	University of Geneva, University of Lausanne
US	United States
UV	Ultraviolet
VTU	Danish Ministry of Science, Technology and Innovation

w	Wavelength
w/o	Water-in-oil
WR	Weight ratio
w(X)	Width of the entity X
1D	One-dimension
^{1}H NMR	Proton nuclear magnetic resonance spectroscopy
3D	Three-dimension
4-HA	Hyaluronic acid tetrasaccharide
6-HA	Hyaluronic acid hexasaccharide
8-HA	Hyaluronic acid octasaccharide
10-HA	Hyaluronic acid decasaccharide
12-HA	Hyaluronic acid dodecasaccharide
14-HA	Hyaluronic acid tetradecasaccharide
α	Swelling coefficient
δ	Chemical shift
$[\eta]$	Intrinsic viscosity
λ_0	Wavelength of the laser light in vacuum
θ	Scattering angle
μ	Non-dimensional fitting parameter representing the mean polymeric micelle diameter
ρ(X)	Density of the entity X
σ	Non-dimensional fitting parameter representing the standard deviation of the polymeric micelle diameter
§	Paragraph

List of figures

Figure I.1: Molecular structure of the HA repeating unit....3
Figure I.2: Intramolecular hydrogen bonding and hydrogen bonding with the solvent in aqueous HA solutions....6
Figure I.3: Plan (1) and elevation (2) computer drawn projections of HA and view along the two-fold helix axis (3)....7
Figure I.4: The hydrophilic and non-polar/hydrophobic patches in HA....7
Figure I.5: Illustration of the viscoelastic properties of HA....8
Figure I.6: Distribution of HA in adult human skin....10
Figure I.7: Scheme of HA matrices in aqueous solutions....11
Figure I.8: Scheme of the organisation of proteoglycans and collagen in HA matrices....11
Figure I.9: Illustration of selected hydrophobic modifications of HA....24

Figure II.1: Drug encapsulation in polymeric nanoparticles....43
Figure II.2: Structure of mammalian skin and possible skin penetration pathways....45
Figure II.3: Penetration through the intercellular space between corneocytes....45
Figure II.4: Schematic representation of the skin sandwich model....50

Figure III.A.1: Modification of HA with Ar/AlVS....92
Figure III.A.2: Mechanism of the reaction between HA and Ar/AlVS....93
Figure III.A.3: FT-IR spectra of HA300 and PVS-HA300 (1)....94
Figure III.A.4: ^{1}H NMR spectrum of HA300....96
Figure III.A.5: ^{1}H NMR spectrum of PVS-HA300 (1)....97
Figure III.A.6: Modification of HA with AlkSA....100
Figure III.A.7: Mechanism of the reaction between HA and AlkSA....100
Figure III.A.8: ^{1}H NMR spectrum of OSA-HA30 (2)....102

Figure III.B.i: Competitive reactions accompanying the modification of starch with succinic anhydrides in aqueous alkaline media....109
Figure III.B.1: Molecular structure of the HA repeating unit....115
Figure III.B.2: Scheme of the fishbone structure of OSA-HA....120

Figure III.B.3: ^{1}H NMR spectrum of HA20 121
Figure III.B.4: ^{1}H NMR spectrum of OSA-HA (8) 122
Figure III.B.5: Evaluation of the model used to fit the DS of the OSA-HA derivatives 127
Figure III.B.6: Contour plot of the DS of the OSA-HA derivatives..... 128

Figure III.C.1: HPLC chromatograms of the digestion mixture..... 138
Figure III.C.2: MALDI-TOF-MS spectrum of the product of the reaction between the HA oligosaccharides and OSA 140
Figure III.C.3: Putative reaction mechanism between HA and OSA 143
Figure III.C.4: Illustration of the experimental difficulties encountered when performing MALLS..... 148

Figure IV.1: Molecular structure of the HA repeating unit 156
Figure IV.2: Maximum fluorescence emission wavelength of Nile Red as a function of the OSA-HA concentration..... 162
Figure IV.3: Critical aggregation concentration as a function of the degree of substitution of OSA-HA..... 163
Figure IV.4: Selected TEM micrographs of the OSA-HA polymeric micelles..... 165
Figure IV.5: Number-weighed size distribution of the OSA-HA polymeric micelles based on micelle diameter extraction from TEM micrographs..... 167
Figure IV.6: Number-weighed cumulative size distribution of the OSA-HA polymeric micelles based on micelle diameter extraction from TEM micrographs 168
Figure IV.7: Experimental and simulated hydrodynamic diameter of the OSA-HA polymeric micelles as a function of the scattering angle 169
Figure IV.8: Zeta potential of the OSA-HA polymeric micelles..... 172
Figure IV.9: Putative representation of the structure of the OSA-HA polymeric micelles 173

List of tables

Table I.1: Biomedical applications of HA 14
Table I.2: Preparation methods of HA microparticles 17
Table I.3: Preparation methods of HA nanoparticles 19

Table II.1: Advantages of using the skin as a drug administration route 40
Table II.2: Redistribution of topically applied polymeric nanoparticles on the surface of the skin 54

Table III.A.1: Number of molar equivalents of HA, NaOH and PVS used to prepare the PVS-HA derivatives 86
Table III.A.2: Reaction yields of the PVS-HA derivatives 86
Table III.A.3: Number of molar equivalents of HA and OSA used to prepare the OSA-HA derivatives 88
Table III.A.4: Reaction yields of the OSA-HA derivatives 88
Table III.A.5: Number of molar equivalents of HA and ODSA used to prepare the ODSA-HA derivatives 89
Table III.A.6: Reaction yields of the ODSA-HA derivatives 89
Table III.A.7: Molecular weight of HA300 and selected PVS-HA300 derivatives 93
Table III.A.8: Degree of substitution of the PVS-HA derivatives 98
Table III.A.9: Degree of substitution of the OSA-HA derivatives 102
Table III.A.10: Advantages and drawbacks associated to the preparation of the Ar/AlVS-HA and AlkSA-HA derivatives 105

Table III.B.i: Optimisation of the preparation of AlkSA-starch 111
Table III.B.1: Reaction parameters and ranges used in the experimental plan 118
Table III.B.2: Reaction conditions and degree of substitution of the OSA-HA derivatives 125

Table III.C.1: MALDI-TOF-MS analysis of the digestion mixture after 8 hours 139
Table III.C.2: Molecular weight, root mean square radius and osmotic second virial coefficient of HA20 and of the OSA-HA derivatives 145

List of equations

Equation III.A.1 90

Equation III.C.1 136
Equation III.C.2 136
Equation III.C.3 136

Equation IV.1 160
Equation IV.2 160
Equation IV.3 160
Equation IV.4 174
Equation IV.5 174
Equation IV.6 175
Equation IV.7 175

CHAPTER I
Introduction

I. Hyaluronic acid

I.1. Origin and molecular structure

Hyaluronic acid (HA) belongs to the class of amino sugar-containing polysaccharides known as glycosaminoglycans (GAGs) and is the only non-sulphated GAG. In vertebrates, GAGs are essential components of connective tissues. While *in vivo*, most GAGs are synthesised in the Golgi apparatus and are added to protein cores, HA is produced at the cell surface and is directly extruded in the extracellular space without a protein core. This process is carried out by a group of proteins called HA synthases located in cell membranes [1].

HA was discovered in 1934 by Karl Meyer and John Palmer in the vitreous humour of bovine eyes [2]. It is a linear polysaccharide consisting of D-glucuronic acid and *N*-acetyl-D-glucosamine linked through *β*-1,3 glycosidic bonds while consecutive repeating disaccharide units are linked through *β*-1,4 bonds (Figure I.1). The name *hyaluronic acid* originates from *hyaloid* (vitreous) and *uronic acid* [3].

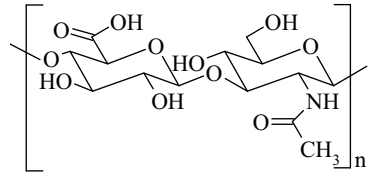

Figure I.1: Molecular structure of the HA repeating unit.

Depending on the ionic strength of the solution in which HA is dissolved, the pKa value of its carboxyl groups is around 3 [4]. As a result, HA does not occur, at physiological pH, as its protonated acid form but as a polyanion which negative

charges are balanced by mobile cations such as Na^+, K^+, Ca^{2+} or Mg^{2+} [5]. Therefore, HA is also often referred to as *hyaluronan* or *hyaluronate*.

I.2. Industrial manufacture

Historically, HA was first produced by extraction from rooster combs. However, this production method is expensive (poor yields) and requires an extensive purification of the crude product to remove antigenic avian proteins [6]. For these reasons, and more importantly, due to ethical issues, alternatives to the animal extraction of HA were pursued and industrial techniques based on microorganism fermentation eventually emerged in the 1990's.

A key breakthrough in the HA production occurred when HA was first obtained by the more sophisticated fermentation of certain strains of *Streptococcus* (S) which naturally synthesise HA as a part of their outer capsule [6]. After this major industrial shift and until recently, the streptococcal production of HA remained the golden standard.
However, S can be difficult and expensive to ferment and is challenging to genetically modify. S is also a known pathogenic microorganism in virtue of which the final HA product can contain both endo- and exotoxins [6]. Finally, the streptococcal production of HA requires the use of substantial volumes of organic solvents.

The newest progress in the manufacture of HA is the use of *Bacillus* (B) as expression host. B strains have long been used as industrial workhorses for the production of specialty chemicals and *Bacillus Subtilis* (BS) was recently shown a superior system for the production of HA:
(i) BS grows on minimal media in contrast to S which is a fastidious microorganism requiring more expensive and complex media for growth;

(ii) BS secretes HA into its surrounding medium and HA is not cell associated which simplifies the recovery step compared to that of the S-based process;
(iii) The BS-based process is aqueous thus environmentally friendly;
(iv) HA molecular weight (MW) and polydispersity are better controlled,
(v) HA yields are higher,
(vi) BS is a non-pathogenic microorganism and the final HA product does not contain any endo- or exotoxins [6].
This last aspect obviously makes BS-HA an advantageous alternative to S-HA for applications requiring HA internalisation in the body.
BS-HA (Novozymes Biopolymer A/S) was used in the present Ph.D. project for its environmentally friendly production process and the ultra-purity of this novel biosynthetic polymer (see Chapters III and IV).

I.3. Structures in aqueous solutions

The structures of HA in aqueous solutions have extensively been studied and only key elements are summarised below which allow to understand some of the fundamental properties and biological functions of HA.

HA is a highly hydrophilic biopolymer capable of binding water molecules and expanding its volume up to 1,000 times [7].
In aqueous solutions, the macromolecular structure of HA is not random as it is stiffened by a combination of intra- and intermolecular hydrogen bonding, hydrogen bonding with the solvent and intermolecular non-polar/hydrophobic interactions. As a result, HA exhibits several preferred structures referred to as the primary, secondary and tertiary structures [5].

The primary structure refers to the sequence of HA disaccharide units [5]. The secondary structure is due to intramolecular hydrogen bonding and hydrogen bonding

with the solvent. The sugar rings being relatively fixed in their shapes, rotation along HA chains is only allowed at the glycosidic bonds through revolution around the oxygen atom joining one disaccharide unit to the next. Although the substituents attached on both sides of this oxygen atom can in principle rotate 360 degrees around, only limited configurations are possible and each disaccharide unit is twisted by 180 degrees compared with the one ahead and behind in the chain due to intramolecular hydrogen bonding and hydrogen bonding with the solvent [5] (Figure I.2).

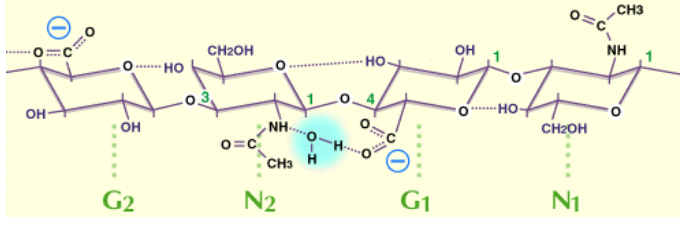

Figure I.2: Intramolecular hydrogen bonding and hydrogen bonding with the solvent in aqueous HA solutions (adapted from [5]).

G and N stand for glucuronate and acetylglucosamine, respectively. The dotted lines represent hydrogen bonding. Hydrogen bonding with the solvent occurs through the water bridge between the N2 acetamido and G1 carboxylate group.

Two disaccharide unit twists bringing the original orientation back, HA assumes a two-fold helix structure [5] (Figure I.3).

Finally, the tertiary structure stems from intermolecular non-polar/hydrophobic interactions and intermolecular hydrogen bonding between neighbouring HA chains. Although HA is a highly hydrophilic molecule due to its equatorial hydroxyl, carboxyl and acetamido groups, it also possesses a number of CH groups stretching along each disaccharide unit. The corresponding axial hydrogen atoms form a non-polar, relatively hydrophobic patch. In addition, the

hydroxymethylene group of the acetylglucosamine moiety can easily rotate to contribute to this patch [8] (Figure I.4).

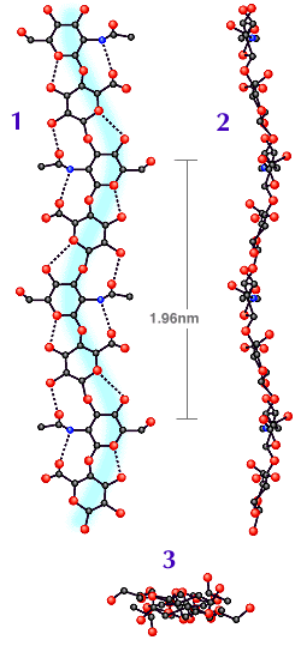

Figure I.3: Plan (1) and elevation (2) computer drawn projections of HA and view along the two-fold helix axis (3) [5].

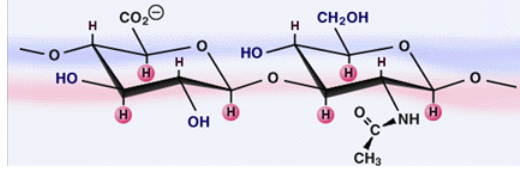

Figure I.4: The hydrophilic and non-polar/hydrophobic patches in HA [8].

The blue and red ribbons represent the hydrophilic and the non-polar/hydrophobic patches in HA, respectively.

The existence of the non-polar/hydrophobic patches in HA explains the association of HA chains in aqueous solutions despite the dense distribution of anionic charges along the polymer backbone. Indeed, the curves in each HA molecules (see Figure I.3, (1) and (2)) closely follow the same course which allows the hydrophobic patches to closely engage with each other in an antiparallel fashion. In addition, in this configuration, the acetamido and carboxylate groups on neighbouring HA chains become within hydrogen bonding distances [5].

It is noteworthy that similar structures are possible for other GAGs such as chondroitin, keratan and dermatan sulfates and mixtures of two or more including HA [9] (also see § I.4).

In vivo, HA occurs in a wide range of MW from a few thousands to several millions Daltons. However, physiological concentrations (e.g. 1-4 g/L) of high MW HA can result in entangled polymeric networks exhibiting viscoelastic properties. Indeed, due to the fundamental structures in aqueous solutions described above, HA networks can resist rapid, short-duration fluid flow and display elastic properties by returning the integrity of the shear forces applied. They can also absorb a fraction of these and feature viscous properties by partially separating and aligning HA molecules under slow, long-duration fluid flow [8] (Figure I.5).

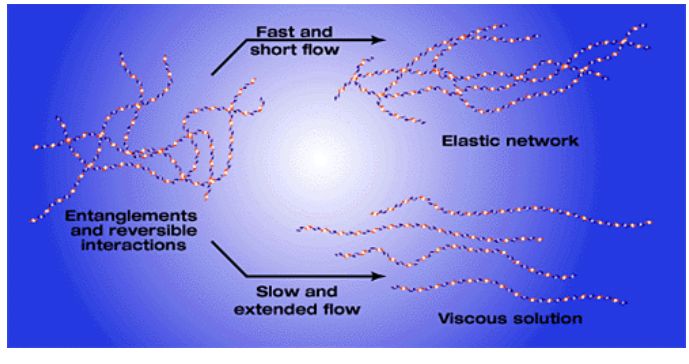

Figure I.5: Illustration of the viscoelastic properties of HA [8].

The viscoelastic properties of HA have important biological consequences. For example, the presence of HA in the synovial fluid contributes to both shock-absorption and lubrication in the knee.

HA networks have another important function related to the regulation of solute transport: small molecules such as water, electrolytes, nutrients and waste products can freely diffuse through the network. However, large molecules such as proteins, proteases and pathogens are partially excluded from the latter due to their larger hydrodynamic dimensions. Since HA chains are constantly in movement, these bulky molecules can in principle statistically diffuse through the network but with various degrees of retardation. As a result, their concentration in the network is limited compared to that of the surrounding HA-free compartments. This allows to avoid the spreading of pathogens and unwanted proteolytic damages [8] (also see § I.4).

I.4. Biological functions in the skin

HA is ubiquitous in the body but is most abundant in the skin where it amounts to approximately 5 g, *i.e.* a third of the total human body's HA content [10]. In normal skin, HA occurs both in the dermis and the epidermis [11] (Figure I.6).
In the dermis, HA is mostly found in the papillary dermis and, in the reticular dermis, at the level of the skin appendages (e.g. the sebaceous glands and hair follicles, Figure I.6, a). Its concentration in the dermis is around 0.5 mg/g of wet tissue [4].
In the epidermis, HA is present in the extracellular space between the keratinocytes in the stratum granulosum, stratum spinosum and stratum basale (Figure I.6, b between the arrow heads and Figure I.6, c). Its concentration in the epidermis approaches 0.1 mg/g of wet tissue [4]. Recently, Sakai *et al.* [12] demonstrated that HA also occurs in the stratum corneum (SC), in the extracellular space between the corneocytes where its dry weight content is about 20 µg/g of SC.

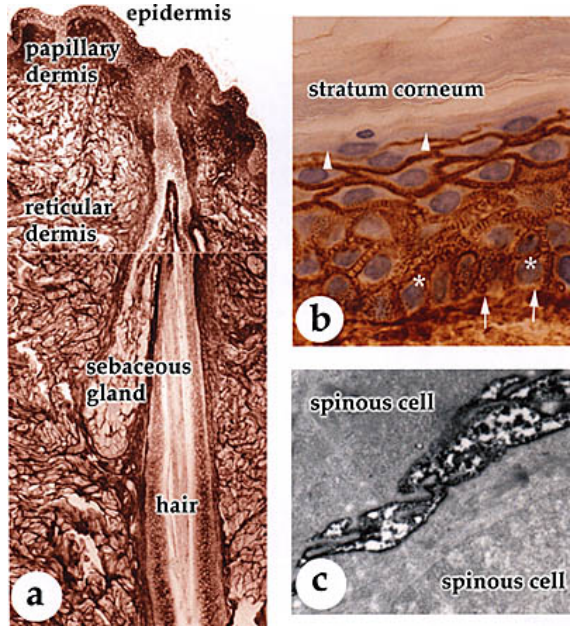

Figure I.6: Distribution of HA in adult human skin [11].

Human skin sections were stained for HA using the system biotinylated G1 protein/link protein complex. The binding of the complex was visualised using the avidin-biotin-peroxidase technique (brown), and nuclei were counterstained with hematoxylin (blue in b). In c, the dark precipitate in the extracellular space between the keratinocytes indicates HA [11].

In the skin, HA possesses a number of important structural and biological functions. Structurally, HA provides a matrix substrate for the distribution and organisation of important molecules of the extracellular matrix (ECM) (Figure I.7). In particular, HA constitutes a backbone for the organisation of proteoglycans (PG), fibrin, fibronectin, collagen and elastin [13] (Figure I.8). For example, HA is thought to associate with chondroitin, keratan and dermatan sulfates in the same fashion as it associates with itself, *i.e.* through non-polar/hydrophobic interactions and intermolecular hydrogen bonding [9] (also see § I.3).

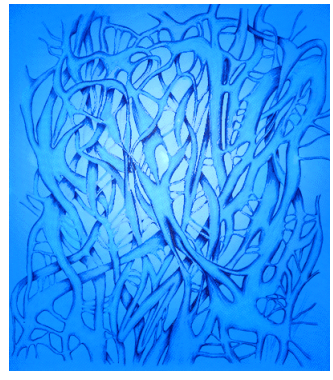

Figure I.7: Scheme of HA matrices in aqueous solutions [5].

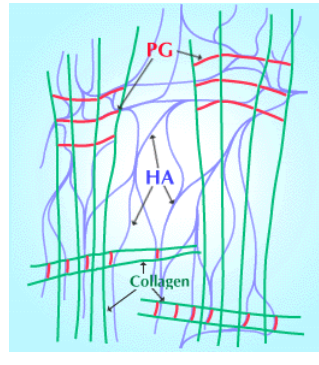

Figure I.8: Scheme of the organisation of proteoglycans and collagen in HA matrices [5].

Due to its naturally forming networks, HA acts as a filler which maintains both space and cohesion between skin cells. This facilitates the diffusion of nutrients to and waste products from upper skin cells and the movement of the immune system cells (*i.e.* lymphocytes and Langerhans cells) while restricting the movement of proteins, proteases and pathogens [8] (also see § I.3).

Finally, due to its strong hygroscopic character, HA is capable of retaining considerable amounts of water over prolonged periods of time. This contributes to tissue hydration and lubrication [14].

Biologically, HA triggers fundamental processes by binding with cells through specific interactions. For example, HA is involved in complex signalling events regulating cell proliferation, differentiation and migration. Such events are mediated by a group of proteins called hyaladherins. These proteins act as cellular receptors for HA. Two major receptors have been studied: CD44 and RHAMM (Receptor for HA-mediated mobility) [11].

CD44 is a major cell receptor for HA and is expressed on the surface of a variety of cells such as the leucocytes, fibroblasts, keratinocytes and some epithelial and endothelial cells [15]. CD44 has been shown to be associated with various cellular processes including cell adhesion, migration, proliferation and activation as well as HA degradation and uptake [16].

RHAMM is found on the surface and in the cytosol and nucleus of a number of cell types [17]. This receptor has been demonstrated to be involved in the regulation of cellular responses to growth factors and in the migration of fibroblasts and smooth muscle cells [17,18].

For more information about the CD44 and RHAMM receptors, the reader is invited to consult references [19] and [20].

Another potential biological function of HA is the scavenging of reactive oxygen species (ROS). ROS are noxious compounds produced as a result of exposure to ultraviolet (UV) radiations and are known to cause damage to cell membrane lipids, nucleic acids, proteins and enzymes and to be responsible for cancer, chronic diseases and aging. It has been demonstrated that HA effectively scavenges ROS *in vitro* [21,22,23]. ROS are now known to attack the C-5 hydrogen in the glucuronic acid moiety [24], the C-1 hydrogen in the acetylglucosamine moiety [25] and the carboxyl

and acetamido groups [26]. ROS clearance from the epidermis is currently speculated to happen through the natural rapid HA turnover [11].

In summary, these selected structural and biological functions of HA in the skin show that HA is the most active guardian of the ECM homeostasis.

I.5. Applications

Due to its unmatched natural biocompatibility, resorbability, physicochemical properties and biological functions (see § I.3 and I.4), HA has been used in numerous cosmetic, pharmaceutical and biomedical applications.

In the cosmetic industry, HA is a well-known and widely spread moisturising and skin softening agent [27,28]. Indeed, the topical application of HA-containing formulations has been reported to restore skin hydration and elasticity and thus provide an anti-ageing effect [4]. In addition, the incorporation of HA in sunscreens could help protect the skin against UV radiation damages.

The biomedical applications of HA are currently considerable [16,29,30]. According to Balazs [31] these can be classified into five main categories, namely (i) visco-surgery, (ii) visco-separation, (iii) visco-protection, (iv) visco-supplementation and (v) visco-augmentation (Table I.1). HA provides tissue protection, lubrication and space during surgery, prevents adhesion and excessive scar formation after surgery and promote wound healing by regulating cell proliferation and migration. Cross-linked HA can also be used to replace or supplement defective tissue fluids such as the synovial fluid in patients affected by osteoarthritis and possesses filling properties that can exploited for tissue augmentation.

Table I.1: Biomedical applications of HA [31].

Biomedical application	HA role
Visco-surgery	Tissue protection and lubrication HA provides space during surgery
Visco-separation	Separation and lubrication of traumatised connective tissue surfaces Prevention of tissue adhesion and excessive scar formation
Visco-protection	Tissue protection from dryness and environmental noxious agents Healing promotion
Visco-supplementation	Tissue fluid replacement or supplementation
Visco-augmentation	Tissue filling and augmentation

As for pharmaceutical applications, HA has been widely studied towards ophthalmic, nasal, pulmonary and parenteral drug delivery [32] for which it is generally thought to act as a mucoadhesive compound retaining the drug at its site of action/absorption and modifying the drug's *in vivo* release/absorption rate.
Recently, HA was envisaged as a potential promising excipient for dermal drug delivery.

II. Hyaluronic acid-mediated dermal drug delivery

Dermal drug delivery has become an important research field due to the advantages the dermal route presents compared to the more conventional enteral and parenteral routes (see Chapter II, § I). It has been estimated that the market for dermal and transdermal drug delivery represented 1.57 billion dollars in the United State (US) in 2002 and will amount to nearly 5.67 billion dollars by 2009, *i.e.* approximately 6 % of the total US drug delivery market [33].

Due to its natural presence in the skin, HA represents an attractive biocompatible and resorbable excipient for the dermal administration of drugs. For example, HA can be co-formulated with drugs (first generation systems) or constitute the building block of more advanced biomaterials (second generation systems).

II.1. First generation systems

The use of HA in dermal drug delivery is relatively recent [34] and has mainly consisted in co-formulating HA with the drugs. Co-formulations of HA and therapeutic agents such as dichlorofenac, ibuprofen, clindamycin and cyclosporin has been rigorously investigated *in vitro*, *in vivo* and in clinical studies and reviewed in an excellent article by Liao *et al.* [32]. These studies have shown that HA significantly enhances drug partitioning into human skin and drug retention and localisation in the epidermis compared to other GAGs and more ordinary pharmaceutical formulations. However, the exact mechanisms by which HA, as an excipient, achieves such performances remains unclear [32].

While HA/drug co-formulations seem to sustain drug absorption in skin layers, drug release, in this configuration, remains non-specific. In cases of more challenging and demanding therapeutic situations, such as when the drugs need to be protected and targeted to specific tissues, more advanced systems than co-formulations are required. These form the basis of the second generation HA-based systems.

II.2. Second generation systems

The interest in nanotechnology in pharmacy is somewhat new and is mainly due to drug-associated issues such as poor solubility and instability in biological milieu (*i.e.* short half-life), poor bioavailability and unspecific targeting. As a result, high drug dosages are used to achieve a therapeutic effect which increases the risk for toxicity in

patients and health cost [35]. Therefore, the design of advanced drug delivery systems addressing these challenges has become more and more crucial. In this perspective, it is believed that drug encapsulation in nanovehicles could allow the formulation of improved systems [35].
With its unusual and beneficial properties, HA represents an attractive candidate for the encapsulation and release of drugs in biological environments, including skin layers. HA-based advanced biomaterials such as colloidal particles therefore constitute potential valuable second generation dermal drug delivery systems.

III. Hyaluronic acid-based colloidal particles

III.1. Microparticles

The preparation of HA-based colloidal particles towards drug delivery first addressed the development of microparticles (MPs). HA MPs in which HA constitutes the only component of the polymeric matrix have been prepared according to a few different methods which are reviewed in Table I.2. These methods can be classified in two main categories according to the type of HA modification involved, namely cross-linking [36,37] or hydrophobic modification [38,39].
In the first case, HA and a cross-linking agent are mixed and emulsified into mineral oil with the aid of a biodegradable surfactant to produce a microemulsion. Cross-linking is then initiated in the microdroplets containing HA and the cross-linking agent by addition of a coupling agent [36]. Alternatively, two auto-cross-linkable HA derivatives can be used [37].
In the second case, HA is first hydrophobically modified (HYAFF®). HYAFF® solutions are then spray-dried into the form of microparticles [38] or emulsified in mineral oil with the aid of a biodegradable surfactant [38,39]. The polar organic solvent in the microdroplets is then either removed by extraction with another polar organic solvent [38] or evaporated by mixing at room temperature [39]. In methods

[38] and [39], the particles are stabilised by hydrophobic interactions between the hydrophobic groups grafted on the HA chains.

Table I.2: Preparation methods of HA microparticles.

ADH, Span 80, EDC, DMSO, Arlacel® A stand for adipic acid dihydrazide, sorbitan monostearate, 1-ethyl-3-[3-dimethyl amino] propyl carbodiimide, dimethyl sulfoxide and mannide monostearate, respectively. HYAFF® is Fidia's trademark for hydrophobically modified HA obtained by reacting HA and alkyliodides in DMSO, using the tetrabutylammonium salt of HA (also see § IV).

Reference	HA MW MP size	Principle
[36]	1,600-3,300 kDa 5-15 µm	▪ Emulsification of HA and ADH into mineral oil with Span 80 ▪ Cross-linking in the presence of EDC
[37]	490-1,300 kDa 10 µm	▪ Emulsification of oxidized HA and ADH-modified HA into mineral oil with Span 80 ▪ Cross-linking in the presence of EDC
[38]	unspecified 1-10 µm	▪ Spray drying of aqueous HYAFF® solutions
[38]	unspecified 1-100 µm	▪ Emulsification of HYAFF® in DMSO into mineral oil with Arlacel® A ▪ Extraction of DMSO with ethyl acetate
[39]	150 kDa 10-100 µm	▪ Emulsification of HYAFF® in hexafluoropropanol into mineral oil with Arlacel® A ▪ Evaporation of hexafluoropropanol by mixing at room temperature

The applications of HA MPs towards drug delivery are numerous and *in vivo* release studies have shown that HA MP-mediated drug delivery presents some advantages compared to conventional drug formulations. For example, HA MPs have been used to modulate the nasal absorption of insulin in sheeps [40], enhance the vaginal assimilation of salmon calcitonin [41], the oral bioavailability of cyclosprorin [42] and piroxicam [43] in rats and the production of growth factors when injected subcutaneously to monkeys and dogs [44]. These examples show that HA MPs are

currently designed in the perspective of targeting all three drug administration routes, namely the topical, enteral and parenteral routes.
However, for topical routes such as the skin, the size of the particulate system is an important factor for its performances since skin penetration is an extremely selective phenomenon. With their large dimensions, MPs have often been considered unsuitable devices for targets other than the surface of the skin or the skin appendages [45]. Nanoparticles (NPs), however, could present more favourable dimensions towards skin penetration and their interaction with the skin is a currently studied topic (see Chapter II).

III.2. Nanoparticles

To the best of our knowledge, and as until January 2008, four patent applications and three articles have since 1995 claimed the preparation of HA NPs in which HA constitutes the only component of the polymeric matrix. The techniques disclosed are reviewed in Table I.3. As for HA MPs, the preparation methods of HA NPs can be classified in the two main categories described before, *i.e.* according to whether HA is hydrophobically modified [46] or cross-linked [47-51].
However, HA can also be directly complexed with the drug to be encapsulated [52].
In the second case, where particles are produced by cross-linking of transient HA colloidal assemblies, the parameter which seems to allow a size reduction from micro- to nanoparticles is the type of solvent used as the continuous phase: mineral oil for HA MPs versus water, water/acetone mixtures or (mixtures of) light non-polar organic solvents for HA NPs. These solvents or solvent mixtures are much less viscous that mineral oil which results in much smaller droplet size and by extension particle size.

Table I.3: Preparation methods of HA nanoparticles.

DMSO, EDC, ADH, ODH, Span 80, HLB, PH, NHSS, Span 85, HLB stand for dimethyl sulfoxide, 1-ethyl-3-[3-dimethyl amino] propyl carbodiimide, adipic acid dihydrazide, oxalic acid dihydrazide, sorbitan monostearate, hydrophilic lipophilic balance, polyhydrazide, sodium *N*-hydroxysulfosuccinimide, sorbitan tristearate, hydrophilic lipophilic balance, respectively. HYAFF® is Fidia's trademark for hydrophobically modified HA obtained by reacting HA and alkyliodides in DMSO, using the tetrabutylammonium salt of HA (also see § IV). For some of the preparation methods, the mechanism underlying the formation of the nanoparticles is explained as claimed by the authors or in the absence thereof as presumed by us in *Comment*.

Reference	HA MW NP size	Principle	Comment
[46]	unspecified 500-1,000 nm	▪ Instillation, under pressure, of pure CO_2 into the HYAFF®/active ingredient solution in DMSO ▪ Calcitonin, granulocyte macrophage colony stimulating factor and human insulin were encapsulated.	Nanoprecipitation of HYAFF® in the supercritical CO_2 antisolvent is induced by DMSO solubilisation in CO_2 and evaporation. Insoluble HYAFF® in CO_2 precipitates into nanoparticles.
[47]	20-2,500 kDa 20 nm- 200 µm	▪ Auto cross-linking of HA carboxyl and hydroxyl groups in the presence of EDC, in aqueous HA solutions or alternatively, ▪ Cross-linking with polyamines, in the presence of EDC, in aqueous HA solutions	Cross-linking of HA in aqueous solutions converts the initially randomly coiled HA into spherical HA nanoparticles.
[48]	200- 1,500 kDa 200 nm	▪ Cross-linking with ADH, in the presence of EDC, in water/acetone mixtures	Water/acetone mixtures provide a poor solvent environment for HA which tends to self-associate into nanoassemblies. Acetone catalyses intra- and intermolecular cross-linking by breaking HA hydrogen bonds.

Table I.3: Preparation methods of HA nanoparticles (continued).

Reference	HA MW NP size	Principle	Comment
[49]	unspecified 50-200 nm	▪ Mixing of HA and EDC with an emulsion of aminophospholipid ▪ Cross-linking with the phospholipids in the presence of EDC ▪ Paclitaxel was encapsulated	We believe that the process involves interfacial cross-linking of HA at the surface of the phospholipid droplets and that the nanoparticles form as the phospholipids are consumed.
[50]	MW > 20 kDa 10-160 nm	▪ Emulsification of HA, ODH and EDC in a non-polar organic solvent with Span 80 ▪ Cross-linking with ODH, in the presence of EDC ▪ Fluorescein isothiocyanate, atrial natriuretic peptide and green fluorescence protein were encapsulated	Despite the fact the authors mention the formation of an o/w emulsion, we believe, according to the Bancroft rule [53], that a w/o emulsion is rather formed due to the low HLB value of Span 80. We therefore presume that the cross-linking reaction takes place inside the water droplets containing HA, ODH and EDC. Interestingly, when this method was applied to 20-40 kDa HA, the size of the nanoparticles was reduced between 10 and 40 nm.
[51]	174 kDa 200-300 nm	▪ Emulsification of HA, PH, EDC and NHSS in ethyl acetate/propylene carbonate with Span 85 ▪ Cross-linking with PH, in the presence of EDC and NHSS	The droplets of the nanoemulsion constitute nanoreactors in which HA is cross-linked with PH. A mixture of EDC and NHSS was used to catalyse the reaction as cross-linking in the presence of EDC alone was too rapid and yielded nanoparticles with uncontrolled properties.
[52]	102 kDa 100-200 nm	▪ Spontaneous complexation between HA and cisplatin	

The preparation methods of Table I.3 present some advantages and drawbacks which are detailed below.

▪ HYAFF®-based NPs [46] contain both hydrophilic and hydrophobic domains where hydrophilic and/or hydrophobic active ingredients can be encapsulated. In addition, HYAFF® polymers are biocompatible and resorbable in rats [54] which makes them potentially suitable for pharmaceutical purposes. However, the nanoprecipitation step requiring relatively high working pressures, the process might be unsuitable for the encapsulation of fragile active ingredients.

▪ The NPs obtained by intra- and intermolecular cross-linking between HA carboxyl and hydroxyl groups [47] do not contain any cross-linking agent molecules making up the bridges between HA chains. As a result, these NPs are potentially completely biocompatible. Similarly, when HA is cross-linked with aminophospholipids naturally present in biological membranes [49], the resulting NPs consist of fully resorbable materials.

Nevertheless, since HA assemblies are randomly formed in method [47], the size of the resulting particles is quite polydisperse. This could limit their use for applications where the latter needs to be accurately controlled and narrowly distributed.

▪ A common advantage to the methods involving HA emulsification [50,51] is the possibility to quite precisely control the NP size by managing that of the nanodroplets. Conversely, a common drawback is the use of organic solvents and surfactants. Organic solvents raise occupational and environmental issues and limit the upscalability of the methods while surfactants are known irritants which complete removal can be problematic.

▪ Native HA-based NPs [47-52] present the disadvantage that only hydrophiphilic/polar ingredients can durably be encapsulated since highly hydrophilic HA represents an unfavourable environment for hydrophobic compounds.

▪ Finally, HA/drug complexes [52] are cross-linking agent-free and do not require modifying HA or using organic solvents, surfactants or harsh conditions. However, the technique is not versatile since HA/drug complexation is not a universal phenomenon.

In summary, the preparation methods of HA NPs are still facing challenges such as (i) environmental unfriendliness, (ii) potential surfactant residues, (iii) NP size polydispersity, (iv) poor versatility of the encapsulated active ingredients and (v) limited upscalability.

When comparing the evolutionary development stage of HA micro- and nanoparticles it becomes clear that that HA MPs are in a paradigmatic stage where dominant designs have emerged and research has been taken beyond the investigation of preparation methods towards *in vivo* release studies. HA NPs, however, are still in a preparadigmatic stage where focus is still drawn on spotting out dominant designs (no two similar methods are described in the existing scarce literature) rather than on investigating the uses and applications of the nanoparticles. HA NP-mediated drug delivery therefore represents a challenging research field with room for innovation, intellectual property and application achievements.

With the exception of Pallado *et al.* [46], there are no reported methods for the preparation of HA NPs based on hydrophobically modified HA (hmHA). Despite the fact the working conditions of this method may be too harsh for the encapsulation of delicate active ingredients, the concept of using hmHA is innovative and currently not widespread according to the literature study. Indeed, with its altered physicochemical properties and HLB, hmHA constitutes a more favourable starting material for the production of nanostructures and the durable encapsulation of hydrophobic ingredients than native HA. For these reasons, some currently available preparation methods of hmHA are reviewed in the next section.

IV. Hydrophobically modified hyaluronic acid

Hydrophobically modified HA is conventionally prepared by targeting reactions at HA carboxyl and/or hydroxyl groups [55].

Historically, Jeanloz and Forchielli [56] were the first to report the modification of HA carboxyl groups with diazomethane, acetic anhydride and triphenylchloromethane towards the preparation of methylated, acetylated and triphenylchloromethylated HA.

In the late 1980's, Della Valle and Romeo [57] patented the modification of HA carboxyl groups with alkyliodides, in DMSO, using the tetrabutylammonium salt of HA. The resulting derivatives currently form the basis of Fidia's trademark HYAFF® which has frequently been used for the preparation of colloidal particles towards drug delivery (see § III).

Other more recent modification methods non-exhaustively include modification of the HA carboxyl groups with:

(i) alkylaldehydes in water/ethanol mixtures, in the presence of sodium cyanoborohydride, using an adipic dihydrazide-modified HA intermediate obtained in the presence of 1-ethyl-3-[3-dimethyl amino] propyl carbodiimide [58],

(ii) alkylbromides in DMSO [59],

and of the HA hydroxyl groups with

(iii) acylchlorides in *N*,*N*-dimethylformamide (DMF), in the presence of pyridine [60],

(iv) alkyloxymethyloxiranes in water/DMSO mixtures [61],

(v) alkylalcohols in DMSO, in the presence of potassium hydroxide, using a *p*-toluene sulfonyl-modified HA intermediate [62] (Figure I.9).

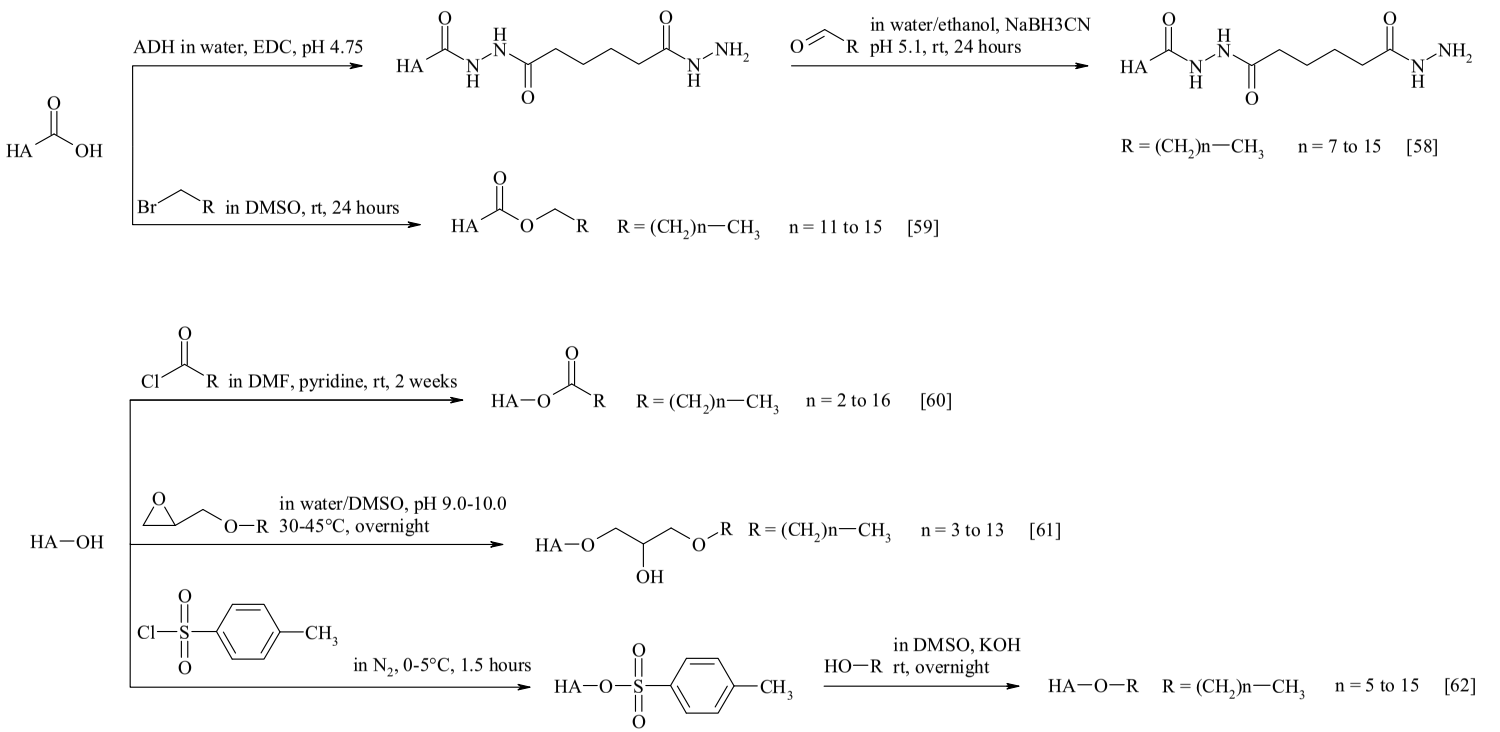

Figure I.9: Illustration of selected hydrophobic modifications of HA.

However, the modification methods currently available for the preparation of amphiphilic HA present some drawbacks.

First, the modification reactions are often conducted in organic solvents or organic solvent/water mixtures. In addition to raise occupational and environmental issues and limit the upscalability of the preparation methods, the use of organic solvents or mixtures of these often requires converting HA into its tetraalkylammonium salt or preparing reactive HA intermediates. This not only adds complex steps to the preparation methods but also often results in HA degradation [59].

Secondly, the modification reactions involving HA carboxyl groups modify the distribution of negative charges along the polymer backbone at physiological pH. This could potentially affect some of the attractive biological and/or pharmacological properties of native HA [62].

Therefore, simple modification reactions in aqueous media, under mild conditions and exclusively involving HA hydroxyl groups could represent advantageous alternatives for the preparation of amphiphilic HA derivatives.

V. The Ph.D. project

V.1. Objectives and challenges

For the reasons outlined all along this introduction chapter, HA currently represents one of the most attractive building block for the preparation of advanced biomaterials with applications in pharmacy.

While the superficial administration of certain HA/drug co-formulations has been shown to enhance drug partitioning into human skin and drug retention and localisation in the epidermis, there is a lack of truly biocompatible and resorbable solutions for more challenging and demanding therapeutic situations requiring drug protection and targeting (see § II).

It is well known that tumourous cells generally over-express HA-binding receptors at their surface. Consequently, these show enhanced HA binding and internalisation [63]. Anti-cancer drug-containing HA-based systems therefore potentially represent valuable and efficient multi-functional targeting devices towards superficial tumoured tissues. In addition, due to HA's natural presence in the skin, HA-based systems are likely to interact with the skin without altering the epithelium's physiology.
Therefore, the overall objective of this project was to design and develop advanced HA-based drug delivery systems such as HA nanoparticles towards the encapsulation and targeted delivery of chemically instable and/or poorly soluble drugs in aqueous media. In the first place, it was envisaged to evaluate these devices for dermal drug delivery and later extend their use to other delivery routes.

The methods currently available for the preparation of HA NPs are still facing challenges such as (i) environmental unfriendliness, (ii) potential surfactant residues, (iii) NP size polydispersity, (iv) poor versatility of the encapsulated active ingredients and (v) limited upscalability. In addition, they use native HA which is unsuitable for the encapsulation of hydrophobic ingredients. It is believed that hydrophobically modified HA with its altered physicochemical properties and HLB, constitutes a more favourable starting material for the production of stable nanostructures and the durable encapsulation of hydrophobic ingredients (see § III.2).
However, the current preparation methods of amphiphilic HA present some drawbacks such as the (i) use of organic solvents, (ii) potential alteration of some fundamental biological and/or pharmacological properties of HA through modification of the carboxyl groups and (iii) limited upscalability (see § IV).
Therefore, other important objectives of this project were to elaborate simple and easily upscalable, aqueous and versatile techniques for both the preparation of amphiphilic HA and of HA NPs. Focus was drawn on exclusively modifying the HA hydroxyl groups in order to preserve the distribution of anionic charges along the polymer backbone and on avoiding the use of surfactants to formulate reasonably

uniformly distributed NPs capable of encapsulating both hydrophilic and hydrophobic compounds.

V.2. Experimental approach

Due to its high hydrophilicity, native HA possesses physicochemical properties incompatible with the spontaneous and stable formation of segregated structures in aqueous media and the durable encapsulation of hydrophobic active ingredients. In addition, native HA displays a poor *in vivo* biological stability and residence time as evidenced by its high turnover rate [64].

Therefore, HA was first rendered amphiphilic by the covalent binding of hydrophobic groups onto its backbone. For this purpose, two novel proprietary methods were evaluated and one was eventually selected for further study based on the superior versatility and functionality of the resulting HA derivatives.
This method was then optimised in order to develop a reproducible and robust process for the routine preparation of functionalised HA polymers with tailored degrees of substitution.
Fundamental properties such as the structure, degree of hydrophobicity, substitution pattern as well as intra- and intermolecular interactions of a selection of derivatives were subsequently studied.
Submicronic multiphasic physically cross-linked nanogel particles capable of solubilising a model hydrophobic substance were prepared by spontaneous self-association and characterized with regard to their morphology, size and surface charge. A multivesicular model was finally put forward to explain their internal structure.
Finally, methods to prepare stable NPs based on the chemical stabilisation of self-assembled HA templates were explored. Indeed, while the methods currently available for the preparation of HA NPs rely on random collisions in the medium to create structures, focus was here drawn on the development of a novel molecular approach

based on self-assembling multiphasic nanoarchitectured HA templates potentially yielding more complex NP configurations than single ingredient or core-shell structures.

V.3. Thesis structure

After this introduction chapter, the thesis is organised in four more chapters written in the form of research reports and/or articles to be submitted shortly.

Chapter II is a review article about the current knowledge about the mechanisms underlying polymeric nanoparticle-mediated (trans)dermal drug delivery. It investigates, among others, the potential of this delivery route, the research gaps and the challenges still faced by this branch of research.

Chapter III is organised in three different sections. Section A reports the initial investigation of novel modification methods to prepare amphiphilic HA and the selection of one class of HA derivatives for further study. Section B concerns the optimisation of the preparation of these HA derivatives which detailed molecular structure and solution properties in aqueous media is investigated in section C.

Chapter IV reports the physicochemical properties of the selected class of HA derivatives and the preparation of multiphasic nanostructured HA templates.

Chapter V reviews the work achieved, gives a conclusion for the thesis and outlines some possible future work. It also suggests some potential applications for the systems developed.

Finally, a record of the educational activities conducted during the industrial Ph.D. programme is presented in the appendices.

References

[1] Lee, J. Y.; Spicer, A. P. Hyaluronan: a multifunctional, megaDalton, stealth molecule. *Curr. Opin. Cell Biol.* **2000**, *12*, 581-586.

[2] Meyer, K.; Palmer, J. The polysaccharide of the vitreous humor. *J. Biol. Chem.* **1934**, *107*, 629-634.

[3] Weissman, B.; Meyer, K. The structure of hyalobiuronic acid and of hyaluronic acid from umbilical cord. *J. Am. Chem. Soc.* **1954**, *76*, 1753-1757.

[4] Brown, M. B.; Jones, S. A. Hyaluronic acid: a unique topical vehicle for the localized delivery of drugs to the skin. *J. Eur. Acad. Dermatol. Venereol.* **2006**, *20*, 1348-1349.

[5] Glycoforum, http://www.glycoforum.gr.jp/science/hyaluronan/HA02/HA02E.html, last updated March 15, 1998.

[6] Widner, B.; Behr, B.; Von Dollen, S.; Tang, M.; Heu, T.; Sloma, A.; Sternberg, D.; DeAngelis, P. L.; Weigel, P. H.; Brown, S. Hyaluronic acid production in bacillus subtilis. *Appl. Environ. Microbiol.* **2005**, *71*, 3747-3752.

[7] Laurent, T. C.; Fraser, J. R. E. Hyaluronan. *Faseb J.* **1992**, *6*, 2397-2404.

[8] Glycoforum, http://www.glycoforum.gr.jp/science/hyaluronan/HA01/HA01E.html, last updated December 15, 1997.

[9] Scott, J. E.; Presti, D. Hyaluronan-mediated protective effect against cell damage caused by enzymatically produced hydroxyl radicals is dependent on hyaluronan molecular mass. *Cell Biochem. Funct.* **1994**, *12*, 281-288.

[10] Banks, J.; Kreider, J. W.; Bhavanadan, V. P.; Davidson, E. A. Anionic polysaccharide production and tyrosine activation in cultured human melanoma cells. *Cancer Res.* **1976**, *36*, 424-431.

[11] Glycoforum, http://www.glycoforum.gr.jp/science/hyaluronan/HA04/HA04E.html, last updated June 15, 1998.

[12] Sakai, S.; Yasuda, R.; Sayo, T.; Ishikawa, O.; Inoue, S. Hyaluronan exists in the normal stratum corneum. *J. Invest. Dermatol.* **2000**, *114*, 1184-1187.

[13] Chen, W. Y. J.; Abatangelo, G. Functions of hyaluronan in wound repair. *Wound Rep. Reg.* **1999**, *7*, 79-89.

[14] Yates, J. R. Mechanism of water uptake by skin. In *Biophysical properties of the skin*; Eden, N. R., Ed.; Wiley Interscience: New York, 1971.

[15] Isacke, C. M.; Yarwood, H. The hyaluronan receptor, CD44. *Int J. Biochem. Cell Biol.* **2002**, *34*, 718-721.

[16] Leach, J. B.; Schmidt, C. E. Hyaluronan. In *Encyclopedia of biomaterials and biomedical engineering*; Bowlin, G. L.; Wnek, G., Eds.; Marcel Dekker: New York, 2004.

[17] Cheung, W. F.; Cruz, T. F.; Turley, E. A. Receptor for hyaluronan-mediated motility (RHAMM), a hyaladherin that regulates cell responses to growth factors. *Biochem. Soc. Trans.* **1999**, *27*, 135-142.

[18] Toole, B. P. Hyaluronan in morphogenesis. *Semin. Cell Dev. Biol.* **2001**, *12*, 79-87.

[19] Glycoforum, http://www.glycoforum.gr.jp/science/hyaluronan/HA10/HA10E.html, last updated January 13, 2005.

[20] Glycoforum, http://www.glycoforum.gr.jp/science/hyaluronan/HA11/HA11E.html, last updated July 25, 1999.

[21] Tokita, Y.; Sakashita, H.; Okamoto, A.; Kubota, K. Kinetic study of a radical scavenging effect of hyaluronic acid. *Polymer Int.* **1995**, *38*, 161-164.

[22] Trommer, H.; Wartewig, S.; Böttcher, R.; Pöppl, A.; Hoentsch, J.; Ozegowski, J. H.; Neubert, R. H. H. The effects of hyaluronan and its fragments on lipid models exposed to UV irradiation. *Int. J. Pharm.* **2003**, *254*, 223-234.

[23] Campo, G. M.; Avenoso, A.; Campo, S.; D'Ascola, A.; Ferlazzo, A. M.; Calatroni, A. The antioxidant and antifibrogenic effects of the glycosaminoglycans hyaluronic acid and chondroitin-4-sulphate in a subchronic rat model of carbon tetrachloride-induced liver fibrogenesis. *Chem. Biol. Interact*. **2004**, *148*, 125-138.

[24] Gilbert, B. C.; King, D. M.; Thomas, C. B. The oxidation of some polysaccharides by the hydroxyl radical: an E.S.R. investigation. *Carbohydr. Res.* **1984**, *125*, 217-235.

[25] Uchiyama, H.; Dobashi, Y.; Ohkouchi, K.; Nagasawa, K. Chemical change involved in the oxidative reductive depolymerization of hyaluronic acid. *J. Biol. Chem.* **1990**, *265*, 7753-7759.

[26] Lapcik, L.; Chabrecek, P.; Stasko, A. Photodegradation of hyaluronic acid: EPR and size exclusion chromatography study. *Biopolymers* **1991**, *31*, 1429-1435.

[27] Balazs, E. A.; Band, P. Hyaluronic acid: its structure and use. *Cosmetics & Toiletries* **1984**, *99*, 65-72.

[28] Oka, T.; Ueno, N.; Yanaki, T. Differential scanning calorimetry studies on the mechanism of skin-softening effect on sodium acethylhyaluronate. *Polymer* **2000**, *41*, 6055-6059.

[29] Lapcik, L. Jr.; Lapcik, L.; De Smedt, S.; Demeester, J.; Chabrecek, P. Hyaluronan: preparation, structure, properties and applications. *Chem. Rev.* **1998**, *98*, 2663-2684.

[30] Kogan, G.; Soltes, L.; Stern, R.; Gemeiner, P. Hyaluronic acid: a natural biopolymer with a broad range of biomedical and industrial applications. *Biotechnol. Lett.* **2007**, *29*, 17-25.

[31] Balazs, E. A. Viscoelastic properties of hyaluronan and its therapeutic use. In *Chemistry and biology of hyaluronan*; Garg, H. G.; Hales, C. A., Eds.; Elsevier: Amsterdam, 2004.

[32] Liao, Y. H.; Jones, S. A.; Forbes, B.; Martin, G. P.; Brown, M. B. Hyaluronan: pharmaceutical characterization and drug delivery. *Drug Deliv.* **2005**, *12*, 327-342.

[33] Frost & Sullivan, U.S. Emerging Transdermal Drug Delivery Technologies Markets. http://www.frost.com, May 9, 2003.

[34] Brown, M. B.; Forbes, B.; Martin, G. P. The use of hyaluronan in topical drug delivery. In *Hyaluronan: biomedical, medical and clinical aspects*; Kennedy, J.; Phillips, G. O.; Williams, P. A.; Hascall, V., Eds.; Woodhead Publishing: Cambridge, 2002.

[35] Rawat, M.; Singh, D.; Saraf, S.; Saraf, S. Nanocarriers: promising vehicle for bioactive drugs. *Biol. Pharm. Bull.* **2006**, *29*, 1790-1798.

[36] Yun, Y. H.; Goetz, D. J.; Yellen, P.; Chen, W. Hyaluronan microspheres for sustained gene delivery and site-specific targeting. *Biomaterials* **2004**, *25*, 147-157.

[37] Jia, X. Q.; Yeo, Y.; Clifton, R. J.; Jiao, T.; Kohane, D. S.; Kobler, J. B.; Zeitels, S. M.; Langer, R. Hyaluronic acid-based microgels and microgel networks for vocal fold regeneration. *Biomacromolecules* **2006**, *7*, 3336-3344.

[38] Ghezzo, E.; Benedetti, L.; Rochira, M.; Biviano, F.; Callegaro, L. Hyaluronate derivative microspheres as NGF delivery devices: preparation methods and in vitro release characterization. *Int. J. Pharm.* **1992**, *87*, 21-29.

[39] Benedetti, L. M.; Topp, E. M.; Stella, V. J. Microspheres of hyaluronic acid esters. Fabrication methods and in vitro hydrocortisone release. *J. Controlled Release* **1990**, *13*, 33-41.

[40] Illum, L.; Farraj, N. F.; Fisher, A. N.; Gill, I.; Miglietta, M.; Benedetti, L. M. Hyaluronic acid ester microspheres as a nasal delivery system for insulin. *J. Controlled Release* **1994**, *29*, 133-141.

[41] Richardson, J. L.; Ramires, P. A.; Miglietta, M. R.; Rochira, M.; Bacelle, L.; Callegaro, L.; Benedetti, L. M. Novel vaginal delivery systems for calcitonin: I. Evaluation of HYAFF/calcitonin microspheres in rats. *Int. J. Pharm.* **1995**, *115*, 9-15.

[42] Woo, J. S.; Piao, M. G.; Li, D. X.; Ryu, D. S.; Choi, J. Y.; Kim, J. A.; Kim, J. H.; Jin, S. G.; Kim, D. D.; Lyoo, W. S.; Yong, C. S.; Choi, H. G. Development of cyclosporin A-loaded hyaluronic microspheres with enhanced oral bioavailability. *Int. J. Pharm.* **2007**, *345*, 134-141.

[43] Piao, M. G.; Kim, J. H.; Kim, J. O.; Lyoo, W. S.; Lee, M. H.; Yong, C. S.; Choi, H. G. Enhanced oral bioavailability of piroxicam in rats by hyaluronate microspheres. *Drug Dev. Ind. Pharm.* **2007**, *33*, 485-491.

[44] Kim, S. J.; Hahn, S. K.; Kim, M. J.; Kim, D. H.; Lee, Y. P. Development of a novel sustained release formulation of recombinant human growth hormone using sodium hyaluronate microparticles. *J. Controlled Release* **2005**, *104*, 323-335.

[45] Toll, R.; Jacobi, U.; Richter, H.; Lademann, J.; Schaefer, H.; Blume-Peytavi, U. Penetration profile of microspheres in follicular targeting of terminal hair follicles. *J. Invest. Dermatol.* **2004**, *123*, 168-176.

[46] Pallado, P.; Benedetti, L.; Callegaro, L. Nanospheres comprising a biocompatible polysaccharide. WO 96/29998, October 10, 1996.

[47] Borbely, J.; Tunde, R.; Magnolna, B. Hyaluronic acid-based cross-linked nanoparticles. US 2007/0224277 A1, September 27, 2007.

[48] Hu, Z.; Xia, X.; Tang, L. Process for synthesizing oil and surfactant-free hyaluronic acid nanoparticles and microparticles. US 2006/0040892 A1, February 23, 2006.

[49] Yerushalmi, N.; Peer, D.; Margalit, R.; Rivkin, I. Formulations of water insoluble or poorly water soluble drugs in lipidated glycosaminoglycan particles and their use for diagnostics and therapy. WO 2006/050246 A2, May 11, 2006.

[50] Mohapatra, S. S.; Sahoo, B.; Kumar, A.; Behera, S. A method of transdermal drug delivery using hyaluronic acid nanoparticles. US 2007/0036728 A1, September 27, 2007.

[51] Pitarresi, G.; Craparo, F.; Palumbo, F. S.; Carlisi, B.; Giammona, G. Composite nanoparticles based on hyaluronic acid chemically cross-linked with α,β-polyaspartylhydrazide. *Biomacromolecules* **2007**, *8*, 1890-1898.

[52] Jeong, Y. I.; Kim, S. T.; Jin, S. G.; Ryu, H. H.; Jin, Y. H.; Jung, T. Y.; Kim I. Y.; Jung, S. Cisplatin-incorporated hyaluronic acid nanoparticles based on ion-complex formation. *J. Pharm. Sci.* **2008**, *97*, 1268-1276.

[53] Bancroft, W. D. Theory of emulsification. *J. Phys. Chem.* **1913**, *17*, 501-519.

[54] Benedetti, L.; Cortivo, R.; Berti, T.; Berti, A.; Pea, F.; Mazzo, M.; Moras, M.; Abatangelo, G. Biocompatibility and biodegradation of different hyaluronan derivatives (Hyaff) implanted in rats. *Biomaterials* **1993**, *14*, 1154-1160.

[55] Vercruysse, K. P.; Prestwich, G. D. Hyaluronate derivatives in drug delivery. *Crit. Rev. Ther. Drug Carrier Syst.* **1998**, *15*, 513-555.

[56] Jeanloz, R. W.; Forchielli, E. Studies on hyaluronic acid and related substances. I. Preparation of hyaluronic acid and derivatives from human umbilical cord. *J. Biol. Chem.* **1950**, *186*, 495-511.

[57] Della Valle, F.; Romeo, A. Esters of hyaluronic acid. US 4,851,521, July 25, 1989.

[58] Creuzet, C.; Kadi, S.; Rinaudo, M.; Auzely-Velty, R. New associative systems based on alkylated hyaluronic acid. Synthesis and aqueous solution properties. *Polymer* **2006**, *47*, 2706-2713.

[59] Pelletier, S.; Hubert, P.; Payan, E.; Marchal, P.; Choplin, L.; Dellacherie, E. Amphiphilic derivatives of sodium alginate and hyaluronate for cartilage repair: rheological properties. *J. Biomed. Mater. Res.* **2001**, *54*, 102-108.

[60] Kawaguchi, Y.; Matsukawa, K.; Gama, Y.; Ishigami, Y. New polysaccharide surfactants from hyaluronate. *Chem. Express* **1991**, *6*, 647-650.

[61] Mlochova, P.; Hajkova, V.; Steiner, B.; Bystricky, S.; Koos, M.; Medova, M.; Velebny, V. Preparation and characterization of biodegradable alkylether derivatives of hyaluronan. *Carbohydr. Polym.* **2007**, *69*, 344-352.

[62] Benesova, K.; Pekar, M.; Lapcik, L.; Kucerik, J. Stability evaluation of *n*-alkyl hyaluronic acid derivatives by DSC and TG measurement. *J. Therm. Anal. Calorim.* **2006**, *83*, 341-348.

[63] Slevin, M.; Krupinski, J.; Gaffney, J.; Matou, S.; West, D.; Delisser, H.; Savani, R. C.; Kumar, S. Hyaluronan-mediated angiogenesis in vascular disease: uncovering RHAMM and CD44 receptor signaling pathways. *Matrix Biol.* **2007**, *26*, 58-68.

[64] Fraser, J. R.; Laurent, T. C.; Laurent, U. B. Hyaluronan: its nature, distribution, functions and turnover. *J. Intern. Med.* **1997**, *242*, 27-33.

CHAPTER II
Review

Towards an understanding of the mechanisms underlying polymeric nanoparticle-mediated (trans)dermal drug delivery

Corinne Eenschooten[1,2], Fanny Guillaumie[1], Georgios M. Kontogeorgis[2], Khadija Schwach-Abdellaoui[1]

[1]Novozymes Biopolymer A/S, Krogshøjvej 36, 2880 Bagsværd, Denmark

[2]Technical University of Denmark, Department of Chemical and Biochemical Engineering, Centre for Phase Equilibria and Separation Processes (IVC-SEP), Building 229, 2800 Lyngby, Denmark

---

Abstract

Due to their unmatched properties, polymeric nanoparticles represent promising and versatile devices towards drug delivery. In the field of (trans)dermal drug delivery, they have been shown to enhance the percutaneous penetration and/or sustain the release within dermal layers of active ingredients. However, the mechanisms by which such feats are achieved are still not fully elucidated. Understanding the interactions between polymeric nanoparticles and the skin is nevertheless crucial in order to design suitable systems towards specific delivery scenari. This article reviews the current knowledge about the mechanisms underlying polymeric nanoparticle-mediated (trans)dermal drug delivery. It appraises some technical advances to assess skin penetration and examines the research gaps and future challenges of this research field.

Key words nanoparticle, skin penetration, drug release, confocal and multiphoton laser scanning microscopy, skin sandwich model, differential stripping, nanoparticle risk assessment

---

I. Introduction

Due to its large surface and significant advantages compared to the more conventional enteral and parenteral administration routes, the skin has been recognised as a valuable possible pathway for a variety of penetrants with heterogeneous properties. Indeed, drug administration to the skin presents some technical, patient-related and societal advantages such as the circumvention of the first pass metabolism, convenient and painless administration and overall reduction of health costs [1] (Table II.1).

Table II.1: Advantages of using the skin as a drug administration route (adapted from [1]).

Technical advantages	▪ Circumvention of the first pass metabolism
	▪ Direct access to superficial diseased sites
	▪ Sustained and controlled drug delivery over time
	▪ More efficient dose management ▪ Easier dose termination in case of dose adverse reactions
Patient-related advantages	▪ Convenient and painless drug administration
	▪ Better patient acceptance and compliance
	▪ Reduction of the side effects associated with systemic toxicity ▪ Minimisation of peaks and troughs in the blood drug concentration
Societal advantages	▪ Overall reduction of health costs ▪ Lesser need for trained personnel ▪ Dose reduction

Consequently, an important market has developed for (trans)dermal drug delivery which, according to some estimates, represented 1.57 billion dollars in the United States (US) in 2002 and will amount to nearly 5.67 billion dollars by 2009, *i.e.* approximately 6 % of the total US drug delivery market [2].

Dermal and transdermal drug delivery follow two different approaches. On the one hand, dermal drug delivery refers to the treatment of pathologies within the skin and requires concentrating drugs in the superficial skin layers. Transdermal drug delivery, on the other hand, is related to the treatment of diseases located in other organs than the skin and necessitates drugs' systemic absorption [1].

Due to its intrinsic structure, the skin and, in particular, the stratum corneum (SC) naturally acts as a protective barrier against exogenous matter and constitutes an obstacle for the transport of drugs within or through its layers. Strategies to circumvent this barrier and enhance the skin uptake of topically applied drug formulations can be classified in passive or active methods.

Passive strategies have involved the use of chemical enhancers [3], supersaturated formulations [4], prodrugs [5], metabolites [6] and particulate systems such as soft carriers [7] (for example, liposomes [8], ethosomes [9], niosomes [10], transferosomes [11]) and rigid carriers (for instance, solid lipid [12] and polymeric [13] nanoparticles).

Active strategies can be classified in electrical (electroporation [14]), mechanical (microneedle-assisted perforation [15]) and iontophoretic [16] methods. Sonophoresis [17], phonophoresis [18], thermophoresis and magnetophoresis [1] constitute additional active methods for enhancing the penetration of topically applied substances.

In some instances, passive and active methods have even been combined to yield a synergetic effect [19,20].

Although efficient, most active methods and some passive methods, such as those involving chemical enhancers, rely on altering the skin barrier function by either chemically or physically disrupting the SC organisation or mechanically by-passing the SC (perforation). This can induce irritation and possible irreversible damages to skin tissues. In addition, such methods are inefficient towards the protection of chemically unstable drugs and can alter their activity [21].
Passive methods based on particulate systems however represent non-invasive techniques which can enhance the penetration of topically applied drugs while minimizing the deterioration of the skin barrier function and preserving drug activity.

Among the currently available particulate systems towards (trans)dermal drug delivery, soft carriers and, in particular, liposomes, have been criticised for their poor stability, low encapsulation efficiency and rapid drug leakage [13]. In contrast to liposomes, polymeric nanoparticles would be more stable and offer a better control of the drug release [22]. Therefore, these currently constitute one of the most promising modern tools towards (trans)dermal drug delivery.

Polymeric nanoparticles are characterised by a mean diameter inferior to 1 µm and a matrix consisting of a natural or synthetic polymer or a combination of several of these. As anticipated, the choice of the polymer(s) is driven by qualities such as biocompatibility and biodegradability. Certain polymers present these features to various degrees, namely, poly(D,L-lactide), poly(lactic acid), poly(D,L-glycolide), poly(lactide-co-glycolide), poly(cyanoacrylate), poly(alkylcyanoacrylate), poly(ε-caprolactone), poly(methylidene malonate) [13] and polysaccharides such as chitosan, dextran, pectin, heparin, pullulan and sodium alginate.
Encapsulation in polymeric nanoparticles is usually achieved by dispersion in the polymer matrix (a), concentration in the nanoparticle core (b), chemical conjugation or physical adsorption on the surface of the nanoparticles (c) [23] (Figure II.1).

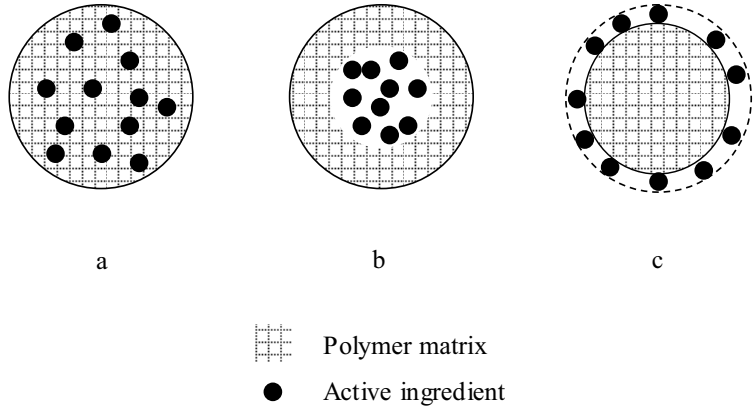

Figure II.1: Drug encapsulation in polymeric nanoparticles.

Some studies have shown that polymeric nanoparticles can noticeably enhance the topical delivery of, for example, chlorhexidine [24], octyl methoxycinnamate [25] and flufenamic acid [26]. However, the mechanisms of such achievements are still questioned.

In view of this, the objective of this article was to take stock of the current knowledge about the mechanisms underlying polymeric nanoparticle-mediated (trans)dermal drug delivery. First, new and improved methods for detecting skin penetration pathways are reviewed. Then, polymeric nanoparticle fate subsequent to topical administration is discussed based on the available experimental data. This discussion in particular addresses the current hypothesis with regards to how polymeric nanoparticles can enhance percutaneous penetration and/or sustain drug release within dermal skin layers. Finally, the research gaps and future challenges of the research field are examined.

II. Technical advances in assessing skin penetration pathways

II.1. Skin penetration pathways

The skin is composed of a dermis and an epidermis consisting of several morphologically distinct layers. These are, from the inside to the outside, the stratum basale, stratum spinosum, stratum granulosum and stratum corneum. The first three layers constitute the viable epidermis which is a dynamic and constantly self-renewing tissue. Cells proliferate in the basal layer and differentiate while migrating towards the surface of the skin. At the interface between the stratum granulosum and SC, they undergo a major terminal differentiation and are transformed into flattened, dead and keratin-filled cells without nuclei (corneocytes). In the SC, the ultimately differentiated corneocytes are covered by a densely cross-linked protein layer, the cell envelope, and are embedded in lipid lamellar regions parallelly oriented to the corneocyte surface. This results in a densely packed structure [27].
Hair follicles and the sweat apparatus are important skin structures resulting from epidermal invaginations and which present orifices at the surface of the skin.

Considering the general anatomy of the skin (Figure II.2), three penetration pathways potentially contribute to the transport of exogenous matter from the surface of the skin into epidermal or dermal layers. These consist of the intercellular space between corneocytes and of the two skin appendages mentioned above namely, hair follicles and sweat ducts.
Historically, the intercellular path has first and foremost been considered the main skin penetration route and is by far the most studied and discussed pathway for the infusion of a variety of chemical substances [28].

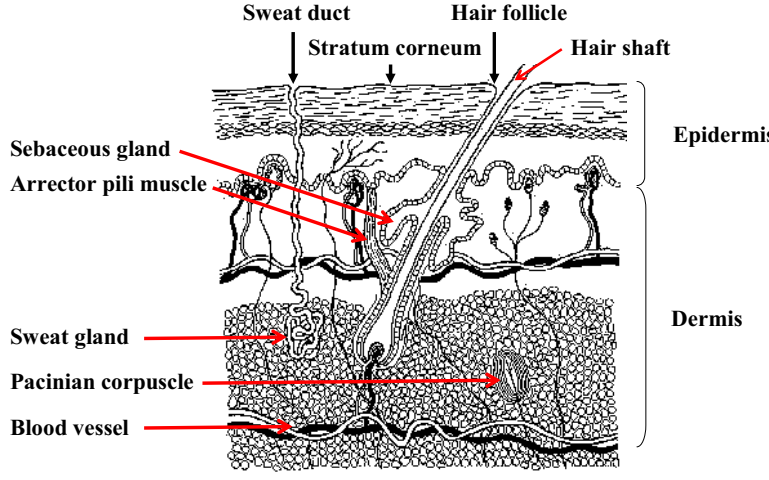

Figure II.2: Structure of mammalian skin and possible skin penetration pathways (adapted from [29]).

The black arrows point to the potential skin penetration pathways.

It is usually agreed that the barrier function of the skin is primarily provided by the SC. Due to the rather impermeable character of the cornified envelope around the corneocytes, substances entering the skin through this pathway are believed to penetrate along the tortuous intercellular space [27] (Figure II.3).

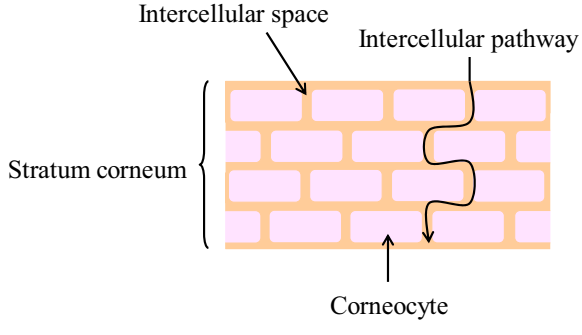

Figure II.3: Penetration through the intercellular space between corneocytes.

Although skin appendage orifices only represent a small fraction of the total surface of the skin, hair follicles and sweat ducts constitute possible additional skin penetration pathways.
An interest for drug delivery via hair follicles has existed for several decades [30-33] and recent reviews have addressed the potential of using this pathway for therapeutic purposes [34,35,36]. It is usually agreed, that the advantages of follicular delivery lie in the possibility to more directly access deep compartments of the skin and in the large and long-term storage capacity of the hair follicle reservoir [37] which has been estimated equal to that of the SC [38]. Interestingly, the follicular pathway is currently considered to play a significant role in particulate drug delivery [33,39].

In contrast to hair follicles, sweat ducts have been a relatively poorly studied system and attempts to elucidate their role in skin penetration processes remain sparse and at an early stage of investigation. Wilke *et al*. [40] have addressed the question of the sweat duct barrier function by studying the distribution of tight junction proteins such as occludin, claudin 1 and claudin 4 throughout the eccrine and apocrine apparatuses. They showed that the sweat duct barrier function was a non-homogeneous property throughout these two structures. Whereas the co-localisation of occludin and claudin 4 in sweat glands and dermal sweat ducts was considered to provide tight junctions (*i.e.* a good barrier function), the sole presence of occludin in intra-epidermal sweat ducts was recognised as being a sign of looser junctions (*i.e.* a reduced barrier function). The authors therefore speculated that the intra-epidermal region of sweat ducts could serve as an alternative penetration pathway. Although an important finding, this theory necessitates further confirmation by specific and quantitative penetration studies through sweat ducts. Some qualitative studies have been reported on this subject [41,42] with only a few examples of positive penetration [42].

For an extensive insight into the various skin penetration routes, the reader is invited to consult the excellent book chapter by Schaefer and Redelmeier [43].

The existence of the three (potential) skin penetration pathways implies that chemical substances and formulated systems may penetrate through the skin by following different paths. However, in order to understand the penetration process(es) of a given system, a deconvolution of its parallel fluxes is necessary in order to reason out the main entry route for this system.
Whereas microscopic imaging can provide a qualitative picture of penetration routes into and through the skin, selective diffusion experiments or diffusion experiments followed by selective extractions offer the possibility to quantify the amount of penetrated matter into the various compartments of the skin and establish a hierarchy between the different penetration routes observed by microscopy.

II.2. Microscopic imaging

Advances in microscopic imaging have crystallised into modern laser scanning microscopy (LSM) with two major variations, namely confocal and multiphoton laser scanning microscopy (CLSM and MPLSM).
In LSM, the sample is illuminated by a beam of laser light focused into a point at the focal plane. This beam can be scanned in the X, Y and Z directions by a computer-controlled scanning mirror. The fluorescence emission created at the successively scanned points is detected by a photon multiplier tube. This information is processed by computer hardware into an image. Spatial scanning of the sample allows reconstructing 3-dimension (3D) images [44].

II.2.1. Confocal laser scanning microscopy

In CLSM, gas lasers are used as the illumination source. Since illumination of the focal plane is inherently accompanied by the creation of out-of-focus fluorescence above and below the focal plane, a pin hole is placed between the specimen and the photon multiplier tube to avoid blurring of the final images. This pin hole

discriminates out-of-focus information so that the focal plane of illumination and detection are confounded or *confocal*. Sharp images of the specimen can thus be derived [44].

II.2.2. Multiphoton laser scanning microscopy

MPLSM uses solid state lasers as the illumination source. These lasers have the particularity to generate photons in pulses and light characterised by a longer wavelength than in CLSM. Due to technical considerations that are beyond the scope of this review, the region of the specimen excited by MPLSM is much more confined than that by CLSM. As a consequence, minimum or no out-of-focus fluorescence is generated in this mode and all the information arising from the focal plane directly reaches the photon multiplier tube without the need for a pin hole [44].

CLSM and MPLSM present decisive advantages over other more conventional microscopy techniques such as light microscopy, transmission electron microscopy:
(i) the endogenous fluorescence of the skin allows achieving images on which the structural details of this tissue can clearly be identified,
(ii) mechanical sectioning is no longer necessary which allows circumventing artefacts related to sample fixation and traditional histological investigations,
(iii) samples are non-invasively studied and high-resolution 3D images can be derived [45].

However, some technical differences between CLSM and MPLSM give further advantages to MPLSM which is more sensitive than CLSM because all the information generated at the focal plane directly reaches the detector. Besides, the longer wavelength light used in MPLSM is less damaging to samples though more penetrating than the shorter wavelength light used in CLSM [44].

For further technical information on CLSM and MPLSM, the reader is invited to consult the reviews by Oheim *et al*. [46] and Diaspro *et al*. [47], respectively.

CLSM and MPLSM have allowed significant improvements in the observation and understanding of biological phenomena and have recently been used, as will be shown in part II, for the qualitative deconvolution of polymeric nanoparticle skin penetration pathways.
The quantitative assessment of the different skin penetration pathways constitutes the second aspect in understanding the fate of topically applied formulations. Advances in this field are the subject of the following paragraph.

II.3. Skin penetration quantification

In the past, the distinction between SC and follicular penetration has been tackled by comparing penetration fluxes through skin containing follicles and skin devoid of these. However, interpretation of the results generated using such an approach is problematic as hairless and hairy skins can exhibit different barrier functions due to their structural and biochemical differences.
Innovative approaches were recently proposed to circumvent this problem and allow to distinguish between SC and appendageal penetration. These are the skin sandwich model and differential stripping.

II.3.1. The skin sandwich model

The skin sandwich model is a composite skin system composed of a stack of a human whole epidermis (nucleated epidermis and SC) and of an additional SC membrane sampled from the same donor. As skin appendage orifices only represent 0.1 % of the total skin surface [38], little chance exists that the shunts of the two different skin components superimpose. Therefore, in this composite skin tissue, the

appendages of both the superficial SC and the underneath whole epidermis are mechanically blocked for penetration (Figure II.4).

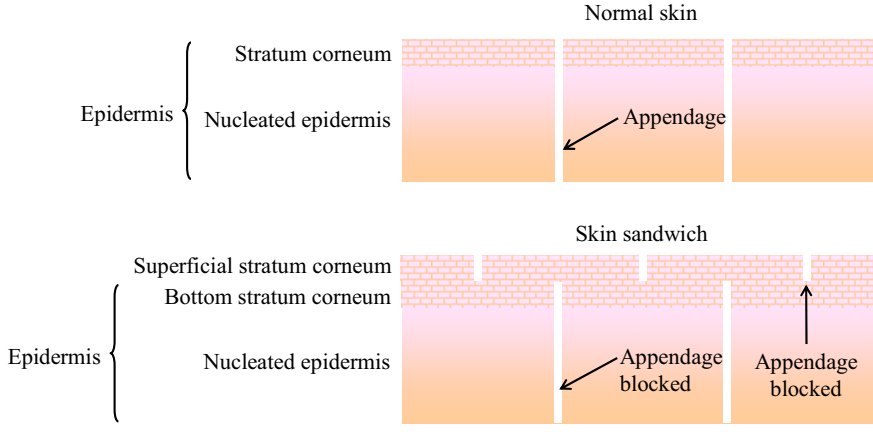

Figure II.4: Schematic representation of the skin sandwich model (adapted from [48]).

A comparison of the penetration fluxes through normal skin and the skin sandwich can be used to isolate the contribution of the appendageal pathway in penetration processes. Indeed, if appendages represent an important pathway for a given system, its flux through the skin sandwich should be much reduced compared to that through normal skin.

The skin sandwich model was first developed by El Maghraby *et al*. [49] to evaluate the importance of the appendageal pathway in the delivery of estradiol from various liposomes in human skin. The authors observed that the permeation of the drug through the skin sandwich was somewhat reduced compared to that through normal skin and that this tendency was independent on the liposomal system employed (ultradeformable or traditional liposomes). However, this reduced drug permeation flux was close to the expected theoretical flux arising from the thicker barrier provided by the skin sandwich. The latter, composed of a stack of two SC layers was indeed

twice as thick as the barrier provided by normal skin. The authors therefore excluded the appendageal pathway as the main penetration route for the delivery of estradiol from liposomes in human skin.

Barry [48] later systematically evaluated the performances of the skin sandwich model using various model compounds such as estradiol (lipophilic), mannitol (hydrophilic) and L-glutamic acid (negatively charged) administered by iontophoresis. A repeated consistency between the theoretical and experimental behaviours of these compounds confirmed the accuracy and validity of the skin sandwich model. For instance, due to its negative charge, L-glutamic acid was expected to follow the path of least resistance and to penetrate through damaged regions of the skin and skin appendages. In addition, the creation of artificial pores due to the temporary disruption of the intercellular lipids was expected to contribute to the enhancement of its transport. Experimentally, the flux ratio between sandwiched skin and normal skin was close to zero for L-glutamic acid which confirmed that the appendageal pathway dominated the iontophoretic transport of L-glutamic acid. However, when electroporation was used the flux ratio did not fall to zero evidencing that the electrical pulses created transient aqueous pores in the intercellular lipids through which L-glutamic acid was transported across sandwiched skin.

The identical source between the skin sandwich and normal skin and the mechanical shunt obstruction without exogenous material circumvent interpretational difficulties related to the different barrier functions of hairless and hairy skins. In addition, Barry [48] demonstrated using the Monte Carlo approach that results remained consistent even in the case of slightly imperfect adherence between the two different skin components in the skin sandwich. Interestingly, the author emphasised that the skin sandwich model could potentially be used to deconvolute the penetration pathways of colloidal particles.

II.3.2. Differential stripping

Differential stripping is based on the combination of two existing techniques namely, tape stripping and the cyanoacrylate follicular biopsy.
On the one hand, tape stripping is a frequently used method to investigate the penetration of topically applied substances into the skin [50]. After applying a formulation onto the skin, several successive skin layers are removed with adhesive films. Each skin strip contains corneocytes and variable amounts of the topically applied system which can further be extracted by adequate techniques. The correlation between the amount of extracted substance from each individual strip and the strip number allows tracking the penetration profile of a given system.
On the other hand, the cyanoacrylate follicular biopsy uses a quick-setting polymer to extract the infundibular content of pilosebaceous units [51]. This technique is useful for studying the contents of follicles and can be employed for analysing the penetration of topically applied compounds or formulations through hair follicles.

Teichmann *et al*. [52] were the first to combine the two above described techniques to selectively and non-invasively study the penetration of topically applied substances into the SC and follicular structures. This method called *differential stripping* uses tape stripping to first collect the amount of topically applied substances penetrated into the SC and the cyanoacrylate follicular biopsy to secondly collect the amount penetrated into follicular structures.
By using these two successive stripping techniques, the authors determined the amount of sodium fluorescein penetrated *in vivo* in the SC and hair follicles of human back skin. After 30 min, 54 % ± 8.1 % of the dye was recovered of which 95 % ± 14 % in the SC and 5 % ± 0.9 % in the follicular infundibula. After 24 and 48 hours, sodium fluorescein was still detected in follicular structures although the concentration of the dye decreased over time.

Differential tape stripping therefore constitutes a novel method to selectively study skin penetration pathways. It gives a number of opportunities for the study of the pharmacokinetics of topically applied substances and more generally for research in the field of dermatology.

The use of CLSM and MPLSM and/or selective extraction techniques has allowed new insights into the mechanisms underlying polymeric nanoparticle-mediated drug delivery which are reviewed hereafter.

III. Mechanisms underlying polymeric nanoparticle-mediated drug delivery

III.1. Redistribution and accumulation of polymeric nanoparticles in the skin

As shown in Table II.2, the redistribution of topically applied polymeric nanoparticles on the surface of the skin has been shown to occur towards the (i) skin's superficial reliefs [26,53,54], (ii) hair follicles [55,56,57], (iii) intercellular space in the SC and (iv) subepidermal skin tissues [58].

In studies [53] and [54], for which the nanoparticles were founds in the skin furrows/dermatoglyphs, optical cross-sections of non-follicular skin regions further showed that the nanoparticle distribution was only superficial. This suggested that skin furrows/dermatoglyphs were not penetration pathways for the nanoparticles.

Studies [55] to [57] reported that hair follicles constituted a significant penetration pathway for nanoparticles with a diameter between 40 and 320 nm.

However, polymer-coated intrinsically fluorescent quantum dots with hydrodynamic diameters between 14 and 45 nm were localised in the SC and in the skin subepidermal layers [58]. This shows that the intercellular space constitute another penetration pathway for nanoparticles with small diameters.

Table II.2: Redistribution of topically applied polymeric nanoparticles on the surface of the skin.

NP stands for nanoparticle.

Reference	NP type/encapsulated substance/size	Administration and detection conditions	Results
[26]	Poly(lactide-co-glycolide)/flufenamic acid/330 nm	▪ 30-min incubation with human skin *in vitro* ▪ MPLSM imaging	▪ Uniform NP distribution on the surface of the skin and within the skin dermatoglyphs ▪ No NPs found between or within corneocytes
[53]	Carboxylate-modified FluoSpheres® (fluorescent polystyrene)/fluorescein-5-isothiocyanate/20 or 200 nm	▪ 30-, 60- or 120-min incubation with porcine skin *in vitro* ▪ CLSM imaging	▪ Time dependent NP accumulation around the follicular openings and in the furrows of the skin ▪ The longer the incubation time, the higher the detected fluorescence
[54]	5-fluoresceinamine-covalently-labelled poly(lactide-co-glycolide)/Texas Red/300 nm	▪ 5-hour incubation with human skin *in vitro* ▪ MPLSM imaging	▪ NP location in the skin dermatoglyphs
[55]	▪ Poly(ε-caprolactone)-block-poly(ethylene glycol)/rubrene/40 or 130 nm	▪ 12-hour incubation with guinea pig skin *in vivo* ▪ CLSM imaging of biopsied guinea pig skin	▪ NP accumulation in hair follicles and their surrounding tissues
[56]	▪ FluoSpheres® (fluorescent polystyrene/40 nm	▪ 15 to 16-hour incubation with human skin *in vitro* ▪ CLSM imaging of follicular cryosections of cyanacrylate stripped human skin	▪ Presence in hair follicles down to a depth of 225±34 µm (corresponding to the occurrence of sebaceous glands)

Table II.2: Redistribution of topically applied polymeric nanoparticles on the surface of the skin (continued).

[57]	▪ Resomer®/5-fluoresceinamine/320 nm	▪ 1-hour incubation with porcine skin *in vitro* LSM imaging of physical skin cross-sections	▪ Penetration along hair follicles down to a depth of 1500 µm when the nanoparticles were massaged on the surface of the skin
[58]	Polymer-coated intrinsically fluorescent quantum dots/14-45 nm	▪ 8 or 24-hour incubation with porcine skin *in vitro* ▪ CLSM imaging	▪ NP penetration and localisation in the SC and subepidermal layers

In summary, according to the recent studies focusing on understanding the fate of topically applied nanoparticles, these can superficially redistribute to skin reliefs such as the skin furrows/dermatoglyphs and follicular openings. They can also penetrate along hair follicles down to macroscopic depths or through the intercellular space down to subepidermal layers. This last finding by Ryman-Rasmussen *et al*. [58] is unusual and in apparent contradiction with the results of Alvarez-Roman *et al*. [53], Shim *et al*. [55] and Vogt *et al*. [56]. However, it is not the only one of its kind since Menzel *et al*. [59] demonstrated using an ion beam analysis that lanceolate metal (titanium oxide) nanoparticles (45- to 150-nm long, 17- to -35-nm wide) penetrated porcine skin from the SC to the stratum granulosum through the intercellular space between corneocytes after an 8 hour incubation of the nanoparticles *in vivo*.

Considering the similarity in size of 20- [53] and 40-nm [55,56] polystyrene nanoparticles on the one hand and 14- to 45-nm [58] polymer-coated quantum dots on the other hand and their different penetration profiles, polymeric nanoparticle skin penetration seems a more complex phenomenon than one just dependant on the size of the nanoparticles. Some possible mechanisms of their transport into the skin are presented in the following paragraph.

III.2. Possible mechanisms underlying polymeric nanoparticle skin penetration

Logically, it can be conceived that the dimensions of the penetration pathway is a major factor for the selective diffusion of polymeric nanoparticles.

Penetration though the SC can therefore be imagined to require that the nanoparticle size complies with the narrow dimensions of the intercellular space between corneocytes. Bouwstra *et al*. [60] described the structure of the intercellular lipids as a stack of lamellae with characteristic periodicities of 6.4 and 13.4 nm [61] (the average thickness of the intercellular space is about 100 nm). Nanoparticles presenting at least one dimension within the order of magnitude of that of the periodic phases can hypothetically penetrate through the intercellular space [58].

Penetration of larger particles may also be possible when the lipid organisation is disrupted such as in the case of high tissue hydration [62,63] and certain skin diseases [64].
In addition, the physicochemical properties of the nanoparticles can also be accountable for the penetration through the intercellular space of larger particles. For example, the poor solubility of the polymer matrix in the intercellular lipids can cause a decrease in the apparent hydrodynamic diameter of the nanoparticles facilitating their penetration through the intercellular space [58].

Nanoparticle penetration along hair follicles however seems to be less restricted than through the intercellular space due to larger dimensions of follicular infundibula [65,66]. Ossadnik *et al*. [57] explained that nanoparticle penetration along hair follicles might occur owing to a pumping effect by hair shafts caused by hair tilting. Indeed, the cuticles arising from keratinocyte desquamation form a structured surface, which can be assimilated to a zigzag relief. The latter is determined by the thickness of the keratin cells which is between 500 and 800 nm. With the continuous movement of hair, the cuticle cells may act as a geared pump and push particles down to the hair infundibulum. According to Ossadnik *et al*. [57], the structural characteristics of follicular infundibula imply that the optimum nanoparticle size for penetration along hair follicles is below 700 nm.

Based on these general mechanisms, the study of the influence of characteristics such as the nanoparticle size, surface charge and shape can further give valuable insight in explaining the mechanism of their skin penetration.

III.2.1. Influence of nanoparticle size

Shim *et al*. [55] correlated the efficiency of mixnoxidil permeation through hairy guinea pig skin to the size of the poly(ε-caprolactone)-block-poly(ethylene glycol) nanoparticles. They found that the *in vitro* permeation of mixnoxidil encapsulated in 40-nm nanoparticles was 1.7-fold higher than that of mixnoxidil encapsulated in 130-nm nanoparticles after 18 hours. Interestingly, no significant influence of the size of the nanoparticles on the permeation of mixnoxidil could be evidenced in hairless guinea pig skin. Moreover, mixnoxidil permeation was substantially lower in hairless than in hairy guinea pig skin.

Alvarez-Roman *et al*. [53] observed that 20-nm fluorescent polystyrene nanoparticles (carboxylate-modified FluoSpheres®) redistributed more rapidly and selectively to the follicular openings of porcine skin *in vitro* than the 200-nm nanoparticles after 120 min. This phenomenon was attributed to the higher specific surface area developed by the smaller nanoparticles.

Vogt *et al*. [56] detected 40-nm polystyrene nanoparticles (FluoSpheres®) in follicular CD1a+ cells in cyanoacrylate stripped human skin after 15 to 16 hours *in vitro*. By contrast, the 750- and 1,500-nm nanoparticles (Fluoresbrite^{TM}) were not detected in these cells. CLSM imaging of follicular cryosections evidenced the penetration of the 40-nm nanoparticles along hair follicles down to a maximum depth of 225 ± 34 µm whereas the larger nanoparticles (750 and 1,500 nm) remained in the uppermost part of the follicles.

Ryman-Rasmussen *et al.* [58] however demonstrated a rather size-independent penetration of differently sized (hydrodynamic diameters between 14 and 45 nm) and coated (poly(ethylene glycol), carboxylic acids and poly(ethylene glycol

amine)) spherical quantum dots in porcine skin. All nanoparticle types penetrated down epidermal or dermal skin layers after 8 hour *in vitro*.

These results suggest that the size of the nanoparticles is an important factor of the penetration kinetics [53,55] and pathway. Nanoparticles presenting dimensions incompatible with that of the penetration pathway are retained superficially [56] while those presenting dimensions under several tens of nanometres penetrate the SC through the intercellular space between corneocytes [58]. Larger nanoparticles but which diameters do not exceed 700 nm preferentially follow the follicular pathway [53,55,56]. Within this size range, differences in nanoparticle size result in differences in penetration velocity and extent: the smaller the nanoparticles, the faster and deeper their transport in the follicles.

III.2.2. Influence of nanoparticle surface charge

Ryman-Rasmussen *et al*. [58] observed a charge-independent penetration of spherical quantum dots and a charge-dependent penetration of ellipsoid quantum dots in porcine skin. Whether coated with neutral poly(ethylene glycol) (PEG), anionic carboxylic acids (CA) or cationic poly(ethylene glycol amine) (PEG-amine), similarly sized spherical quantum dots penetrated epidermal (PEG and CA) and dermal (PEG-amine) skin layers after 8 hours *in vitro*. However, only PEG and PEG-amine coated ellipsoid quantum dots penetrated epidermal skin layers after 8 hours whereas CA ellipsoid quantum dots only penetrated epidermal skin layers after 24 hours. This suggested that the negatively charged ellipsoid quantum dots were more retained in the intercellular space than the neutral and positively charged ellipsoid quantum dots.

Kohli and Alpar [67] however evidenced the *in vitro* penetration and accumulation in porcine SC and viable epidermis of negatively charged fluorescent latex nanoparticles (diameters 50 and 500 nm) after 6 hours. Although unable to fully

explain the mechanism by which these nanoparticles penetrated the in the SC, the authors speculated that the repulsive forces between the negatively charged nanoparticles and skin lipids might have resulted in the formation of temporary channels through which the 50- and 500-nm nanoparticles could be transported.

The scarcity of specific studies on the influence of nanoparticle surface charge on their skin penetration makes it a difficult task to draw general conclusions about this phenomenon. The negative charge of the lipid bilayers in the intercellular space should logically favour the transport of positively charged species. However, the study by Kohli and Alpar [67] is in apparent contradiction with this hypothesis. Further investigation of this topic will be necessary to understand the electrokinetic interactions between polymeric nanoparticles and skin tissues.

III.2.3. Influence of nanoparticle shape

Ryman-Rasmussen *et al*. [58] observed that PEG-amine-coated spherical quantum dots penetrated down to dermal skin layers whereas similarly coated ellipsoid quantum dots only penetrated down to epidermal skin layers in porcine skin after 8 hours *in vitro*. CA-coated spherical quantum dots penetrated and accumulated in the epidermis faster (after 8 hours) than similarly coated ellipsoid quantum dots (after 24 hours). As the difference in hydrodynamic diameter between these spherical and ellipsoid quantum dots was minor (less than 5 nm) the variation in their penetration depths/times was attributed to their shape. The more homogenously shaped spherical quantum dots penetrated in deeper skin layers than their heterogeneously shaped ellipsoid analogues.
These results suggest that the more homogeneous the shape of the nanoparticles the easier their penetration into the intercellular space.

With a better knowledge of the fate of topically applied nanoparticle and of the mechanisms underlying their penetration, it is now possible to formulate hypothesis with regards to how these enhance and/or sustain drug release.

III.3. Hypothesis with regards to how polymeric nanoparticles enhance percutaneous penetration and/or sustain drug release

In most of the cases, due to the relatively large dimensions of most of the currently available polymeric nanoparticles (> 40 nm), enhancement of the percutaneous penetration and/or sustained release of encapsulated substances through non-follicular regions of the skin cannot be attributed to the co-penetration of the carrier and the encapsulated substance through skin tissues.

For example, Luengo *et al*. [26] observed an increase in the flufenamic acid *in vitro* transport through human abdominal skin when the drug was encapsulated in poly(lactide-co-glycolide) (PLGA) nanoparticles compared to that of the free drug after 12 hours. However, the PLGA nanoparticles remained homogeneously distributed on the surface of the skin and within skin dermatoglyphs and no nanoparticles were detected within or between corneocytes.

Stracke *et al*. [54] followed the release, accumulation and penetration of Texas Red-containing PLGA nanoparticles by MPLSM. Multi fluorescence labelling of this system enable the authors to follow the fate of both the nanoparticles and the encapsulated compound. The Texas Red concentration profiles over time in various skin compartment acquired by multiphoton spectral imaging showed that Texas Red started to be absorbed by the SC immediately after topical application. This suggested that release from the nanoparticle had probably already begun before the penetration experiment within the hydrogel used for the formulation.

Alvarez-Roman *et al*. [53] have put forward that the penetration improvement achieved by using nanoparticles is due to an efficient liberation of the encapsulated substance into the SC.

Certain interactions between polymeric nanoparticles and the surface of the skin can explain the sustained release of the encapsulated substances.

For example, Olvera-Martinez *et al*. [68] observed lower penetrated amounts of the sunscreen octyl methoxycinnamate into human skin *in vivo* from cellulose acetate phthalate nanocapsules (diameter 460 nm) than from a conventional oil-in-water emulsion or a nanoemulsion prepared with the non-ionic emulsifying agent poly(vinyl alcohol). The authors suggested that the slower and more superficial release achieved by the nanocapsules was probably due to the formation of a nanoparticle superficial depot from which the sunscreen was progressively infused to the outermost layers of the skin.

Lboutounne *et al*. [24] showed that chlorhexidine-loaded poly(ε-caprolactone) nanoparticles partially wetted porcine skin. The contact angle determined by scanning electron microscopy and surface tension for these nanoparticles were 124 degrees and 147 dyn/cm, respectively. The authors argued that this partial wetting was responsible for the sustained release, enhanced concentration within SC and reduced percutaneous absorption of chlorhexidine. Indeed, the sufficient flexibility of the nanoparticles allowed their adherence to the skin and their sufficient rigidity permitted avoiding rapid drug diffusion [69].

Other studies have shown that nanoparticles could penetrate through hair follicles [37,53,55,56] and could be stored in the follicular structures of human claves for up to 10 days [39]. However the different authors admit that the release mechanisms in such conditions remain unclear.

Finally, nanoparticle penetration through non-follicular skin structures could be a possible mechanism to explain the penetration enhancement of encapsulated substances [58]. However, to the best of our knowledge, very few studies using microscopic imaging have specifically demonstrated this phenomenon.

Although recent advances have been achieved in the understanding of polymeric nanoparticles-mediated (trans)dermal drug delivery, this research field remains fraught with both scientific and regulatory challenges. These are examined hereafter.

IV. Future challenges in polymeric nanoparticle-mediated (trans)dermal drug delivery

IV.1. Nanoparticle design

Polymeric nanoparticles possessing a high drug loading capacity and which can target diseased body sites, be triggered at the right moment and sustain drug release for an appropriate period of time, represent the *Holy Grail* of (trans)dermal drug delivery.

However, drug loading in polymeric nanoparticles is limited by their size. It can therefore be expected that the improved skin penetration of small nanoparticles will be at the expense of the amount of encapsulated drug. For this reason, an optimal balance will have to be found for each given application between the desired extent of penetration (partly determined by the size of the nanoparticles) and the dose required to achieve a therapeutic effect.

Nanoparticle targeting, triggering and sustained drug release represent other major challenges of polymeric nanoparticle design.

Nanoparticle targeting is probably the most complex feature to achieve. It requires the modification of the nanoparticle surface in order to avoid non-specific interactions with cells and proteins and drug accumulation in non-target tissues [70].

Barry [21] commented that (trans)dermal drug delivery would be optimal if it could be coordinated with a continuous diagnosis of the actual physiological condition of each specific patient. Drugs could thus be delivered only when required and for the time

needed. The release of encapsulated substances from topically applied nanoparticles is however currently more often undergone than controlled. Studies on this subject have been limited to the observation of the fate of nanoparticulate systems when administered on the skin. Controlled triggering is not yet an achieved feature of polymeric nanoparticles. It will require the development of advanced devices able to respond to external stimuli. For dermal applications, these stimuli could consist in light illumination or the delayed application of a kick-off agent able to induce a therapeutic cascade effect [54].

Optimisation and conjugation of the above-described complex aspects of polymeric nanoparticle design are necessary to create "smart" nanoparticles. To appreciate the performances of these advanced devices, it will be necessary to overcome some of the remaining technical limitations in their detection for an accurate assessment of their *in situ* behaviour.

IV.2. Nanoparticle performance assessment

IV.2.1. Fate

In the past, encapsulation of a fluorescent label into polymeric nanoparticles was usually used to follow their fate by fluorescence microscopy. However, this approach only truly allows monitoring the fate of the label and not specifically that of the whole system. Indeed, it can difficult to control the diffusion of the label outside the nanoparticles during the experiment.
Alvarez-Roman *et al*. [53] circumvented this issue by covalently binding fluorescein 5-isothiocyanate (FITC) to non-biodegradable polystyrene nanoparticles before following their fate in porcine skin. The covalent binding of the label to the nanoparticles and nanoparticle non-biodegradability ensured that the fluorescence

detected for FITC could unambiguously be attributed to the presence of intact polystyrene nanoparticles.
Similarly, Stracke *et al*. [54] used a dually labelled system consisting of 5-fluoresceinamine-bound PLGA nanoparticles and encapsulated Texas Red.

In summary, intrinsic fluorescence or in the absence of thereof, covalent fluorescence labelling of the nanoparticles combined with fluorescence (labelling) of the encapsulated substance are means to ensure selective monitoring in skin tissues. Non-biodegradability of the nanoparticles is a further guarantee that these will be identified as integral structures.

IV.2.2. Skin penetration

The methods currently available for evaluating polymeric nanoparticle skin penetration still entail artefacts related to the nature of the analytical technique chosen. The lack of skin vasculature in *in vitro* penetration/permeation experiments, possible modification of the skin lipid organisation and redistribution of the penetrants while handling the samples, are aspects which can affect the veracity of the experimental results.
However, systematic *in vivo* assessments in animals or humans involving biopsies represent invasive methods. Future analytical techniques will therefore have to focus on the development of systems mimicking or approaching actual *in vivo* conditions and analytical tools involving minimal disturbance of these systems.
For skin visualisation, Stracke *et al*. [54] emphasise that samples should ideally be visualised *in vivo*, without fixation, non-invasively, on the same sample of human skin examined at different time in order to avoid the problem of sample variability in time-dependent penetration studies.

The accurate assessment of polymeric nanoparticle penetration is essential to measure the benefits but also the risks of such systems. Risk assessment will in the future be a crucial step towards using polymeric nanoparticles for actual therapeutic applications.

IV.3. Nanoparticle risk assessment

Due to their unique properties, polymeric nanoparticles are expected in the near future to dramatically improve humans' quality of life. However, unequalled features such as their size, specific area and surface properties make them potential triggering agents of reactions at the cellular levels that are currently unknown. As with many emerging and promising research fields there is a risk that the development of nanoparticle technologies overtakes investigations to assess their health and environment entailments.

To date only little formal research exist on the health and environmental impact of nanoparticles and scientific reviews with only a few exceptions [71] mainly addressed the risk assessment of airborne nanoparticles [72,73,74]. Morgan [75] recently underlined that due to the scarcity of scientific data on nanoparticle risk assessment, scientific and regulatory workers have the opportunity to address this question strategically by driving research to selected crucial areas for the understanding of the risk involved in each given nanoparticle applications. Therefore, general screening strategies have been proposed [75,76].

The working group of Oberdorster *et al.* [76] proposed a general data gathering strategy for the hazard identification of engineered nanomaterials for the oral, dermal, inhalation and injection routes. The three key element of this strategy are physicochemical characterisation, *in vitro* (cellular and non-cellular) and *in vivo* assays.

Nanomaterial physico-chemical characterisation is indeed essential if experimental data are to be interpreted in relation with the material properties and should encompass particle size distribution, agglomeration state, shape, crystal structure, chemical composition surface area, surface chemistry, surface charge and porosity. Nanomaterial characterisation after administration *in vitro* or *in vivo* is considered ideal although it currently presents significant analytical challenges. Alternatively, characterisation of the material as administered can provide valuable information.
Although there exists some well-documented issues with *in vitro* tests, these are considered important adjuncts to *in vivo* studies since they allow specific pathways to be isolated and tested under controlled conditions which is not feasible *in vivo*. Non-cellular *in vitro* tests can provide information about nanomaterial biopersistence, free radical generation, interaction with proteins and activation of humoral systems.
In vivo tests constitute a crucial step in nanomaterial risk assessment since they provide an evaluation of the systems' performances *in situ*. However, these are currently limited by research gaps in the design of viable *in vivo* detection techniques and in the development of standardized and well characterized nanomaterial samples.
Oberdorster *et al.* [76] further provide recommendations with regards to how these three key fields can be investigated. Their work is a major contribution to the emerging nanomaterial risk assessment.

Morgan [75] also proposed a preliminary and general framework for nanomaterial hazard identification in the form of an *influence diagram*. The latter was developed based on expert elicitation and describes the presumed variables, their inter-connexions and influence on the *uptake*, *transport, fate*, and *toxicity* of nanoparticles, four properties considered as closely related human health and ecological risk. The purpose of the expert elicitation was to collect and organise the knowledge of experienced people working with various aspects of nanoparticle technology in order to create a valuable tool for the systematic identification and prioritisation of crucial research areas.

For the (trans)dermal use of nanoparticles, the influence diagram spots nanoparticle size distribution, surface reactivity, shape and potential binding to a matrix as the main properties affecting nanoparticle *uptake* by the skin. It anticipates that nanoparticle size distribution, surface reactivity and coating (including added molecular groups), adsorption tendency and durability are likely to influence nanoparticle *transport and fate*. Finally nanoparticle size distribution, surface reactivity and coating, adsorption tendency and chemical composition are expected to impact nanoparticle *toxicity*.
The advantages of Morgan's approach lie in its capacity to incorporate new knowledge as it is generated and to remain in the long run a relevant tool for nanoparticle risk assessment.

V. Conclusion

The purpose of this article was to review the current knowledge about the mechanisms underlying polymeric nanoparticle-mediated (trans)dermal drug delivery, spot out research gaps and outline the challenges faced by this scientific field.

From the data available today, it appears that topically applied polymeric nanoparticles on the skin redistribute towards its superficial reliefs or penetrate along hair follicles or through the intercellular space. The penetration pathways followed by the particles certainly depend on a variety of properties such as nanoparticle shape, surface composition and charge but a number of studies have reported that nanoparticle size is probably the most determining factor. However, it is difficult to draw general rules due to the behavioural variability of nanoparticles presenting similar properties.

Although the mechanisms by which nanoparticles enhance and/or sustain drug release within the skin still remain partially questioned, there are some indications that the formation of a nanoparticle depot at the surface of the skin or in the hair follicles

from which drugs are efficiently released may be involved. Release in the intercellular space has not yet been unequivocally evidenced but is a priori not to be excluded.

Many past studies have followed the fate of fluorescent encapsulated substances in the nanoparticles. This does not allow understanding release mechanisms and more recent studies have underlined the need for labelling each of the individual components of a given nanoparticulate system and performing selective penetration studies (skin sandwich model, differential stripping).

Scientific limitations are mainly related to research gaps in the development of standardized and well characterized nanomaterial samples and in the design of viable *in vivo* non-invasive detection techniques. Nanoparticle targeting and release triggering will also represent major technical challenges.
The future of polymeric nanoparticles-mediated (trans)dermal drug delivery will rely on how well our present and next generations of researchers will take up these challenges and coordinate interdisciplinary collaborations for the improvement of patient condition worldwide.

References

[1] Brown, M. B.; Martin, G. P.; Jones, S. A.; Akomeah, F. K. Dermal and transdermal drug delivery systems: current and future prospects. *Drug Deliv.* **2006**, *13*, 175-187.

[2] Frost & Sullivan. U.S. emerging transdermal drug delivery technologies markets. Business report from 2003 available at http://www.frost.com/prod/servlet/frost-home.pag.

[3] Trommer, H.; Neubert, R. H. H. Overcoming the stratum corneum: the modulation of skin penetration. *Skin Pharmacol. Physiol.* **2006**, *19*, 106-121.

[4] Moser, K.; Kriwet, K.; Naik, A.; Kalia, Y. N.; Guy, R. H. Passive skin penetration enhancement and its quantification in vitro. *Eur. J. Pharm. Biopharm.* **2001**, *52*, 103-112.

[5] Sloan, K. B.; Wasdo, S. C.; Rautio, J. Design for optimized topical delivery: prodrugs and a paradigm change. *Pharm. Res.* **2006**, *23*, 2729-2747.

[6] Paudel, K. S.; Nalluri, B. N.; Hammell, D. C.; Valiveti, S.; Kiptoo, P.; Hamad, M. O.; Crooks, P. A.; Stinchcomb, A. L. Transdermal delivery of naltrexone and its active metabolite 6-beta-naltrexol in human skin in vitro and guinea pigs in vivo. *J. Pharm. Sci.* **2005**, *94*, 1965-1975.

[7] Malmsten, M. Soft drug delivery systems. *Soft Matter* **2006**, *2*, 760-769.

[8] Fang, J. Y.; Hwang, T. L.; Huang, Y. L. Liposomes as vehicles for enhancing drug delivery via skin routes. *Curr. Nanosci.* **2006**, *2*, 55-70.

[9] Godin, B.; Touitou, E. Ethosomes: new prospects in transdermal delivery. *Crit. Rev. Ther. Drug Carrier Syst.* **2003**, *20*, 63-102.

[10] Choi, M. J.; Maibach, H. I. Liposomes and niosomes as topical drug delivery systems. *Skin Pharmacol. Physiol.* **2005**, *18*, 209-219.

[11] Nanda, A.; Nanda, S.; Dhall, M.; Rao, R. Transferosomes: a novel ultradeformable vesicular carrier for transdermal drug delivery. *Drug Deliv. Technol.* **2005**, *5* available at http://www.drugdeliverytech.com.

[12] Muller, R. H.; Mader, K.; Gohla, S. Solid lipid nanoparticles (SLN) for controlled drug delivery - A review of the state of the art. *Eur. J. Pharm. Biopharm.* **2000**, *50*, 161-177.

[13] Soppimath, K. S.; Aminabhavi, T. M.; Kulkarni, A. R.; Rudzinski, W. E. Biodegradable polymeric nanoparticles as drug delivery devices. *J. Controlled Release* **2001**, *70*, 1-20.

[14] Gehl, J. Electroporation: theory and methods, perspectives for drug delivery, gene therapy and research. *Acta Physiol. Scand.* **2003**, *177*, 437-447.

[15] Teo, A. L.; Shearwood, C.; Ng, K. C.; Lu, J.; Moochhala, S. Transdermal microneedles for drug delivery applications. *Mater. Sci. Eng. B-Solid State Mater. Adv. Technol.* **2006**, *132*, 151-154.

[16] Kalia, Y. N.; Naik, A.; Garrison, J.; Guy, R. H. Iontophoretic drug delivery. *Adv. Drug Deliv. Rev.* **2004**, *56*, 619-658.

[17] Sivakumar, M.; Tachibana, K.; Pandit, A. B.; Yasui, K.; Tuziuti, T.; Towata, A.; Iida, Y. Transdermal drug delivery using ultrasound: theory, understanding and critical analysis. *Cell. Mol. Biol.* **2005**, *51*, 767-784.

[18] Machet, L.; Boucaud, A. Phonophoresis: efficiency, mechanisms and skin tolerance. *Int. J. Pharm.* **2002**, *243*, 1-15.

[19] Lee, S.; McAuliffe, D. J.; Kollias, N.; Flotte, T. J.; Doukas, A. G. Permeabilization and recovery of the stratum corneum in vivo: the synergy of photomechanical waves and sodium lauryl sulfate. *Lasers Surg. Med.* **2001**, *29*, 145-150.

[20] Nicoli, S.; Santi, P.; Couvreur, P.; Couarraze, G.; Colombo, P.; Fattal, E. Design of triptorelin loaded nanospheres for transdermal iontophoretic administration. *Int. J. Pharm.* **2001**, *214*, 31-35.

[21] Barry, B. W. Is transdermal drug delivery research still important today? *Drug Discov. Today* **2001**, *6*, 967-971.

[22] Suh, H.; Jeong, B. M.; Rathi, R.; Kim, S. W. Regulation of smooth muscle cell proliferation using paclitaxel-loaded poly(ethylene oxide)-poly(lactide/glycolide) nanospheres. *J. Biomed. Mater. Res.* **1998**, *42*, 331-338.

[23] Hans, M. L.; Lowman, A. M. Biodegradable nanoparticles for drug delivery and targeting. *Curr. Opin. Solid State Mater. Sci.* **2002**, *6*, 319-327.

[24] Lboutounne, H.; Chaulet, J. F.; Ploton, C.; Falson, F.; Pirot, F. Sustained ex vivo skin antiseptic activity of chlorhexidine in poly(ε-caprolactone) nanocapsule encapsulated form and as a digluconate. *J. Controlled Release* **2002**, *82*, 319-334.

[25] Alvarez-Roman, R.; Naik, A.; Kalia, Y. N.; Guy, R. H.; Fessi, H. Enhancement of topical delivery from biodegradable nanoparticles. *Pharm. Res.* **2004**, *21*, 1818-1825.

[26] Luengo, J.; Weiss, B.; Schneider, M.; Ehlers, A.; Stracke, F.; Koenig, K.; Kostka, K. H.; Lehr, C. M.; Schaefer, U. F. Influence of nanoencapsulation on human skin transport of flufenamic acid. *Skin Pharmacol. Physiol.* **2006**, *19*, 190-197.

[27] Bouwstra, J. A.; Ponec, M. The skin barrier in healthy and diseases state. *Biochim. Biophys. Acta* **2006**, *1758*, 2080-2095.

[28] Honeywell-Nguyen, P. L.; Groenink, H. W. W.; Bouwstra, J. A. Elastic vesicles as a tool for dermal and transdermal delivery. *J. Liposome Res.* **2006**, *16*, 273-280.

[29] University of Trieste, Department of Physiology and Pathology (Trieste, Italy) http://fc.units.it/ppb/neurobiol/neuroscienze%20per%20tutti/receptor.html (July 2008).

[30] Hueber, F.; Wepierre, J.; Schaeffer, H. Role of transepidermal and transfollicular routes in percutaneous absorption of hydrocortisone and testosterone: in vivo study in the hairless rat. *Skin Pharmacol.* **1992**, *5*, 99-107.

[31] Matschiner, S.; Neubert, R.; Wohlrab, W.; Matschiner, F. Influence of ion pairing on ex vivo penetration of erythromycin into sebaceous follicles. *Skin Pharmacol.* **1996**, *9*, 270-273.

[32] Ogiso, T.; Shiraki, T.; Okajima, K.; Tanino, T.; Iwaki, M.; Wada, T. Transfollicular drug delivery: penetration of drugs through human scalp skin and comparison of penetration between scalp and abdominal skins in vitro. *J. Drug Target.* **2002**, *10*, 369-378.

[33] Jung, S.; Otberg, N.; Thiede, G.; Richter, H.; Sterry, W.; Panzner, S.; Lademann, J. Innovative liposomes as a transfollicular drug delivery system: penetration into porcine hair follicles. *J. Invest. Dermatol.* **2006**, *126*, 1728-1732.

[34] Lademann, J.; Otberg, N.; Jacobi, U.; Hoffman, R. M.; Blume-Peytavi, U. Follicular penetration and targeting. *J. Investig. Dermatol. Symp. Proc.* **2005**, *10*, 301-303.

[35] Meidan, V. M.; Bonner, M. C.; Michniak, B. B. Transfollicular drug delivery: is it a reality? *Int. J. Pharm.* **2005**, *306*, 1-14.

[36] Vogt, A.; Mandt, N.; Lademann, J.; Schaefer, H.; Blume-Peytavi, U. Follicular targeting: a promising tool in selective dermatotherapy. *J. Investig. Dermatol. Symp. Proc.* **2005**, *10*, 252-255.

[37] Lademann, J.; Richter, H.; Schaefer, U. F.; Blume-Peytavi, U.; Teichmann, A.; Otberg, N.; Sterry, W.; Hair follicles - A long-term reservoir for drug delivery. *Skin Pharmacol. Physiol.* **2006**, *19*, 232-236.

[38] Otberg, N.; Richter, H.; Schaefer, H.; Blume-Peytavi, U.; Sterry, W.; Lademann, J. Variations of hair follicle size and distribution in different body sites. *J. Invest. Dermatol.* **2004**, *122*, 14-19.

[39] Lademann, J.; Richter, H.; Teichmann, A.; Otberg, N.; Blume-Peytavi, U.; Luengo, J.; Weiss, B.; Schaefer, U. F.; Lehr, C. M.; Wepf, R.; Sterry, W. Nanoparticles - An efficient carrier for drug delivery into the hair follicles. *Eur. J. Pharm. Biopharm.* **2007**, *66*, 159-164.

[40] Wilke, K.; Wepf, R.; Keil, F. J.; Wittern, K. P.; Wenck, H.; Biel, S. S. Are sweat glands an alternate penetration pathway? Understanding the morphological complexity of the axillary sweat gland. *Skin Pharmacol. Physiol.* **2006**, *19*, 38-49.

[41] Grams, Y. Y.; Whitehead, L.; Lamers, G.; Sturmann, N.; Bouwstra, J. A. On-line diffusion profile of a lipophilic model dye in different depths of a hair follicle in human scalp skin. *J. Invest. Dermatol.* **2005**, *125*, 775-782.

[42] Changez, M.; Chander, J.; Dinda, A. K. Transdermal permeation of tetracaine hydrochloride by lecithin microemulsion in vivo. *Colloids Surf. B Biointerfaces* **2006**, *48*, 58-66.

[43] Schaefer, H.; Redelmeier, T. E. Skin Penetration. In *Contact Dermatitis. Fourth edition*; Frosch, P. J.; Lepoittevin, J. P.; Menne, T., Eds; Springer: Berlin Heidelberg, 2006.

[44] Radboud University Nijmegen, Department of Cellular Animal Physiology (Nijmegen, The Netherlands) http://www.ru.nl/celanphy/, last updated April 2006.

[45] Alvarez-Roman, R.; Naik, A.; Kalia, Y. N.; Fessi, H.; Guy, R. H. Visualization of skin penetration using confocal laser scanning microscopy. *Eur. J. Pharm. Biopharm.* **2004**, *58*, 301-316.

[46] Oheim, M.; Michael, D. J.; Geisbauer, M.; Madsen, D.; Chow, R. H. Principles of two-photon excitation fluorescence microscopy and other nonlinear imaging approaches. *Adv. Drug Deliv. Rev.* **2006**, *58*, 788-808.

[47] Diaspro, A.; Chirico, G.; Collini, M. Two-photon fluorescence excitation and related techniques in biological microscopy. *Q. Rev. Biophys.* **2005**, *38*, 97-166.

[48] Barry, B. W. Drug delivery routes in skin: a novel approach. *Adv. Drug Deliv. Rev.* **2002**, *54*, S31-S40.

[49] El Maghraby, G. M. M.; Williams, A. C.; Barry, B. W. Skin hydration and possible shunt route penetration in controlled estradiol delivery from ultradeformable and standard liposomes. *J. Pharm. Pharmacol.* **2001**, *53*, 1311-1322.

[50] Surber, C.; Schwarb, F. P.; Smith, E. W. Tape-stripping technique. *J. Toxicol. Cutaneous Ocul. Toxicol.* **2001**, *20*, 461-474.

[51] Mills, O. H.; Kligman, A. M. The follicular biopsy. *Dermatologica* **1983**, *167*, 57-63.

[52] Teichmann, A.; Jacobi, U.; Ossadnik, M.; Richter, H.; Koch, S.; Sterry, W.; Lademann, J. Differential stripping: determination of the amount of topically applied substances penetrated into the hair follicles. *J. Invest. Dermatol.* **2005**, *125*, 264-269.

[53] Alvarez-Roman, R.; Naik, A.; Kalia, Y. N.; Guy, R. H.; Fessi, H. Skin penetration and distribution of polymeric nanoparticles. *J. Control. Release* **2004**, *99*, 53-62.

[54] Stracke, F.; Weiss, B.; Lehr, C. M.; Konig, K.; Schaefer, U. F.; Schneider, M. Multiphoton microscopy for the investigation of dermal penetration of nanoparticle-borne drugs. *J. Invest. Dermatol.* **2006**, *126*, 2224-2233.

[55] Shim, J.; Kang, H. S.; Park, W. S.; Han, S. H.; Kim, J.; Chang, I. S. Transdermal delivery of mixnoxidil with block copolymer nanoparticles. *J. Controlled Release* **2004**, *97*, 477-484.

[56] Vogt, A.; Combadiere, B.; Hadam, S.; Stieler, K. M.; Lademann, J.; Schaefer, H.; Autran, B.; Sterry, W.; Blume-Peytavi, U. 40 nm, but not 750 or 1,500 nm nanoparticles enter epidermal CD1a+ cells after transcutaneous application on human skin. *J. Invest. Dermatol.* **2006**, *126*, 1316-1322.

[57] Ossadnik, M.; Richter, H.; Teichmann, A.; Koch, S.; Schäfer, U.; Wepf, R.; Sterry, W.; Lademann, J. Investigation of differences in follicular penetration of particle- and nonparticle-containing emulsions by laser scanning microscopy. *Laser Phys.* **2006**, *16*, 747-750.

[58] Ryman-Rasmussen, J. P.; Riviere, J. E.; Monteiro-Riviere, N. A. Penetration of intact skin by quantum dots with diverse physicochemical properties. *Toxicol. Sci.* **2006**, *91*, 159-165.

[59] Menzel, F.; Reinert, T.; Vogt, J.; Butz, T. Investigations of percutaneous uptake of ultrafine TiO_2 particles at the high energy ion nanoprobe LIPSION. *Nucl. Instrum. Methods Phys. Res. B* **2004**, *219*, 82-86.

[60] Bouwstra, J. A.; Gooris, G. S.; Dubbelaar, F. E. R.; Ponec, M. The lipid organisation in the skin barrier. *Acta Derm. Venereol. Supp.* **2000**, *208*, 23-30.

[61] Bouwstra, J. A.; Gooris, G. S.; Van der Spek, J. A.; Bras, W. Structural investigations of human stratum corneum by small-angle X-ray scattering, *J. Invest. Dermatol.* **1991**, *97*, 1005-1012.

[62] Tang, H.; Blankschtein, D.; Langer, R. Prediction of steady-state skin permeabilities of polar and non-polar permeants across excised pig skin based on measurements of transient diffusion: characterization of hydration effects on the skin porous pathway. *J. Pharm. Sci.* **2002**, *91*, 1891-1907.

[63] Warner, R. R.; Stone, K. J.; Boissy, Y. L. Hydration disrupts human stratum corneum ultrastructure. *J. Invest. Dermatol.* **2003**, *120*, 275-284.

[64] Grando, S. A.; Terman, A. K.; Stupina, A. S.; Glukhenky, B. T.; Romanenko, A. B. Ultrastructural study of clinically uninvolved skin of patients with pemphigus vulgaris. *Clin. Exp. Dermatol.* **1991**, *16*, 359-363.

[65] Corcuff, P.; Roguet, R.; Kermici, M. A method for measuring the various constituents of the human-hair follicle. *J. Microsc.* **1989**, *156*, 115-123.

[66] Lee**,** M. S.; Kossard, S.; Wilkinson, B.; Doyle, J. A. Quantification of hair follicle parameters using computer image analysis: a comparison of androgenetic alopecia with normal scalp biopsies. *Australas. J. Dermatol.* **1995**, *36*, 143-147.

[67] Kholi, A. K.; Alpar, H. O. Potential use of nanoparticles for transcutaneous vaccine delivery: effect of particle size and charge. *Int J Pharm.* **2004**, *275*, 13-17.

[68] Olvera-Martinez, B. I.; Cazares-Delgadillo, J.; Calderilla-Faardo, S. B.; Villalobos-Garcia, R.; Ganem-Quintanar, A.; Quintanar-Guerrero, D. Preparation of polymeric nanocapsules containing octyl methoxycinnamate by the emulsification-diffusion technique: Penetration across the stratum corneum. *J. Pharm. Sci.* **2005**, *94*, 1552-1559.

[69] Lboutounne, H.; Faivre, V.; Falson, F.; Pirot, F. Characterization of transport of chlorhexidine-loaded nanocapsules through hairless and Wistar rat skin. *Skin Pharmacol. Physiol.* **2004**, *17*, 176-182.

[70] Lemarchand, C.; Gref, R.; Couvreur, P. Polysaccharide-decorated nanoparticles. *Eur. J. Pharm. Biopharm.* **2004**, *58*, 327-341.

[71] Tsuji, J. S.; Maynard, A. D.; Howard, P. C.; James, J. T.; Lam, C.; Warheit, D. B.; Santamariak, A. B. Research strategies for safety evaluation of Nanomaterials. Part IV: risk assessment of nanoparticles. *Toxicol. Sci.* **2006**, *89*, 42-50.

[72] Kreyling, W. G.; Semmler-Behnke, M.; Moller, W. Health implications of nanoparticles. *J. Nanopart. Res.* **2006**, *8*, 543-562.

[73] Seaton, A. Nanotechnology and the occupational physician. *Occup. Med.* **2006**, *56*, 312-316.

[74] Herve-Bazin, B. Potential health impacts of nanoparticles. *Anal. Chim. Sci. Mater.* **2006**, *31*, 339-350.

[75] Morgan, K. Development of a preliminary framework for informing the risk analysis and risk management of nanoparticles. *Risk Anal.* **2005**, *25*, 1621-1635.

[76] Oberdörster, G.; Maynard, A.; Donaldson, K.; Castranova, V.; Fitzpatrick, J.; Ausman, K.; Carter, J.; Karn, B.; Kreyling, W.; Lai, D.; Olin, S.; Monteiro-Riviere, N; Warheit, D.; Yang, H. Principles for characterizing the potential human health effects from exposure to nanomaterials: elements of a screening strategy. *Part. Fibre Toxicol.* **2005**, *2* (8) available at http://www.particleandfibretoxicology.com.

CHAPTER III

Preparation and structural characterisation of amphiphilic hyaluronic acid derivatives

A. Investigation of novel modification methods for the preparation of amphiphilic hyaluronic acid derivatives

Abstract

Amphiphilic hyaluronic acid (HA) derivatives were prepared and structurally characterised by size exclusion chromatography–multi-angle laser light scattering (SEC-MALLS), Fourier transform infrared spectroscopy (FT-IR) and proton nuclear magnetic resonance spectroscopy (^{1}H NMR). HA was chemically modified in aqueous alkaline media and at room temperature with on the one hand phenyl and ethyl vinyl sulfone and on the other hand octenyl and octadecenyl succinic anhydride. The influence of reaction parameters such as the reaction medium alkalinity, reagent concentration and type on the degree of substitution (DS) of the resulting HA derivatives was investigated. Amphiphilic HA derivatives with a maximum DS of 55 % per disaccharide unit according to ^{1}H NMR were obtained. A comparison between the versatility of the two modification methods ultimately led to the selection of the succinic anhydride-based technology for further study.

I. Introduction

Alteration of the physicochemical properties of HA and introduction of a self-associative behaviour of this biopolymer towards the preparation of nanocarriers requires modifying the hydrophilic/hydrophobic balance of HA. This can be achieved by covalently grafting hydrophobic moieties onto the hydrophilic HA backbone.

Amphiphilic HA has mainly been prepared by modification of the HA carboxyl and hydroxyl groups [1] and a wide range of HA derivatives with a large number of chemistries is currently available (see Chapter I, § IV).

However, the modification methods currently available for the preparation of amphiphilic HA present some drawbacks, namely the (i) use of organic solvents, (ii) complexity and (iii) limited upscalability of the techniques and (iv) potential alteration of some of the fundamental biological and/or pharmacological properties of HA through modification of the polymer's carboxyl groups (see Chapter I, § IV).

With this in mind, the objective of this work was to design and implement a new and improved modification method for the preparation of amphiphilic HA based on simple and easily upscalable reactions in aqueous media exclusively involving the HA hydroxyl groups. Accordingly, two novel modification methods based on the reaction of HA with aryl/alkyl vinyl sulfone (Ar/AlVS) and alkenyl succinic anhydride (AlkSA) reagents were investigated.

The first technique is an extension of the use of divinyl sulfone (DVS) to cross-link HA in aqueous alkaline media [2]. The method involves fast reaction of the HA hydroxyl groups and typically results in the formation of macroscopic solid HA hydrogels insoluble in water. The lone reactive site CH_2=CH–SO_2–R of monofunctional vinyl sulfone compounds is believed to react with the HA hydroxyl groups in the same fashion as DVS and yield HA derivatives with grafted R hydrophobic groups.

The second technique is an application to HA of an existing method to hydrophobically modify starch with cyclic dicarboxylic acid anhydrides in aqueous alkaline media [3] (also see section B of this chapter, Foreword). This technology which also involves the modification of the HA hydroxyl groups is believed to be easily transferable to HA.

The prepared HA derivatives were structurally characterised by size exclusion chromatography–multi-angle laser light scattering (SEC-MALLS), Fourier transform infrared spectroscopy (FT-IR) and proton nuclear magnetic resonance spectroscopy (^{1}H NMR).

II. Materials and methods

II.1. Materials

Medium molecular weight (MW) HA (HyaCare®, MW~750,000 Da, HA750) was provided by Novozymes Biopolymer A/S (Bagsværd, Denmark). Low MW HA (HA300 and HA30) was prepared using the procedure described hereafter. Phenyl vinyl sulfone (PVS, 168.22 Da, purity ≥ 99 %) and ethyl vinyl sulfone (EVS, 120.17 Da, purity ≥ 98 %) were purchased from Fluka (Buchs, Switzerland) and Sigma-Aldrich (Saint Louis, Missouri, United States), respectively. Octenyl succinic anhydride (OSA, 210.27 Da, purity ≥ 97 %, mixture of *cis* and *trans*) was obtained from Sigma-Aldrich (Saint Louis, Missouri, United States). Octadecenyl succinic anhydride (ODSA, 352.56 Da, mixture of molecules with a random distribution of the unsaturation along the octadecenyl chains) was a non-commercial product kindly provided by Pentagon (Workington, United Kingdom). The water used for the sample preparation and analysis was distilled and purified to a resistivity of 18.2 MΩ.cm in a milli-Q apparatus (Millipore, Billerica, Massachusetts, United States).

II.2. Methods

II.2.1. Preparation of low molecular weight hyaluronic acid

HA300 was prepared from HA750 by acid degradation using phosphoric acid (H_3PO_4), at 60 °C. HA750 (70 g) was first dissolved in milli-Q water (7 L) for 16 hours (overnight), at 4 °C. H_3PO_4 (85 %, 30 mL) was added to HA750 and the resulting acidic solution was stirred for 10 min. This mixture was then incubated for 3.5 hours, at 60 °C, in a water bath. 1 mL of the digestion mixture was sampled after 1, 2.5 and 3 hours and used to determined the MW of HA by SEC-MALLS (see § II.2.4). The degradation was stopped when the MW of HA was close to

300,000 Da. The pH of the mixture was then adjusted to 7.0 with sodium hydroxide (NaOH, 4 M). The resulting product was purified by filtration through glass microfiber filters (GF/F 1825 110, porosity 0.7 µm; Whatman, Maidstone, United Kingdom). The permeate was purified by ultra filtration (Centramate™ Tangential Flow Systems; Pall, East Hills, New York, United States) through a membrane cassette (Omega™ Centramate™, MW cut-off (MWCO) 3,000 Da; Pall, East Hills, New York, United States). The purification was monitored by conductivity measurements of the permeate and was stopped when the conductivity had reached a value inferior to 5 µS/cm. The purified retentate containing HA300 was finally freeze-dried.

HA30 was prepared using the same method as that described for HA300 but with 160 mL of H_3PO_4 and a 25-hour incubation time.

Approximately 52 g of HA300 and 48 g of HA30, *i.e.* 74 and 69 %, respectively of the starting HA750 were recovered.

SEC-MALLS

The exact MW of HA300 and HA30 was 346,900 ± 1,387 and 33,930± 339 Da, respectively.

FT-IR

(KBr, 4000-500 cm^{-1}) w 3431 (O–H and N–H st), 2931 (C–H st), 1700-1600 (COO^- st as, N–H bd), 1423 (COO^- st sy), 1392 (C–O–H bd), 1154 (C–O–C st as), 1077 and 1038 (C–OH st), 954 and 900 (COO^- bd), 808 (C–O–C st sy) (see Figure III.A.3).

^{1}H NMR

(D_2O, 400 MHz) δ 2.0 (s, 3 H, H-m), 3.2-4.2 (m, 10 H, H-2, H-5', H-4', H-3, H-3', H-5, H-6'b, H-4, H-6'a, H-2), 4.3-4.6 (d, 2 H, H-1, H-1') (see Figure III.A.4).

II.2.2. Preparation of aryl/alkyl vinyl sulfone-modified hyaluronic acid

Phenyl vinyl sulfone-modified HA (PVS-HA)

PVS-HA was prepared by reacting HA300 or HA750 with PVS in water/acetone mixtures, under alkaline conditions, at room temperature. HA (100 mg) was first dissolved in milli-Q water (10 mL) for 6 hours, at room temperature. A NaOH solution (0.2 M) was prepared from concentrated NaOH (4 M) by dilution in milli-Q water. PVS was dissolved in acetone (10 mL) for 10 min. NaOH (0.2 M) was added to the HA solution and mixed for 10 min. The PVS solution was added drop-wise to the alkaline HA solution using a separation funnel. The mixture was then stirred for 16 hours (overnight), at room temperature. The resulting product was dialysed against milli-Q water (7.5 L), at 4 °C, using molecularporous membrane tubing (Spectra/Por®4, MWCO 12,000-14,000 Da; Spectrum Laboratories, Rancho Dominguez, California, United States). The surrounding milli-Q water was changed every third hour three times, then once after 16 hours (overnight) until the conductivity had reached a value inferior to 5 µS/cm. Purified PVS-HA was finally freeze-dried [4]. The number of molar equivalents of HA, NaOH and PVS used to prepare the PVS-HA derivatives and the reaction yields of the products are reported in Table III.A.1 and Table III.A.2, respectively.

SEC-MALLS

The MW values of PVS-HA300 (1) and PVS-HA300 (3) were 242,400 ± 4,848 and 148,300 ± 2,966 Da, respectively.

FT-IR

(KBr, 4000-500 cm^{-1}) w 3431 (O–H and N–H st), 2931 (C–H st), 1700-1600 (COO^- st as, N–H bd, ar C=C st), 1450 (ar C=C st), 1423 (COO^- st sy), 1392 (C–O–H bd), 1308 (S=O st as), 1154 (C–O–C st as, S=O st sy), 1077 and 1038 (C–OH st), 954 and 900 (COO^- bd), 808 (C–O–C st sy), 730 and 690 (ar C–H bd oop) (see Figure III.A.3).

^{1}H NMR

(D_2O, 400 MHz) δ 2.0 (s, 3 H, H-m), 3.0-4.2 (m, 12 H, H-2, H-5', H-4', H-3, H-3', H-5, H-6'b, H-4, H-6'a, H-2, H-2''), 4.2-4.6 (d, 4 H, H-1, H-1', H-1''), 7.6-8.0 (t, 5 H, H-3''-H-7'') (see Figure III.A.5).

Table III.A.1: Number of molar equivalents of HA, NaOH and PVS used to prepare the PVS-HA derivatives.

PVS-HAX (A) stands for PVS-HA prepared from HAX (X = 300 or 750) with the combination of molar equivalents A. One molar equivalent of HA corresponded to 0.250 mmol of disaccharide units. For the calculations, the MW of one disaccharide unit was approximated to 400 Da.

Sample	Number of molar equivalents		
	HA	NaOH	PVS
PVS-HAX (1)	1	1	1.5
PVS-HAX (2)	1	5	1.5
PVS-HAX (3)	1	10	1.5
PVS-HAX (4)	1	1	5
PVS-HAX (5)	1	1	10

Table III.A.2: Reaction yields of the PVS-HA derivatives.

Sample	Yield (mg)
PVS-HA300 (1)	93
PVS-HA300 (2)	88
PVS-HA300 (3)	85
PVS-HA300 (4)	97
PVS-HA300 (5)	118
PVS-HA750 (1)	94
PVS-HA750 (4)	96
PVS-HA750 (5)	115

Ethyl vinyl sulfone-modified HA (EVS-HA)

EVS-HA was prepared using the same method as that described for PVS-HA. EVS-HA300 was obtained from 1, 1 and 1.5 molar equivalents of HA300, NaOH and EVS, respectively (1 molar equivalent of HA corresponded to 0.250 mmol of disaccharide units). The reaction yield of EVS-HA300 was 96 mg.

FT-IR

(KBr, 4000-500 cm^{-1}) w 3431 (O–H and N–H st), 2931 (C–H st), 1700-1600 (COO^- st as, N–H bd), 1423 (COO^- st sy), 1392 (C–O–H bd), 1308 (S=O st as), 1154 (C–O–C st as, S=O st sy), 1077 and 1038 (C–OH st), 954 and 900 (COO^- bd), 808 (C–O–C st sy).

^{1}H NMR

(D_2O, 400 MHz) δ 1.2-1.4 (s, 3 H, SO_2–CH_2–C*H*$_3$), δ 2.0 (s, 3 H, H-m), 3.2-4.0 (m, 14 H, H-2, H-5', H-4', H-3, H-3', H-5, H-6'b, H-4, H-6'a, H-2, SO_2–C*H*$_2$–CH_2–O, SO_2–C*H*$_2$–CH_3), 4.2-4.6 (d, 4 H, H-1, H-1', SO_2–CH_2–C*H*$_2$–O).

II.2.3. Preparation of alkenyl succinic anhydride-modified hyaluronic acid

Octenyl succinic anhydride-modified HA (OSA-HA)

OSA-HA was prepared by reacting HA30 with OSA in aqueous media, under alkaline conditions, at room temperature. HA30 was first dissolved in milli-Q water at a concentration of 5 mg/mL, for 6 hours, at room temperature. A NaOH solution (0.5 M) was prepared from concentrated NaOH (4 M) by dilution in milli-Q water. OSA was added drop-wise to the HA solution with a volumetric pipette, under vigorous agitation. The pH of the resulting mixture was adjusted to 8.5 with NaOH (0.5 M). The mixture was then stirred for 16 hours (overnight), at room temperature. The pH of the reaction mixture was maintained at 8.5 by a titration manager (TIM856; Radiometer analytical, Lyon, France) using NaOH (0.5 M). The resulting product was dialysed as described in § II.2.2. Purified OSA-HA was finally freeze-

dried [5]. The number of molar equivalents of HA and OSA used to prepare the OSA-HA derivatives and the reaction yields of the products are reported in Table III.A.3 and Table III.A.4, respectively.

Table III.A.3: Number of molar equivalents of HA and OSA used to prepare the OSA-HA derivatives.

OSA-HA30 (A) stands for OSA-HA prepared from HA30 with the combination of molar equivalents A. One molar equivalent of HA corresponded to 0.125 mmol of disaccharide units. For the calculations, the MW of one disaccharide unit was approximated to 400 Da.

Sample	Number of molar equivalents	
	HA	OSA
OSA-HA30 (1)	10	2
OSA-HA30 (2)	1	1
OSA-HA30 (3)	10	20

Table III.A.4: Reaction yields of the OSA-HA derivatives.

Sample	Yield (mg)
OSA-HA30 (1)	4,840
OSA-HA30 (2)	470
OSA-HA30 (3)	4,780

^{1}H NMR

(D_2O, 400 MHz) δ 0.9 (s, 3 H, H-10), 1.3-1.5 (m, 6 H, H-7-H-9), 2.0 (s, 3 H, H-m), 3.3-4.0 (m, 10 H, H-2, H-5', H-4', H-3, H-3', H-5, H-6'b, H-4, H-6'a, H-2), 4.4-4.7 (d, 2 H, H-1, H-1') (see Figure III.A.8).

Octadecenyl succinic anhydride-modified HA (ODSA-HA)

ODSA-HA was prepared using the same method as that described for OSA-HA. The number of molar equivalents of HA and ODSA used to prepare the ODSA-HA derivatives and the reaction yields of the products are reported in Table III.A.5 and Table III.A.6, respectively.

Table III.A.5: Number of molar equivalents of HA and ODSA used to prepare the ODSA-HA derivatives.

ODSA-HA30 (A) stands for ODSA-HA prepared from HA30 with the combination of molar equivalents A. One molar equivalent of HA corresponded to 0.125 mmol of disaccharide units. For the calculations, the MW of one disaccharide unit was approximated to 400 Da.

Sample	Number of molar equivalents	
	HA	ODSA
ODSA-HA30 (1)	5	1.25
ODSA-HA30 (2)	5	12.5

Table III.A.6: Reaction yields of the ODSA-HA derivatives.

Sample	Yield (mg)
ODSA-HA30 (1)	2,060
ODSA-HA30 (2)	2,130

^{1}H NMR

(D_2O, 400 MHz) δ 1.0 (s, 3 H, ODSA terminal methyl protons), 1.2-1.5 (m, 26 H, ODSA methylene protons), 2.0 (s, 3 H, H-m), 3.3-4.0 (m, 10 H, H-2, H-5', H-4', H-3, H-3', H-5, H-6', H-4, H-6'a, H-2), 4.4-4.7 (d, 2 H, H-1, H-1').

II.2.4. Characterisation techniques

SEC-MALLS

Each sample (10 mg) was dissolved in the mobile phase (10 mL) which was prepared as followed: NaCl (45.0 g), NaH_2PO_4 (7.8 g) and NaN_3 (1.25 g) on the one hand and NaCl (45.0 g), Na_2HPO_4 (22.4 g) and NaN_3 (1.25 g) on the other hand were first dissolved in milli-Q water (5.0 L) in two volumetric flasks to constitute two distinct solutions (S_1 and S_2). S_1 and S_2 were mixed. The pH of the mixture was measured and, if necessary, adjusted to 7.0 with either HCl (4 M) or NaOH (4 M). The resulting mobile phase was finally filtered through glass microfiber filters (GF/F 1825 110, porosity 0.7 µm; Whatman, Maidstone, United Kingdom). Each sample was first fractionated by high performance liquid chromatography (HPLC, Alliance Waters 2695; Waters, Milford, Massachusetts, United States) through a HPLC column (7.8 x 300 mm TSK-GEL®, G5000PW$_{XL}$; Tosoh Corporation, Tokyo, Japan). The various sample fractions were then analysed by the MALLS (DAWN EOS; Wyatt Technology Corporation, Santa Barbara, California, United States) and refractive index (Optilab Rex; Wyatt Technology Corporation, Santa Barbara, California, United States) detection instruments. The flow rate was kept constant at 0.5 mL/min. The values of the osmotic second virial coefficient and of the variation of the polymer solution refractive index n as a function of the polymer concentration c (dn/dC) were 0.0023 mol.mL/g^2 and 0.153 mL/g, respectively. The HPLC on the one hand and the MALLS and RI instruments on the other hand were piloted by the softwares Empower 1154 (Waters, Milford, Massachusetts, United States) and ASTRA 5.3.1.4 (Wyatt Technology Corporation, Santa Barbara, California, United States).

The MW loss of the PVS-HA derivatives was calculated as followed:

$$MWloss = \frac{MW(PVS - HA300) - MW(HA300)}{MW(HA300)} \times 100 \qquad \text{Equation III.A.1}$$

Thin layer chromatography (TLC)

Drops of PVS (1 mg/mL in acetone) and of the crude and purified PVS-HA products (10 mg/mL in milli-Q water) were spotted on the bottom line of a TLC plate (Silica gel 60 F254; Merck, Whitehouse Station, New Jersey, United States). The compounds were eluted using a heptane/ethyl acetate mixture (50:50, v/v). The plate was revealed under ultraviolet light (254 nm). The retention time of each spot was the ratio between the distance travelled by the spot and that travelled by the elution system (control).

FT-IR

Each sample (1 mg) was ground in potassium bromide (KBr, ~25 mg) and a pellet was prepared using a Qwik Handi-Press (P/N 0016-125; Thermo Spectra-Tech, Shelton, Connecticut, United States) and a 3-mm Die Set (P/N 0016-115; Thermo Spectra-Tech, Shelton, Connecticut, United States). The spectra were acquired at room temperature, in the wavelength range 4000-500 cm^{-1} (Nicolet Nexus 470 FT-IR, equipped with a Smart ARK^{TM} system; Thermoelectron, Copenhagen, Denmark). Each spectrum was an overlap of 64 scans.

The spectra of native HA and of the HA derivatives were assigned based on Alkrad *et al.* [6], Haxaire *et al.* [7] and Pretsch *et al.* [8].

^{1}H NRM

Each sample (10 to 30 mg) was dissolved in D_2O (0.8 mL) and transferred into an NMR glass tube. The spectra were acquired at 80 °C and 400 MHz (Varian Mercury TX 400 MHz; Varian, Palo Alto, California, United States). The DS of the derivatives, which corresponds to the number of grafted reagent molecules per 100 disaccharide units, was calculated by comparing the intensity per proton of the phenyl protons (PVS-HA, δ = 7.6-8.0 ppm), the terminal methyl protons close to the sulfonyl group (EVS-HA, δ = 1.2-1.4 ppm) or the terminal methyl protons on the

alkenyl chain (δ = 0.9 ppm for OSA-HA and δ = 1.0 ppm for ODSA-HA) to that of the methyl protons on native HA (δ = 2.0 ppm).

The spectra of native HA and of the HA derivatives were assigned based on Welti *et al.* [9], Pavia *et al.* [10] and Pretsch *et al.* [8].

III. Results and discussion

III.1. Characterisation of aryl/alkyl vinyl sulfone-modified hyaluronic acid

HA was reacted with phenyl and ethyl vinyl sulfone in water/acetone mixtures, under alkaline conditions, at room temperature and the influence of the NaOH/HA and PVS/HA molar ratios, reagent type and HA MW on the DS of the resulting derivatives was investigated.

The reaction between HA and Ar/AlVS is illustrated in Figure III.A.1 and its mechanism is presented in Figure III.A.2.

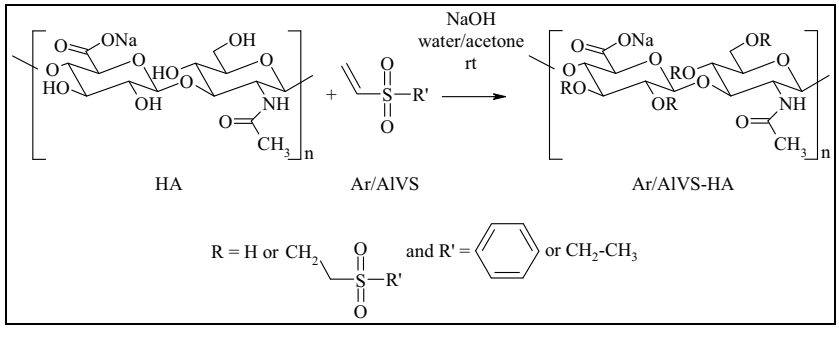

Figure III.A.1: Modification of HA with Ar/AlVS.

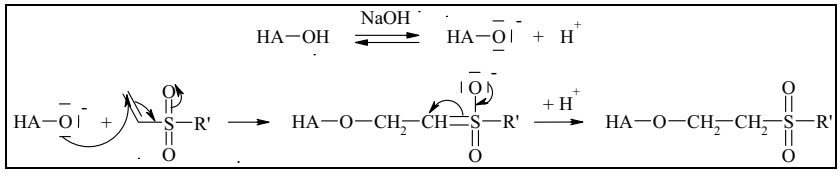

Figure III.A.2: Mechanism of the reaction between HA and Ar/AlVS.

The products obtained were white spongy materials partially soluble in milli-Q water. At concentrations above 1 mg/mL in milli-Q water, all products gave slightly turbid solutions. This was not the case for native HA which evidenced that the products had different properties than the starting HA.

Residual ungrafted PVS in the crude and purified PVS-HA products was assessed by TLC. The results showed that the crude PVS-HA products contained phenyl-based compounds while the purified PVS-HA products were free of these. This demonstrated that ungrafted PVS was eliminated during the purification step. Dialysis was thereby proved efficient to purify the products of the reaction between HA and PVS and by extension HA and EVS.

The MW values of HA300, PVS-HA300 (1) and PVS-HA300 (3) were determined by SEC-MALLS to evaluate the extent of HA degradation during the preparation of PVS-HA (Table III.A.7).

Table III.A.7: Molecular weight of HA300 and selected PVS-HA300 derivatives.

Sample	MW (Da)	MW loss (%)
HA300	346,900 ± 1387	-
PVS-HA300 (1)	242,400 ± 4848	30
PVS-HA300 (3)	148,300 ± 2966	57

The results showed that the alkaline treatment needed to activate the HA hydroxyl groups led to a manifest polymer degradation and that the latter was an increasing function of the NaOH/HA molar ratio between 1 (PVS-HA300 (1)) and 10 (PVS-HA300 (3)). The treatments with NaOH/HA molar ratios equal to 1 and 10 led to 30 % and 57 % HA degradation, respectively, suggesting that NaOH/HA molar ratios lower than 1 are more suitable to limit the degradation of HA and retain its MW. This was taken into consideration when preparing PVS-HA300 (4) and (5) and PVS-HA750 (1), (4) and (5) (see Table III.A.1).

The structure of the vinyl sulfone-based HA derivatives was qualitatively confirmed by FT-IR by comparing the spectra of native HA300 and of the derivatives. As an example, the spectra of HA300 and PVS-HA300 (1) are shown in Figure III.A.3.

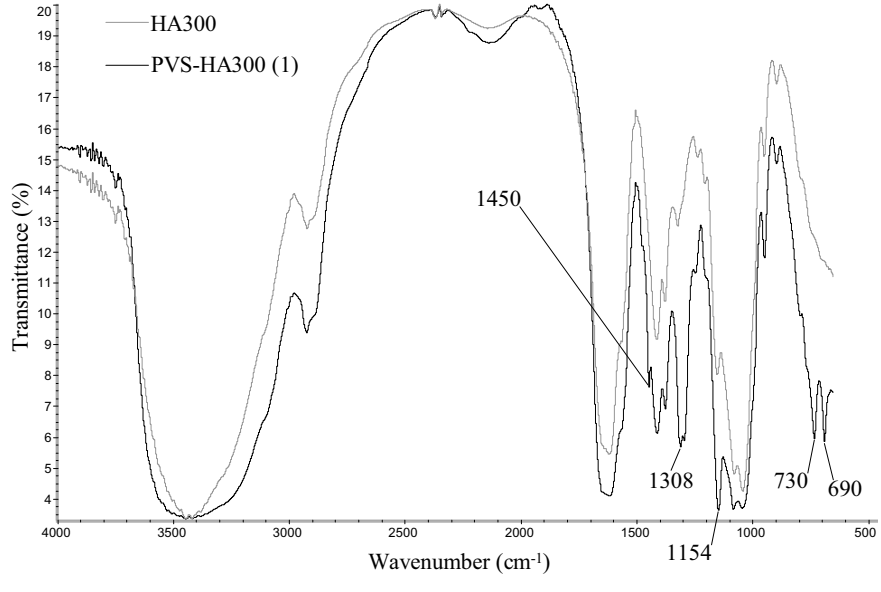

Figure III.A.3: FT-IR spectra of HA300 and PVS-HA300 (1).

Compared to the spectrum of HA300, additional bands at 1450, 1308, 730 and 690 cm-^{1} were found on the spectrum of PVS-HA300 (1). These correspond to aromatic C=C stretching (second band), S=O asymmetric stretching and aromatic C–H out-of-plane bending (bands at 730 and 690 cm^{-1}), respectively. In addition, the two bands at 730 and 690 cm^{-1} were typical of monosubstituted aromatic rings.
The intensity of the broad band between 1700 and 1600 cm^{-1} and that of the band at 1154 cm^{-1} was significantly higher in the case of PVS-HA300 (1). On the spectrum of HA300, the band between 1700 and 1600 cm^{-1} was most likely due to COO^{-} asymmetric stretching and N–H bending. However, on the spectrum of PVS-HA300 (1), this band probably also additionally resulted from aromatic C=C stretching (first absorption). Similarly, the sharp band at 1154 cm^{-1} most certainly arose from C–O–C asymmetric stretching on the spectrum of HA300 and to a combination of the latter and S=O symmetric stretching on the spectrum of PVS-HA300 (1) (see § II.2.2).
The univocal presence of aromatic C=C and C–H and S=O bands on the spectrum of PVS-HA300 (1) qualitatively confirmed the modification of HA with PVS.

Similar spectra were observed for the other PVS-HA derivatives while only S=O asymmetric stretching around 1300 cm^{-1} on the spectrum of EVS-HA300 could confirm the modification of HA with EVS (see § II.2.2).

^{1}H NMR was used to quantitatively confirm the structure of the vinyl sulfone-based HA derivatives and calculate their DS. As an example, the spectra of native HA300 and PVS-HA300 (1) are shown in Figure III.A.4 and Figure III.A.5, respectively.
Due to the large MW of HA300 and to peak overlapping in the region 3.2 to 4.2 ppm, it was not possible to clearly assign the shifts of protons 3 to 5 and 2' to 6' (see § II.2.1). For this reason, lower MW HA was used to prepare the succinic anhydride-modified HA derivatives (see § II.2.3).

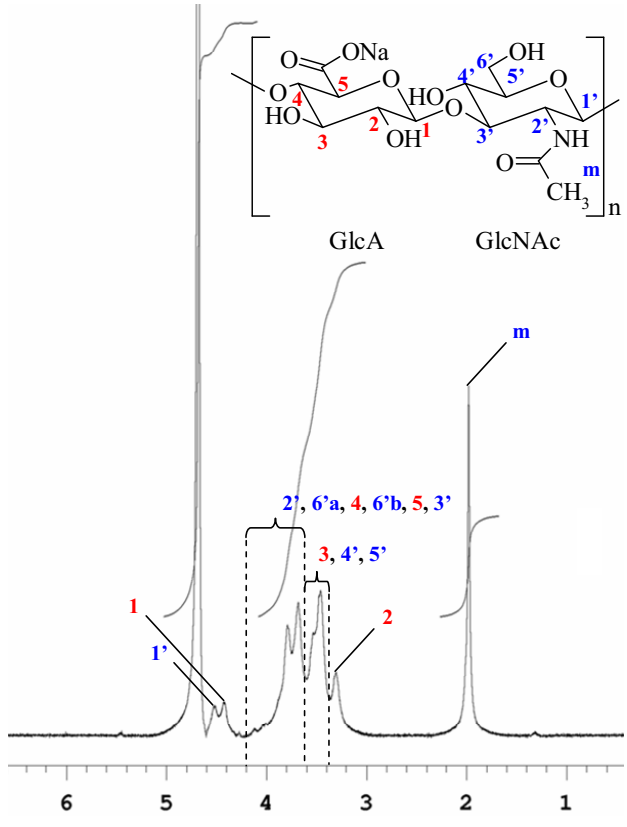

Figure III.A.4: ^{1}H NMR spectrum of HA300.

m stands for methyl. For the multiplet occurring between 3.2 and 4.2 ppm, protons are written in the order of their spectral occurrence according to [9].

Compared to the spectrum of HA300, an additional triplet was found between 7.6 and 8.0 ppm on the spectrum of PVS-HA300 (1). It corresponds to the aromatic protons of grafted PVS (H-3'' to H-7''). In addition, the intensities of the resonances between 3.0 and 4.2 ppm and 4.2 and 4.6 ppm were relatively more important compared to those found in the same regions on the spectrum of HA300 (see Figure III.A.4). This was due to the contribution of the methylene protons vicinal to the sulfonyl group

(H-2'') and those vicinal to the ether bond (H-1''), respectively (see § II.2.2). The DS of PVS-HA300 (1) was 11 % per disaccharide unit.

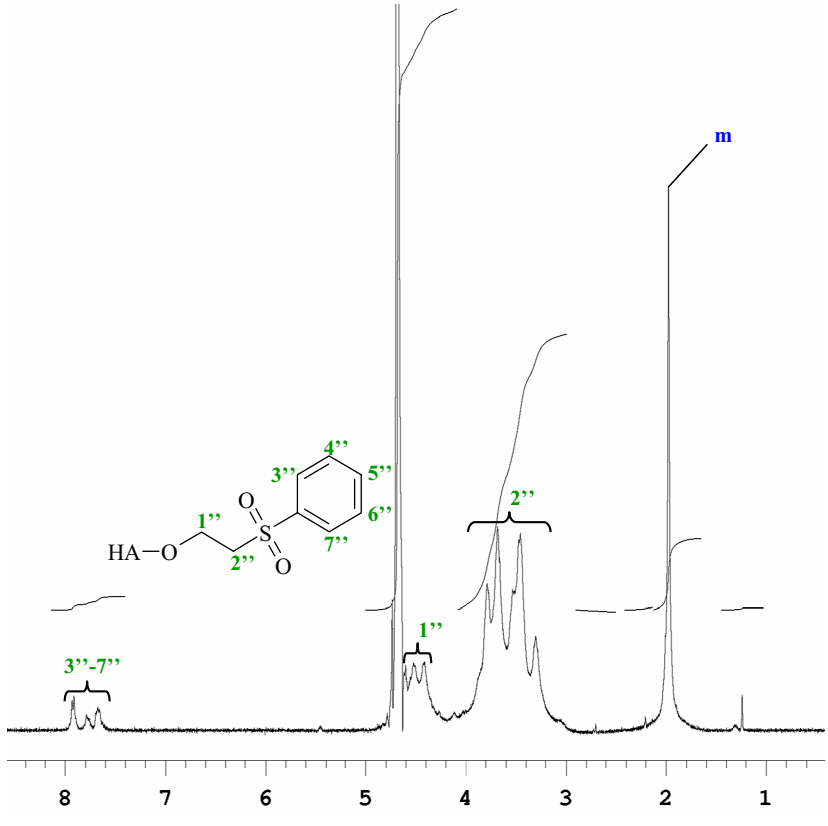

Figure III.A.5: ^{1}H NMR spectrum of PVS-HA300 (1).

Similar spectra were observed for the other PVS-HA derivatives. However, the relative intensity of the triplet between 7.6 and 8.0 ppm and therefore the DS of the derivatives were dependent on the reaction conditions. The DS values of the PVS-HA derivatives are reported in Table III.A.8.

Table III.A.8: Degree of substitution of the PVS-HA derivatives.

Sample	DS (%)
PVS-HA300 (1)	11
PVS-HA300 (2)	< 1
PVS-HA300 (3)	< 1
PVS-HA300 (4)	19
PVS-HA300 (5)	55
PVS-HA750 (1)	3
PVS-HA750 (4)	18
PVS-HA750 (5)	52

When the NaOH/HA molar ratio was increased from 1 to 10 (PVS-HA300 (1), (2) and (3)), the DS of PVS-HA decreased from 11 to values inferior to 1 % (the PVS/HA molar ratio was 1.5). Formation of inert moieties by hydrolysis of DVS under alkaline conditions has been reported [11]. The probability of forming this by-product being naturally proportional to the alkaline strength of the reaction medium, it is likely that this side reaction extensively occurred while preparing PVS-HA300 (2) (NaOH/HA molar ratio = 5) and PVS-HA300 (3) (NaOH/HA molar ratio = 10) yielding derivatives with very low DS.

As expected, the DS of PVS-HA increased when the PVS/HA molar ratio was increased from 1.5 to 10 (PVS-HA300 (1), (4) and (5), on the one hand and PVS-HA750 (1), (4), (5), on the other hand, the NaOH/HA molar ratio was 1). This increase was from 11 to 55 % for PVA-HA300 and from 3 to 52 % for PVS-HA750.

The DS of PVA-HA300 (4) (19 %) and PVS-HA750 (4) (18 %) (the PVS/HA molar ratio was 5) and of PVA-HA300 (5) (55 %) and PVS-HA750 (5) (52 %) (the PVS/HA molar ratio was 10) were very similar suggesting that at fixed NaOH/HA and PVS/HA molar ratios, the DS of the resulting PVS-HA derivatives was rather independent of the MW of native HA for MW values of 300,000 and 750,000 Da. This was not the case for the low PVS/HA molar ratio (1.5) since the DS of PVS-

HA300 (1) (11 %) was much higher compared to that of PVS-HA750 (1) (3 %). This could be due to the higher viscosity of HA750 aqueous solutions which might have limited the mixing and diffusion of small quantities of PVS.

The spectrum of EVS-HA300 showed an additional triplet between 1.2 and 1.4 ppm corresponding to the terminal methyl protons close to the sulfonyl group (SO_2–CH_2–C*H*$_3$). In addition, as for PVS-HA, the intensities of the resonances between 3.2 and 4.2 ppm and 4.2 and 4.6 ppm was relatively more important compared to that found in the same regions on the spectrum of HA300. This was due to the contribution of the methylene protons vicinal to the sulfonyl group (SO_2–C*H*$_2$–CH_2–O and SO_2–C*H*$_2$–CH_3) and of those vicinal to the ether bond (SO_2–CH_2–C*H*$_2$–O), respectively (see § II.2.2).

The DS of EVS-HA300 was 13 % per disaccharide unit. This value was close to that obtained for PVS-HA300 (1) (11 %) suggesting that at fixed NaOH/HA and vinyl sulfone reagent/HA molar ratios the DS of the resulting derivatives was rather independent of the pendant group attached for the substituents PVS and EVS.

III.2. Characterisation of alkenyl succinic anhydride-modified hyaluronic acid

HA was reacted with octenyl and octadecenyl succinic anhydride in aqueous media, under alkaline conditions, at room temperature and the influence of the reagent/HA molar ratio and succinic anhydride reagent type on the DS of the resulting derivatives was investigated.

The reaction between HA and AlkSA is illustrated in Figure III.A.6 and its mechanism is presented in Figure III.A.7.

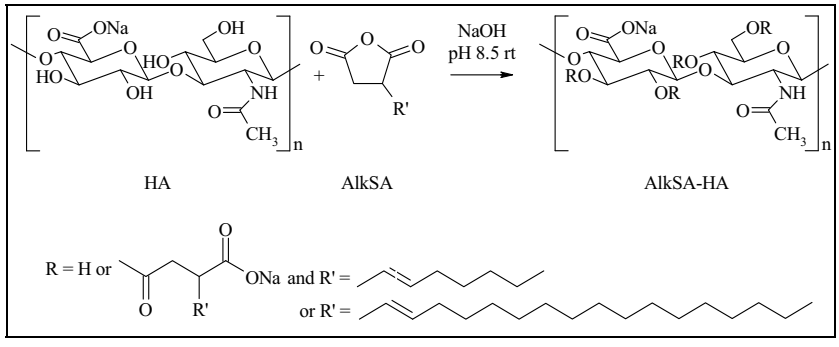

Figure III.A.6: Modification of HA with AlkSA.

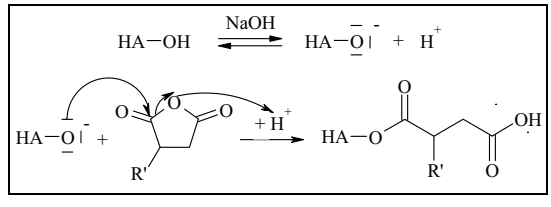

Figure III.A.7: Mechanism of the reaction between HA and AlkSA.

As for PVS- and EVS-HA, the products obtained gave slightly turbid solutions when dissolved at concentrations above 1 mg/mL in milli-Q water.

The MW of the OSA-HA derivatives was studied by SEC-MALLS. However, the MW measurement was impeded by the strong retention of the derivatives on the stationary phase of the fractionation column of the SEC instrument. This phenomenon has been reported for alkylated HA with dodecyl and octadecyl bromide [12]. Circumvention of this limitation was investigated in section C of this chapter.

The structure of the succinic anhydride-based HA derivatives was qualitatively studied by FT-IR by comparing the spectra of native HA30 and of the derivatives. However, these spectra did not show any significant differences,

independently of the DS of the derivatives. This lack of difference was probably due the overlapping of the characteristic bands of HA, OSA- and ODSA-HA. Indeed, vinyl C–H stretching was most likely indiscernible from HA O–H stretching. Likewise, C=C stretching and C=O (ester) stretching were certainly hidden by HA C=O stretching. However, in the region 800-500 cm^{-1}, which was free of any bands on the HA spectrum, CH_2 bending/rocking along the octenyl succinate (OS) chains and vinyl C–H out-of-plane bending could not clearly be detected, probably due to the low DS of the OSA- and ODSA-HA derivatives (see Table III.A.9 and below). As a result, FT-IR could not confirm the modification of HA with OSA or ODSA.

^{1}H NMR, however, confirmed grafting of OSA onto HA and was used to calculate the DS of the OSA-HA derivatives. As an example, the spectrum of OSA-HA30 (2) is shown in Figure III.A.8.
Compared to the spectrum of HA30, an additional singlet and a multiplet were found at 0.9 ppm and between 1.3 and 1.5 ppm, respectively on the spectrum of OSA-HA30 (2). The former corresponds to the terminal methyl protons (H-10) and the latter to the methylene protons (H-7 to H-9) on the octenyl chain of grafted OS. Due to the low signal intensity in the regions 2.2-3.0 and 4.8-5.8 ppm, it was not possible to clearly assign the chemical shifts of protons 1 to 6 (see § II.2.3). The DS of OSA-HA30 (2) was approximately 3 % per disaccharide unit.

Similar spectra were observed for the other OSA-HA derivatives. However, the relative intensity of the singlet at 0.9 ppm and therefore the DS of the derivatives were dependent on the reaction conditions. The DS values of the OSA-HA derivatives are reported in Table III.A.9.

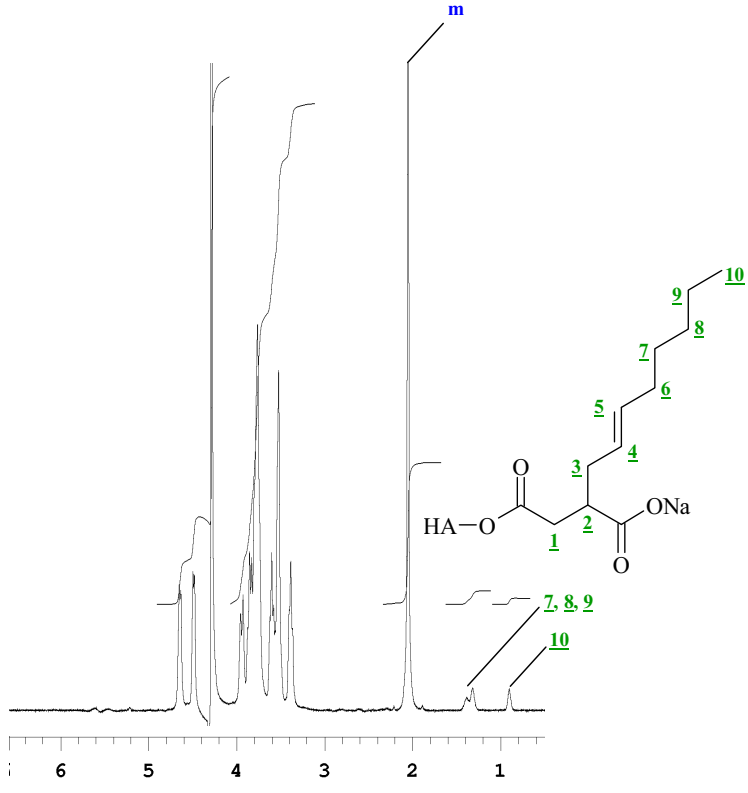

Figure III.A.8: ^{1}H NMR spectrum of OSA-HA30 (2).

Table III.A.9: Degree of substitution of the OSA-HA derivatives.

Sample	DS (%)
OSA-HA30 (1)	< 1
OSA-HA30 (2)	3
OSA-HA30 (3)	4

As expected, the DS of OSA-HA increased when the OSA/HA molar ratio was increased from 0.2 (OSA-HA30 (1)) to 2 (OSA-HA30 (3)). This increase was from < 1 to 4 %.

The spectra of the ODSA-HA derivatives showed two additional singlets at 1.0 ppm and between 1.2 and 1.5 ppm (broad). The former corresponds to the terminal methyl protons and the latter to the 26 methylene protons localised after the unsaturation on the octadecenyl chain of grafted ODSA. As for OSA-HA, the chemical shifts of the remaining protons (H-1 to H-6) were difficult to clearly assign. The DS of ODSA-HA30 (1) and ODSA-HA30 (2) were < 1 and 2 % per disaccharide unit, respectively. Increasing the ODSA/HA molar ratio from 0.25 (ODSA-HA30 (1)) to 2.5 (ODSA-HA30 (2)) did not result in a substantial increase of the DS. This might be due to the low solubility in the aqueous reaction medium of ODSA which in both cases limited the number of reagent molecules available for reaction.

The DS of the ODSA-HA derivatives were lower compared to those of the OSA-HA derivatives when using comparable reaction conditions. This might be due to the lower solubility in aqueous media of ODSA.

III.3. Comparison between the two preparation methods

In summary, the modification of HA with vinyl sulfone and succinic anhydride reagents was not only proved feasible but also efficient under alkaline conditions, at room temperature. In addition, the reactions exclusively involved the HA hydroxyl groups, were simple, well controlled and yielded HA derivatives with high DS (vinyl sulfone-based HA derivatives).

Ar/AlVS-HA derivatives with a DS up to 52-55 % per disaccharide unit according to ^{1}H NMR were prepared from HA300 and HA750. The DS of the derivatives was an increasing function of the reagent/HA molar ratio and was rather independent on the HA MW. In addition, the same reaction conditions (same NaOH/HA and reagent/HA molar ratios) yielded derivatives with a similar DS, independently of the reagents (PVS or EVS). The alkaline treatment with NaOH causing a substantial degradation

of native HA, NaOH/HA molar ratios below 1 were subsequently used to limit the degradation of HA and retain its MW.

AlkSA-HA derivatives with a DS up to 4 % per disaccharide unit according to ^{1}H NMR were obtained from HA30. The DS of the AlkSA-HA derivatives was an increasing function of the reagent/HA molar ratio and was dependent on the reagent type: the use of ODSA yielded derivatives with lower DS most likely due to the lower solubility in the reaction medium of the longer octadecenyl chains.

The DS of the AlkSA-HA derivatives was lower than that of the Ar/AlVS-HA derivatives at comparable reagent/HA molar ratios most likely due to the lower solubility and higher sensitivity to hydration of the AlkSA reagents.

A comparison between the two modification methods is presented in Table III.A.10.

Although both preparation methods involve the HA hydroxyl groups and are easily upscalable, the preparation of AlkSA-HA is more environmentally friendly than that of Ar/AlVS-HA. Indeed, the former is conducted in aqueous media while the latter is achieved in water/acetone mixtures. However, a higher through-put is possible in the case of Ar/AlVS-HA since only one sample of AlkSA-HA can be prepared at a time due to the use of a titration manager to control the pH of the reaction medium.

The vinyl sulfone reagents are fewer, relatively more expensive and less available compared to the succinic anhydride reagents which are very diversified, relatively less expensive and largely available according to three major chemical databases [13]. Vinyl sulfone reagents with substituted groups other than methyl, ethyl and phenyl are scarce. Some suppliers list compounds with larger aliphatic groups or more complex molecular arrangements containing heteroatoms but these are often rare and non commercial compounds with a small production volume [13]. Alternatively, more diverse vinyl sulfone reagents could be prepared by the selective addition of nucleophilic compounds such as secondary amines, alcohols or thiols with various chain lengths on one double bond of divinyl sulfone, as described by

Prilezhaeva and Shapiro [14]. However, these reactions are by nature difficult to control and inevitably result in mixture of mono- and disubstituted sulfone compounds.

Table III.A.10: Advantages and drawbacks associated to the preparation of the Ar/AlVS-HA and AlkSA-HA derivatives.

		Advantages	Drawbacks
Ar/AlVS-HA	Reaction	▪ Involves HA –OH ▪ Easily upscalable ▪ Higher through-put	▪ Water/acetone based
	Reagents	▪ Less sensitive to hydration	▪ Fewer ▪ More expensive ▪ Less available
	Derivatives	▪ Partially water soluble ▪ Higher DS	-
AlkSA-HA	Reaction	▪ Involves HA –OH ▪ Easily upscalable ▪ Water based	▪ Lower through-put
	Reagents	▪ More numerous ▪ Less expensive ▪ More available	▪ Poorly soluble in aqueous media ▪ More sensitive to hydration
	Derivatives	▪ Partially water soluble ▪ Introduction of additional negative charges	▪ Lower DS

By contrast, the succinic anhydride reagents present a large variability of substituted groups ranging, for aliphatic chains, from methyl to tetratetracontenyl (44 carbon atoms) and other more complex molecular arrangements containing heteroatoms are

also listed [13]. However, the modification of HA with succinic anhydride reagents is limited by their relative poor solubility in aqueous media and high sensitivity to hydration. As a result, the derivatives exhibit lower DS values than the vinyl sulfone-based HA derivatives.

Both types of derivatives present a partial solubility in aqueous media but AlkSA-HA possesses a higher charge density than Ar/AlVS-HA at neutral pH. This is due the additional carboxyl groups introduced upon ring opening of AlkSA (see Figure III.A.6) which increases the repulsion between the polymer chains. This property could advantageously be exploited for the electrostatic stabilisation of future nanocarriers based on AlkSA-HA.

Due to the additional advantages of the succinic anhydride-based technology, namely (i) the environmental friendliness, (ii) large variability and availability of the succinic anhydride reagents and (iii) increase of the negative charge density on the polymer, this method was selected for further study.

IV. Conclusion

Aryl/alkyl vinyl sulfone- and alkenyl succinic anhydride-modified HA were prepared and structurally characterised and their preparation methods were compared on the basis of their versatility.

The environmental friendliness of the preparation method of AlkSA-HA, the large variability and availability of the AlkSA reagents and the increase of the negative charge density on the polymer motivated the selection of the succinic anhydride-based technology for further study. Indeed, these properties provide the AlkSA-HA derivatives with a potential higher versatility and functionality compared to the Ar/AlVS-HA derivatives.

However, the lower preparation through-put of AlkSA-HA, poorer solubility and higher sensitivity to hydration of the AlkSA reagents limiting the DS of the HA

derivatives were aspects which remained to be addressed. In addition, the preparation method of AlkSA-HA needed to be optimised in order to develop a reproducible and robust process for the routine production of HA derivatives with a controlled DS. This optimisation work is reported in the following section.

References

[1] Vercruysse, K. P.; Prestwich, G. D. Hyaluronate derivatives in drug delivery. *Crit. Rev. Ther. Drug Carrier Syst.* **1998**, *15*, 513-555.

[2] Balazs, E. A.; Leshchiner, A. Cross-linked gels of hyaluronic acid and products containing such gels. US 4,582,865, December 6, 1984.

[3] Caldwell, C. G.; Wurzburg, O. B. Polysaccharide derivatives of substituted dicarboxylic acids. US 2,661,349, December 1, 1953.

[4] Eenschooten, C.; Christensen, M. W. Aryl/alkyl vinyl sulfone hyaluronic acid derivatives. WO 2007/098770 A1, September 7, 2007.

[5] Tømmeraas, K.; Eenschooten, C. Aryl/alkyl succinic anhydride hyaluronan derivatives. WO 2007/033677 A1, March 29, 2007.

[6] Alkrad, J. A.; Mrestani, Y.; Stroehl, D.; Wartewig, S.; Neubert, R. Characterization of enzymatically digested hyaluronic acid using NMR, Raman, IR, and UV-Vis spectroscopies. *J. Pharm. Biomed. Anal.* **2003**, *31*, 545-550.

[7] Haxaire, K.; Marechal, Y.; Milas, M.; Rinaudo, A. Hydration of polysaccharide hyaluronan observed by IR spectrometry. I. Preliminary experiments and band assignments. *Biopolymers* **2003**, *72*, 10-20.

[8] Pretsch, E.; Buhlmann, P.; Affolter, C. Structure determination of organic compounds. Tables of spectral data. Third edition; Springer: Berlin, 2000.

[9] Welti, D.; Rees, D. A.; Welsh, E. J. Solution conformation of glycosaminoglycans: assignment of the 300-MHz 1H-magnetic resonance spectra of chondroitin 4-sulphate, chondroitin 6-sulphate and hyaluronate, and

investigation of an alkali-induced conformation change. *Eur. J. Biochem.* **1979**, *94*, 505-514.

[10] Pavia, D. L.; Lampman, G. M.; Kriz, G. S. Introduction to spectroscopy. Third edition; Brooks/Cole Cengage Learning: Belmont, 2001.

[11] Cirino, V. O.; Bullock, A. L.; Rowland, S. P. The structure of reagent residues in cotton cellulose treated with divinyl sulfone. *Carbohydr. Res.* **1971**, *17*, 67-78.

[12] Pelletier, S.; Hubert, P.; Lapicque, F.; Payan, E.; Dellacherie, E. Amphiphilic derivatives of sodium alginate and hyaluronate: synthesis and physico-chemical properties of aqueous dilute solutions. *Carbohydr. Polym.* **2000,** *43*, 343-349.

[13] ByersGuideChem (Netvertise, Garbsen, Germany), ChemExpert (Court-St-Etienne, Belgium), ChemIDplus (Advanced, Division of specialized information services, United States national library of medicine, Bethesda, Maryland, United States).

[14] Prilezhaeva, E. N.; Shapiro, E. S. Synthesis based on divinyl sulfone. *Dokl. Akad. Nauk. SSSR* **1967**, *6*, 1345-1348.

B. Optimisation of the preparation of octenyl succinic anhydride-modified hyaluronic acid

Foreword

In order to define the frame of the optimisation work, a preliminary literature study on the preparation of alkenyl succinic anhydride (AlkSA)-modified starch was achieved. The most important conclusions of this study are summarised hereafter.

The succinic anhydride-based modification technology was first patented in 1953 by Caldwell and Wurzburg [1] for the modification of starch with cyclic dicarboxylic acid anhydrides (succinic and glutaric anhydrides). Typically, starch and the reagents were reacted in alkaline sodium carbonate buffers (pH < 11) and at room temperature [1] which led to starch derivatives modified at the polymer's hydroxyl groups.

However, due to competitive reactions, the degree of substitution (DS) of the succinate/glutarate starch derivatives is usually low. Indeed, the modification of starch with anhydrides in aqueous alkaline media is inevitably accompanied by the simultaneous hydrolysis of the reagent molecules and the reverse cleavage of the bonds between starch and the grafted moieties (Figure III.B.i for succinic anhydrides).

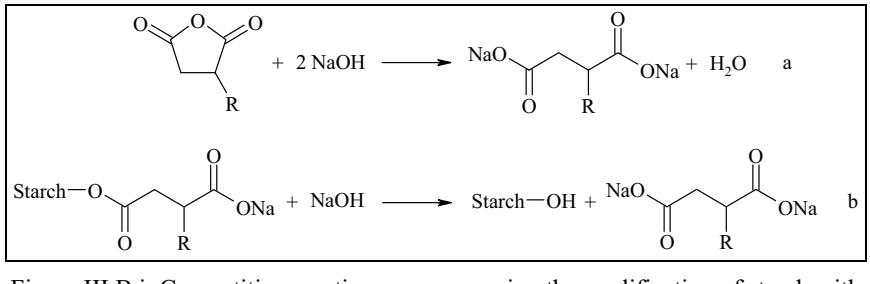

Figure III.B.i: Competitive reactions accompanying the modification of starch with succinic anhydrides in aqueous alkaline media.

In order to improve the DS of succinate/glutarate starch and allow the grafting of a variety of anhydride reagents, it is necessary to limit the extent of the side reactions presented in Figure III.B.i. This can be achieved by finely controlling the reaction conditions and supposes that their influence on the grafting of the anhydride reagents be known.

Most of the literature available on the optimisation of the preparation of modified starch with cyclic dicarboxylic acid anhydrides concerns AlkSA-modified starch. For example, Jeon *et al.* [2], Bhosale and Singhal [3] and Song *et al.* [4] have systematically studied the influence of reaction parameters such as the starch concentration, reagent/starch weight ratio, reaction pH, temperature and time and reagent type on the reaction efficiency (RE*) and DS of AlkSA-starch. Indeed, these parameters potentially all affect, in a more or less complex and/or contradictory fashion, the extent of starch modification.

For example, it may seem desirable to work at high starch concentrations to increase the probability that AlkSA be esterified with starch instead of being hydrolysed. However, concentrated starch suspensions are viscous and can hinder the mixing and diffusion of the AlkSA molecules in the reaction medium. Similarly, one could think that high values of the reaction pH and temperature would enhance the reactivity of the starch hydroxyl groups and the solubility and diffusivity of the AlkSA molecules. However, these conditions can also favour the hydrolysis of AlkSA. It is obvious that sufficiently long reaction times be applied in order to allow the completion of the esterification reactions. Nevertheless, past a certain time the reverse cleavage of the bonds created between starch and alkenyl succinate (AlkS) can occur due to the

*RE is defined as the ratio between the experimental and theoretical DS of the starch derivatives. The theoretical DS is calculated in the hypothetical case where all the reagent molecules added react with starch.

consumption of AlkSA in the esterification and hydrolysis reactions. Finally, the reactivity of AlkSA most likely depends on its chain length.
Consequently, in order to improve the DS of AlkSA-starch, optima for the above-mentioned parameters need to be found.

The reaction parameters tested in references [2] to [4], their range and optima are summarised in Table III.B.i.

Table III.B.i: Optimisation of the preparation of AlkSA-starch.
C(starch), WR, T, t, DDSA and OSA stand for starch concentration, weight ratio, temperature, time, dodecyl succinic anhydride and octenyl succinic anhydride, respectively.

		Jeon *et al.* [2]	Bhosale and Singhal [3]	Song *et al.* [4]
	Starch origin	Waxy corn starch	Amaranth and waxy corn starch	*Indica* rice starch
Reaction parameters	C(starch)	25-65 % w/w	25 % w/w	20-40 % w/w
	AlkSA/starch WR	5-40 % (DDSA)	1-3 % (OSA)	3-15 % (OSA)
	pH	7.5-10.5	7.0-11.0	7.0-10.0
	T	15-45 °C	20-60 °C	25-45 °C
	t	5-95 hours	6-30 hours	2-6 hours
	Alkenyl chain length	8-18 C atoms	8 C atoms	8 C atoms
Optima	C(starch)	no influence	-	35 % w/w
	AlkSA/starch WR	10 % (DDSA)	3 % (OSA)	15 % (OSA)
	pH	8.5-9.0	8.0	8.5
	T	23 °C	30 °C	35 °C
	t	24 hours	6-24 hours	6 hours
	Alkenyl chain length	8 C atoms	-	-
	Maximum DS	4.0 %	2.5 %	4.6 %

The modification methods used in references [2] to [4] were very similar to the original method by Caldwell and Wurzburg [1] and only differed from the latter with regards to the pH control. Typically, AlkSA was progressively added to the starch suspension for 2 hours. The pH was maintained at the desired value by the continuous addition of sodium hydroxide (NaOH). At the end of the reaction, the pH was adjusted to 6.5 with HCl. The resulting AlkSA-starch was filtered, washed and dried.

Despite differences in the starch botanical origin and granule morphology, the results of the studies presented in Table III.B.i were consistent and showed that:

(i) C(starch) had a variable influence on the DS of the derivatives,

(ii) the higher the AlkSA WR, the higher the DS, but the lower the RE,

(iii) the optimal ranges for the reaction pH, T and t were 8.0-9.0, 23-35 °C and 6-24 hours, respectively,

(iv) T above 23 °C did not allow a significant improvement of the DS of the derivatives,

(v) RE and DS decreased rapidly when the alkenyl chain length was increased above 8 carbon atoms,

(vi) finally, the maximum DS of the starch derivatives was approximately 5 % per starch repeating unit.

In references [2] to [4], the reaction parameters tested were varied independently from each other. This method requires that all parameters but one are kept constant and that this parameter is varied until an optimal value is found for it. After the parameter has been set to the optimal value, a second parameter is varied. This is repeated until an optimal value has been found for each of the tested parameters. Although rigorous, this technique exhibits some drawbacks. Firstly, changing one separate parameter at a time does not always lead to the real optimum and gives different implications with different starting points. Secondly, the approach requires a large number of experiments which in turn bring relatively little information

due to the inefficient distribution of the experiments. Finally, this method does not allow detecting interactions between parameters [5].

By contrast, the construction of a carefully prepared set of representative experiments (experimental plan) in which all parameters are simultaneously varied allows drawing more information from fewer experiments and uncovering interactions and synergies between parameters. In addition, this method still permits to evaluate the influence of each separate parameter [5]. Therefore, it is more suitable when screening the parameters mostly influencing the extent of a given chemical reaction.

With this in mind, an experimental plan was used in the following optimisation study which frame was defined based on the conclusions drawn from the optimisation of the preparation of AlkSA-starch.

References

[1] Caldwell, C. G.; Wurzburg, O. B. Polysaccharide derivatives of substituted dicarboxylic acids. US 2,661,349, December 1, 1953.

[2] Jeon, Y. S.; Viswanathan, A.; Gross, R. A. Studies of starch esterification: reactions with alkenyl-succinates in aqueous slurry systems. *Starch/Stärke* **1995**, *51*, 90-93.

[3] Bhosale, R.; Singhal, R. Process optimization for the synthesis of octenyl succinyl derivative of waxy corn and amaranth starches. *Carbohydr. Polym.* **2006**, *66*, 521-527.

[4] Song, X.; He, G.; Ruan, H.; Chen, Q. Preparation and properties of octenyl succinic anhydride modified early *Indica* rice starch. *Starch/Stärke* **2006**, *58*, 109-117.

[5] Montgomery, D. C. Design and analysis of experiments. Sixth edition; Wiley: Hoboken, 2004.

Preparation and structural characterisation of novel and versatile amphiphilic octenyl succinic anhydride-modified hyaluronic acid

Corinne Eenschooten[1,2], Fanny Guillaumie[1], Georgios M. Kontogeorgis[2], Erling H. Stenby[2], Khadija Schwach-Abdellaoui[1].

[1]Novozymes Biopolymer A/S, Krogshøjvej 36, 2880 Bagsværd, Denmark.
[2]Technical University of Denmark, Department of Chemical and Biochemical Engineering, Centre for Phase Equilibria and Separation Processes (IVC-SEP), Building 229, 2800 Lyngby, Denmark.

Abstract

Amphiphilic octenyl succinic anhydride-modified hyaluronic acid (OSA-HA) was prepared in aqueous alkaline media, at room temperature and was structurally characterised by Fourier transform infrared spectroscopy (FT-IR) and proton nuclear magnetic resonance spectroscopy (^{1}H NMR). The influence of reaction parameters such as the HA and buffer concentrations, OSA/HA molar ratio and reaction time on the degree of substitution (DS) of the OSA-HA derivatives was studied by means of an experimental plan. The results showed that the OSA/HA molar ratio, $NaHCO_3$ concentration and interaction between these had the largest influence on the DS of the derivatives while the HA concentration and reaction time only had a negligible effect. The maximum DS achieved was 44 % per disaccharide unit according to ^{1}H NMR. Moreover, optimal reaction conditions were identified for the preparation of versatile OSA-HA derivatives with a DS between 1.5 and 44 %.

Keywords amphiphilic hyaluronic acid derivative, octenyl succinic anhydride, degree of substitution, experimental plan.

I. Introduction

Hyaluronic acid (HA) is a natural linear polysaccharide consisting of D-glucuronic acid and *N*-acetyl-D-glucosamine linked through β-1,3 glycosidic bonds while consecutive repeating disaccharide units are linked through β-1,4 bonds [1] (Figure III.B.1).

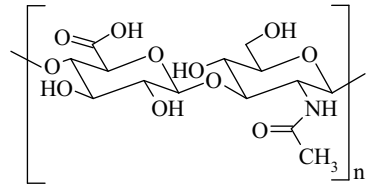

Figure III.B.1: Molecular structure of the HA repeating unit.

HA is found in all vertebrate organs and fluids and is particularly abundant in the extracellular matrix of soft connective tissues [2].

Due to its natural biocompatibility and resorbability, HA is currently one of the most attractive building blocks for the preparation of novel biomaterials with applications in the cosmetic, pharmaceutical and medical industries. However, native HA has limited applications in these fields due to its intrinsic poor mechanical and physicochemical properties [3]. Chemical modifications of HA have therefore been developed to prepare mechanically robust HA derivatives with tailored physicochemical properties.

For example, amphiphilic HA derivatives have been obtained by grafting hydrophobic moieties onto the hydrophilic HA backbone using the carboxyl and hydroxyl functions of the polymer [3]. The resulting derivatives, which possess an altered aqueous solubility compared to native HA [4,5,6], potentially represent attractive starting materials for the formulation of self-associative HA-based systems towards drug encapsulation and delivery.

However, the modification methods currently available for the preparation of amphiphilic HA present some drawbacks. Firstly, the modification reactions are often conducted in organic solvents or organic solvent/water mixtures [7,8,9]. In addition to raise occupational and environmental issues and limit the upscalability of the preparation method, the use of organic solvents or mixtures of these often requires converting HA into its tetraalkylammonium salt [10,11] or preparing reactive intermediates [10,12]. This not only adds complex steps to the preparation method but also often results in HA degradation [4,8]. Secondly, the modification reactions involving HA carboxyl groups modify the distribution of negative charges along the polymer backbone at neutral pH. This could potentially affect some of the attractive biological and/or pharmacological properties of native HA [13].
Therefore, simple modification reactions in aqueous media, under mild conditions and exclusively involving HA hydroxyl groups could represent advantageous alternatives for the preparation of amphiphilic HA derivatives.

In this regard, a novel, simple and easily upscalable modification method for the preparation of amphiphilic HA was previously developed in our laboratories which is based on the reaction between HA and octenyl succinic anhydride (OSA) in aqueous mild alkaline media [14].
The objective of the present work was to optimise this method and prepare versatile HA derivatives with tailored and extended degrees of substitution (DS). To achieve this, an experimental plan was implemented in which four different reaction parameters were simultaneously varied and their influence on the DS of the OSA-HA derivatives was detailedly studied. The chemical structure of the derivatives was characterised by Fourier transform infrared spectroscopy (FT-IR) and proton nuclear magnetic resonance spectroscopy (^{1}H NMR).

II. Materials and methods

II.1. Materials

Medium molecular weight (MW) HA (HyaCare®, MW~750,000 Da, HA750) was provided by Novozymes Biopolymer A/S (Bagsværd, Denmark). Low MW HA (HA20) was prepared using the procedure described hereafter. Octenyl succinic anhydride (OSA, 210.27 Da, purity ≥ 97 %, mixture of *cis* and *trans*) was obtained from Sigma-Aldrich (Saint Louis, Missouri, United States). Sodium bicarbonate ($NaHCO_3$) and potassium bromide (KBr) were used as purchased without further purification. The water used for the sample preparation and analysis was distilled and purified to a resistivity of 18.2 MΩ.cm in a milli-Q apparatus (Millipore, Billerica, Massachusetts, United States).

II.2. Methods

II.2.1. Preparation of low molecular weight hyaluronic acid

HA20 was prepared using the same method as that described for HA300 (see section A of this chapter, § II.2.1) but with 250 mL of H_3PO_4 and a 24-hour incubation time. Approximately 56 g of HA20, *i.e.* 80 % of the starting HA750 were recovered.

SEC-MALLS

The exact MW of HA20 was 19,090 ± 191 Da.

FT-IR

(KBr, 4000-500 cm^{-1}) w 3431 (O–H and N–H st), 2931 (C–H st), 1700-1600 (COO^- st as, N–H bd), 1423 (COO^- st sy), 1392 (C–O–H bd), 1154 (C–O–C st as), 1077 and 1038 (C–OH st), 954 and 900 (COO^- bd), 808 (C–O–C st sy).

^{1}H NMR

(D_2O, 400 MHz) δ 2.0 (s, 3 H, H-m), 3.2-4.0 (m, 10 H, H-2, H-5', H-4', H-3, H-3', H-5, H-6'b, H-4, H-6'a, H-2), 4.3-4.7 (d, 2 H, H-1, H-1') (see Figure III.B.3).

II.2.2. Preparation of octenyl succinic anhydride-modified hyaluronic acid

HA20 was first dissolved in milli-Q water (50 mL) for 6 hours, at room temperature. $NaHCO_3$ was added to the HA solution and mixed for 1 hour, at room temperature. A NaOH solution (0.5 M) was prepared from concentrated NaOH (4 M) by dilution in milli-Q water. The pH of the HA solution was measured and, if necessary, adjusted to 8.5 with NaOH (0.5 M). OSA was added drop-wise to the alkaline HA solution with a volumetric pipette, under vigorous agitation. The mixture was then stirred for the desired time, at room temperature. The resulting product was dialysed against milli-Q water as described in section A of this chapter, § II.2.2.
The reaction parameters studied in the experimental plan and their ranges are reported in Table III.B.1.

Table III.B.1: Reaction parameters and ranges used in the experimental plan.
C(HA), C($NaHCO_3$), OSA/HA MR and t stand for the HA and $NaHCO_3$ concentrations, OSA/HA molar ratio and reaction time, respectively. The number of moles of HA was expressed in terms of number of moles of repeating disaccharides units. For the calculations the MW of one disaccharide unit was approximated to 400 Da.

Reaction parameter	Range
C(HA)	5-25 mg/mL
C($NaHCO_3$)	0.2-1.0 M
OSA/HA MR	1-20
t	6-24 hours

The combinations of reaction conditions tested (see Table III.B.2) were determined using an experimental planning software (MODDE 8; Umetrics, Umeå, Sweden) and a two-level interaction full factorial design. The experimental DS values were fitted with a "linear plus interaction model" using a partial least square (PLS) regression analysis. The accuracy of the model was determined by separating the residual sum of squares into pure error (experimental error) and lack of fit.

^{1}H NMR

(D_2O, 400 MHz) δ 0.9 (s, 3 H, H-10''), 1.3 (m, 6 H, H-7''-H-9''), 1.4-1.8 (m, 2 H, H-6''), 2.0 (s, 3 H, H-m), 2.2-3.0 (m, 5 H, H-1''-H-3''), 3.4-4.2 (m, 10 H, H-2, H-5', H-4', H-3, H-3', H-5, H-6'b, H-4, H-6'a, H-2), 4.6-4.8 (d, 2 H, H-1, H-1'), 4.9-5.7 (m, 2 H, H-4'', H-5'') (see Figure III.B.4).

II.2.3. Characterisation methods

(see section A of this chapter, § II.2.4 for SEC-MALLS, FT-IR and ^{1}H NMR)

III. Results and discussion

III.1. Characterisation of octenyl succinic anhydride-modified hyaluronic acid

OSA-HA was prepared by reacting HA and OSA in aqueous mild alkaline media, at room temperature (see section A of this chapter, Figure III.A.6).

Due to the linear structure of HA, the products obtained can be regarded as fishbone-like polymers consisting of a hydrophiphilic HA backbone and a number of hydrophobic octenyl succinate (OS) side chains which depends on the degree of substitution of the derivative (Figure III.B.2).

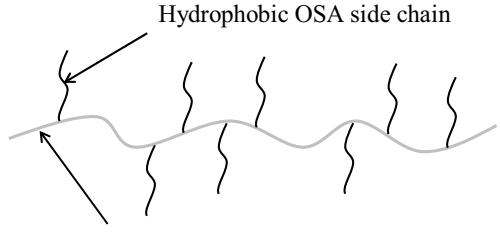

Figure III.B.2: Scheme of the fishbone structure of OSA-HA.

The structure of the OSA-HA derivatives was qualitatively studied by FT-IR by comparing the spectra of native HA20 and of the derivatives. However, these spectra did not show any significant differences, independently of the DS of the derivatives. This lack of difference was probably due the overlapping of the characteristic bands of HA20 and OSA-HA (see section A of this chapter, § III.2). As a result, FT-IR could not confirm the modification of HA with OSA.

^{1}H NMR, however, proved efficient in demonstrating the grafting of OSA onto HA and was used to calculate the DS of the OSA-HA derivatives. The spectrum of native HA20 is presented in Figure III.B.3 while that of OSA-HA (8) (see Table III.B.2 for a definition of the notation) is shown as an example in Figure III.B.4. Due to peak overlapping in the region 3.2-4.0 ppm, it was not possible to clearly assign the shifts of protons 3 to 5 and 2' to 6'.

The spectrum of OSA-HA (8) showed an additional singlet at 0.9 and a multiplet at 1.3 ppm. The former corresponds to the terminal methyl protons 10'' and the latter to the methylene protons 7'' to 9'' on the octenyl chain of grafted OS. Due to the low signal intensity in the regions 1.4-1.8, 2.2-3.0 and 4.9-5.7 ppm, it was not possible to clearly assign the chemical shifts of protons 1'' to 6''.

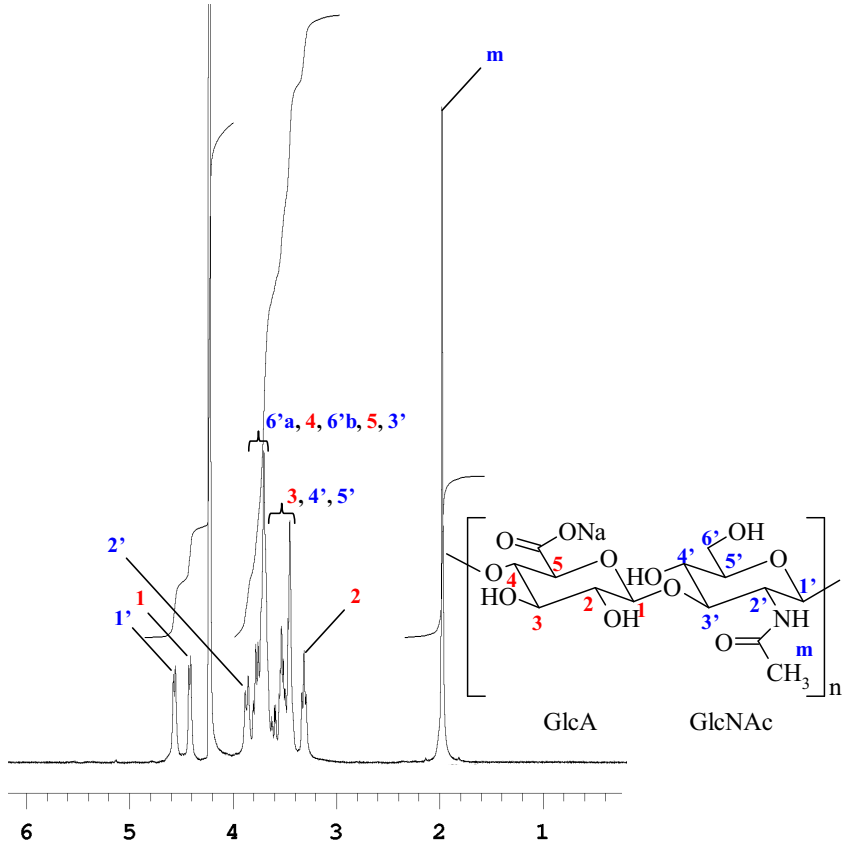

Figure III.B.3: ^{1}H NMR spectrum of HA20.

However, in the group of protons 1'' to 3'' and 6'', the methylene protons 6'' are expected to occur most upfield, possibly in the region 1.4-1.8 ppm due their farthermost position with respect to the anisotropic fields of the carboxylate and ester groups. Conversely, the methylene protons 1'' and the methine proton 2'' are expected to occur most downfield in the region 2.2-3.0 ppm due their closest position with respect to these fields. Finally, the vinyl proton 4'' should appear downfield of the vinyl proton 5'' for a similar reason.

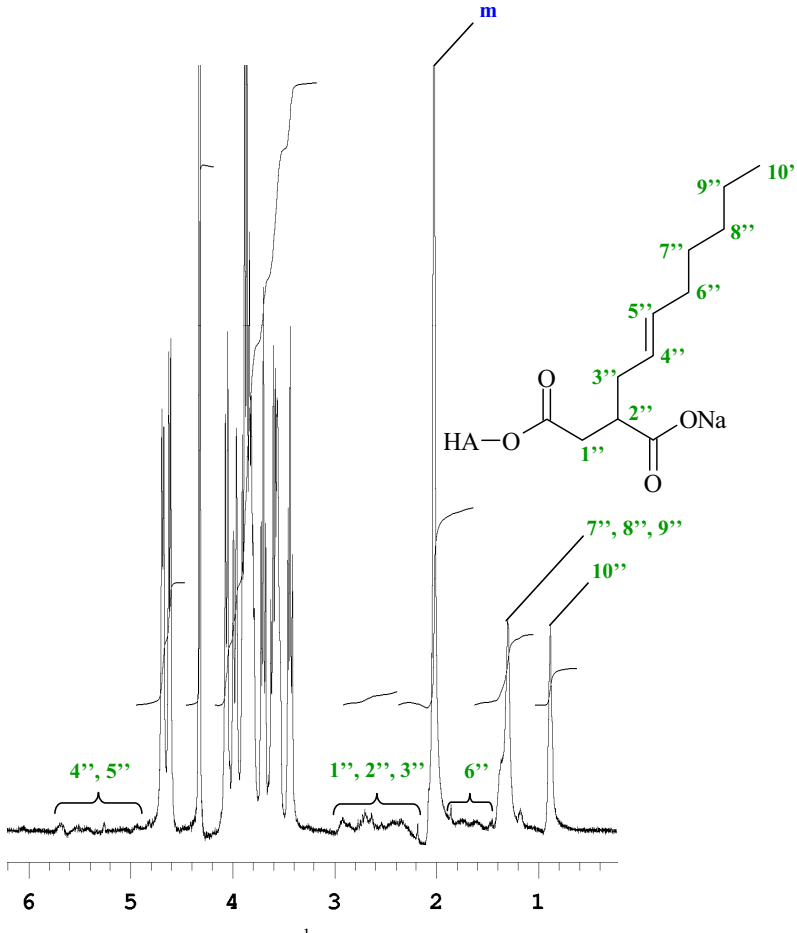

Figure III.B.4: ^{1}H NMR spectrum of OSA-HA (8).

It is noteworthy that the signal of protons 1'' to 6'' is higher than that observed for OSA-HA30 (2) (see section A of this chapter, Figure III.A.8). This is probably due to the higher DS of OSA-HA (8) which was 18 % per disaccharide unit (see Table III.B.2).

Similar spectra were observed for the other OSA-HA derivatives. However, the relative intensity of the singlet at 0.9 ppm and therefore the DS of the derivatives were dependent on the reaction conditions.

III.2. Influence of the reaction conditions on the degree of substitution of octenyl succinic anhydride-modified hyaluronic acid

In order to identify the reaction parameters mostly influencing the DS of the OSA-HA derivatives, an experimental plan (2-level interaction full factorial design) was implemented in which four different reaction parameters were simultaneously varied.

The frame of this experimental plan was defined based on a preliminary literature study on the optimisation of the preparation of alkenyl succinic anhydride (AlkSA)-modified starch [15,16,17] (see Foreword). According to the conclusions of this study, the following settings were applied:

(i) the reaction pH was set to 8.5 and was maintained at this value using a sodium bicarbonate ($NaHCO_3$) buffer,

(ii) the reaction temperature was between 20 and 23 °C (room temperature),

(iii) the reaction parameters studied were the HA and buffer concentrations, OSA/HA molar ratio and reaction time,

(iv) these were varied between 5 and 25 mg/mL, 0.2 and 1.0 M, 1 and 20 and 6 and 24 hours, respectively (see Table III.B.1),

(v) the starting HA used had a molecular weight of 20,000 Da.

The choice of working with low MW HA was made in the perspective of the potential future applications of the OSA-HA derivatives, namely their use for the formulation of nanocarriers.

Kawaguchi *et al*. [7] have indeed shown that the emulsification capacity of palmitoyl chloride-modified HA prepared from 20,000-Da HA (P-HA20, DS = 3 % per

disaccharide unit) was clearly superior to that of the same HA derivative prepared from 2,000,000 Da-HA (P-HA2000). The emulsification of soybean oil and liquid paraffin (5 % w/v) with P-HA20 yielded stable emulsions in which the average oil droplet size was 315 ± 98 and 341 ± 79 nm, respectively. However, when P-HA2000 was used rather instable emulsions were formed which almost immediately phase-separated in the case of liquid paraffin. P-HA20 had a better emulsification capacity than P-HA2000 most likely due to its ability to move faster to interfaces and stabilise smaller oil droplets.

Similarly, Mohapatra *et al.* [18] experienced that the use of 20,000- to 40,000-Da HA for the production of HA nanoparticles by cross-linking in w/o emulsions could reduce the particle size from 160 nm to between 10 to 40 nm. This size reduction was most likely due to the formation of smaller HA-containing water droplets owing to the lower viscosity of low MW HA solutions.

Therefore, it is believed that the use of low MW HA as starting material will be an important factor for the formation of future nanocarriers from OSA-HA.

The low, medium and high levels of the four reaction parameters studied were associated into 17 different combinations including a centre point which was replicated four times in order to calculate the experimental error. This brought the total number of samples to 20. The DS of the resulting OSA-HA derivatives was determined by ^{1}H NMR (see § II.2.3 and Table III.B.2).

The DS of the OSA-HA derivatives was between 1.5 and 18 % per disaccharide unit and the two combinations of reaction conditions allowing a DS of 18 % were those of OSA-HA (8) and OSA-HA (15) (also highlighted in grey in Table III.B.2), *i.e.* when the OSA/HA MR and buffer concentration were the highest.

The DS values of the four replicates OSA-HA (17), (18), (19) and (20), which were prepared on different days, were very similar which indicated a general good reproducibility of the experiments.

Table III.B.2: Reaction conditions and degree of substitution of the OSA-HA derivatives.

$C(NaHCO_3)$, C(HA), OSA/HA MR and t stand for the $NaHCO_3$ and HA concentrations, OSA/HA molar ratio and reaction time, respectively.

Sample name	Reaction conditions				DS
	$C(NaHCO_3)$ (M)	C(HA) (mg/mL)	OSA/HA MR	t (hours)	
OSA-HA (1)	0.2	5	1	6	3.5
OSA-HA (2)	0.2	25	1	6	2.5
OSA-HA (3)	0.2	5	20	6	10
OSA-HA (4)	0.2	25	20	6	7
OSA-HA (5)	1.0	5	1	6	1.5
OSA-HA (6)	1.0	25	1	6	2
OSA-HA (7)	1.0	5	20	6	16
OSA-HA (8)	1.0	25	20	6	18
OSA-HA (9)	0.2	5	1	24	3
OSA-HA (10)	0.2	25	1	24	4
OSA-HA (11)	0.2	5	20	24	13
OSA-HA (12)	0.2	25	20	24	8
OSA-HA (13)	1.0	5	1	24	4
OSA-HA (14)	1.0	25	1	24	2
OSA-HA (15)	1.0	5	20	24	18
OSA-HA (16)	1.0	25	20	24	17
OSA-HA (17)	0.6	15	10.5	15	6
OSA-HA (18)	0.6	15	10.5	15	7
OSA-HA (19)	0.6	15	10.5	15	6
OSA-HA (20)	0.6	15	10.5	15	7.5

The initial coefficient plot showed that only a few parameters and combinations of parameters had a significant influence on the DS of the OSA-HA derivatives, namely the OSA/HA molar ratio, $NaHCO_3$ concentration and interaction between these. Indeed, the amplitude of the confidence intervals for these parameters was much lower than the magnitude of their associated coefficients. This was due to the fact the OSA/HA molar ratio is directly related to the number of available reagent molecules and the $NaHCO_3$ concentration is associated to the buffering capacity of the reaction medium which needs to be sufficient in order to maintain an alkaline pH (8.5) for the activation of the HA hydroxyl groups.

The HA concentration and reaction time had little influence on the DS of the OSA-HA derivatives (see for example OSA-HA (7) and OSA-HA (8) on the one hand and OSA-HA (8) and OSA-HA (16) on the other hand). This suggested that the viscosity of the 25-mg/mL HA solutions did not hinder the mixing and diffusion of the OSA molecules nor limit the competitive hydrolysis of OSA more than the 5-mg/mL HA solutions. This means that OSA-HA can be prepared from relatively concentrated HA solutions without compromising the extent of the modification. Finally, increasing the reaction time from 6 to 24 hours did not result in higher DS values which suggested that the reactions between HA and OSA were already completed after 6 hours.

After elimination of the parameters and combinations of parameters insignificantly influencing the DS of the OSA-HA derivatives, the experimental DS values were fitted with a linear plus interaction model using a PLS regression analysis. The model was evaluated by means of calculating four different coefficients: the regression (R2) and prediction (Q2) coefficients, the model validity (MV) and the reproducibility coefficient (RC) (Figure III.B.5). The high values of R2, Q2, MV and RC suggested that the choice of the mathematical model used to modelise the influence of the reaction conditions on the DS of the OSA-HA derivatives was justified and suitable.

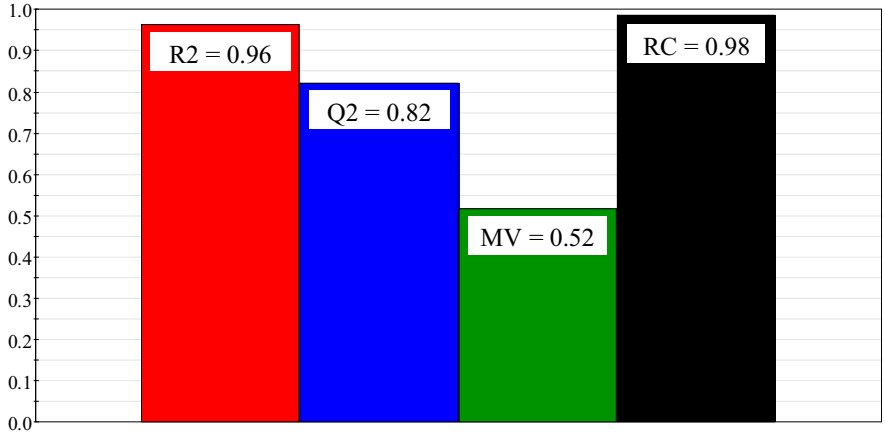

Figure III.B.5: Evaluation of the model used to fit the DS of the OSA-HA derivatives.

R2 and Q2 are measures of fit and prediction of new data from the model according to cross-validations, respectively. MV is a measure of the validity of the model. When MV is larger than 0.25 (which is the case here), the model error is in the same range as the experimental error. RC is an assessment of the reproducibility of the response under the same conditions (experimental error).

Therefore, a contour plot of the DS of the OSA-HA derivatives as a function of the OSA/HA molar ratio and $NaHCO_3$ concentration was computed and is presented in Figure III.B.6.

As already observed, the contour plot predicts that the highest DS values are obtained for the highest OSA/HA molar ratio and buffer concentration, typically 20 and 1.0 M, respectively. Indeed, the higher the OSA/HA molar ratio, the larger the number of OSA molecules available for reaction. Likewise, the higher the $NaHCO_3$ concentration, the greater the buffering capacity and consequently the longer the activation of HA hydroxyl groups.

Interestingly, when a higher OSA/HA molar ratio (50) and $NaHCO_3$ concentration (2.0 M) were used (the HA concentration and reaction time were 25 mg/mL and 24 hours, respectively), the DS of the resulting OSA-HA derivatives

could be increased to 44 % which demonstrated that the OSA modification technology was very versatile. Moreover, this maximum DS was much higher than that reported for OSA-starch which does not exceed 5 % per repeating unit [15,16,17] (see Foreword).

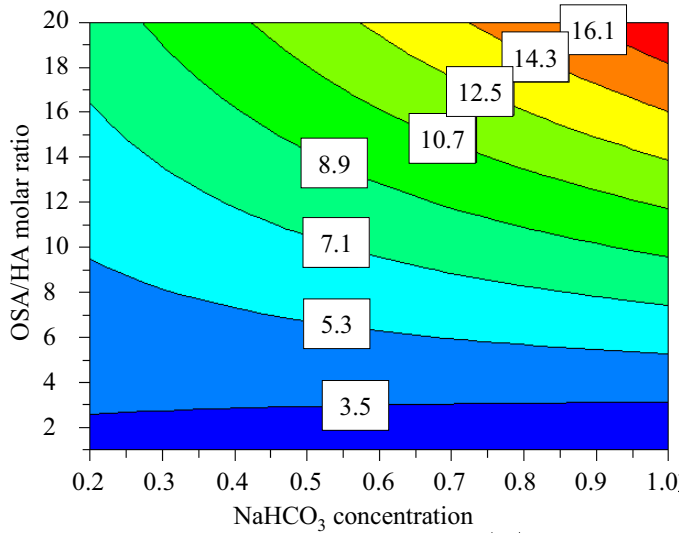

Figure III.B.6: Contour plot of the DS of the OSA-HA derivatives (C (HA) = 15 mg/mL).

IV. Conclusion

Amphiphilic hyaluronic acid derivatives were prepared using a simple water-based modification method targeting the HA hydroxyl groups thus preserving the carboxyl groups of the polysaccharide.

HA was alkenylated with octenyl succinic anhydride to yield fishbone-like OSA-HA polymers and the influence of reaction parameters such as the HA and buffer

($NaHCO_3$) concentrations, OSA/HA molar ratio and reaction time on the degree of substitution of the OSA-HA derivatives was studied by means of an experimental plan. The results showed that the OSA/HA molar ratio, $NaHCO_3$ concentration and interaction between these had the largest influence on the DS of the derivatives while the HA concentration and reaction time only had a negligible effect.

Combinations of reaction conditions allowing the preparation of OSA-HA derivatives with a DS between 1.5 and 44 % per disaccharide unit according to ^{1}H NMR were identified. This represents a wide DS range compared to that reported for OSA-starch (DS < 5 % per repeating unit) and shows that the OSA modification technology is very versatile.
Moreover, it was demonstrated that the reactions were fast (6 hours) and could be conducted in relatively concentrated HA solution (25 mg/mL). These aspects could potentially represent advantages in terms of volume and through-put in the perspective of upscaling the method.

The introduction of octenyl chains onto HA is expected to alter the properties of the native polymer and especially its solution properties. These, together with the detailed structure of OSA-HA, were investigated in the following section.

References

[1] Weissman, B.; Meyer, K. The structure of hyalobiuronic acid and of hyaluronic acid from umbilical cord. *J. Am. Chem. Soc.* **1954**, *76*, 1753-1757.

[2] Baier Leach, J.; Schmidt, C. E. Hyaluronan. In *Encyclopaedia of biomaterials and biomedical engineering*; Wnek, G. E.; Bowlin G. L., Eds.; Marcel Dekker: New York, 2004; pp 779-789.

[3] Vercruysse, K. P., Prestwich, G. D. Hyaluronate derivatives in drug delivery. *Crit. Rev. Ther. Drug Carrier Syst.* **1998**, *15*, 513-555.

[4] Pelletier, S.; Hubert, P.; Lapicque, F.; Payan, E.; Dellacherie, E. Amphiphilic derivatives of sodium alginate and hyaluronate: synthesis and physico-chemical properties of aqueous dilute solutions. *Carbohydr. Polym.* **2000**, *43*, 343-349.

[5] Creuzet, C.; Kadi, S.; Rinaudo, M.; Auzély-Velty, R. New associative systems based on alkylated hyaluronic acid. Synthesis and aqueous solution properties. *Polymer* **2006**, *47*, 2706-2713.

[6] Mlcochova, P.; Bystricky, S.; Steiner, B.; Machova, E.; Koos, M.; Velebny, V.; Krcmar, M. Synthesis and characterization of new biodegradable hyaluronan alkyl derivatives. *Biopolymers* **2006**, *82*, 74-79.

[7] Kawaguchi, Y.; Matsukawa, K.; Gama, Y.; Ishigami, Y. New polysaccharide surfactants from hyaluronates. *Chemistry Express* **1991**, *6*, 647-650.

[8] Bergman, K.; Elvingson, C.; Hilborn, J.; Svensk, G.; Bowden, T. Hyaluronic acid derivatives prepared in aqueous media by triazine-activated amidation. *Biomacromolecules* **2007**, *8*, 2190-2195.

[9] Mlcochova, P.; Hajkova, V.; Steiner, B.; Bystricky, S.; Koos, M.; Medova, M.; Velebny, V. Preparation and characterization of biodegradable alkylether derivatives of hyaluronan. *Carbohydr. Polym.* **2007**, *69*, 344-352.

[10] Della Valle, F.; Romeo, A. Esters of hyaluronic acid. US 4,851,521, July 25, 1989.

[11] Salvatore, F. S.; Pitarresi, G.; Mandracchia, D.; Tripodo, G.; Giammona, G. New graft copolymers of hyaluronic acid and polylactic acid: synthesis and characterization. *Carbohydr. Polym.* **2006**, *66*, 379-385.

[12] Bulpitt, P.; Aeschlimann, D. New strategy for chemical modification of hyaluronic acid: preparation of functionalized derivatives and their use in the formation of novel biocompatible hydrogels. *J. Biomed. Mater. Res.* **1999**, *47*, 152-169.

[13] Benesova, K.; Pekar, M.; Lapcik, L.; Kucerik, J. Stability evaluation of *n*-alkyl hyaluronic acid derivatives by DSC and TG measurement. *J. Therm. Anal. Calorim.* **2006**, *83*, 341-348.

[14] Tømmeraas, K.; Eenschooten, C. Aryl/alkyl succinic anhydride hyaluronan derivatives. WO 2007/033677 A1, March 29, 2007.

[15] Jeon, Y. S.; Viswanathan, A.; Gross, R. A. Studies of starch esterification: reactions with alkenyl-succinates in aqueous slurry systems. *Starch/Stärke* **1995**, *51*, 90-93.

[16] Bhosale, R.; Singhal, R. Process optimization for the synthesis of octenyl succinyl derivative of waxy corn and amaranth starches. *Carbohydr. Polym.* **2006**, *66*, 521-527.

[17] Song, X.; He, G.; Ruan, H.; Chen, Q. Preparation and properties of octenyl succinic anhydride modified early *Indica* rice starch. *Starch/Stärke* **2006**, *58*, 109-117.

[18] Mohapatra, S. S.; Sahoo, B.; Kumar, A.; Behera, S. A method of transdermal drug delivery using hyaluronic acid nanoparticles. US 2007/0036728 A1, September 27, 2007.

C. Additional characterisation of octenyl succinic anhydride-modified hyaluronic acid – Substitution pattern, molecular weight and conformation in aqueous media

Abstract

The substitution pattern, molecular weight (MW) and conformation in aqueous media of octenyl succinic anhydride-modified hyaluronic acid (OSA-HA) were investigated by high performance liquid chromatography (HPLC), matrix-assisted laser desorption/ionisation–time-of-flight–mass spectrometry (MALDI-TOF-MS), nuclear magnetic resonance spectroscopy (NMR) and multi-angle laser light scattering (MALLS). Although these studies were not performed under optimal conditions due to experimental difficulties related to the purification and/or intrinsic nature of the samples, the results suggested that the substitution pattern of OSA-HA was most likely (i) random at the molecular level, *i.e.* all HA hydroxyl groups were potential targets for the grafting of OSA, and (ii) heterogeneous at the macromolecular level due to the biphasic nature of the reaction between HA and OSA. It was also shown that OSA-HA underwent a major conformation change in aqueous media at a concentration which was dependent on its degree of substitution. However, it was not possible to unequivocally evidence the presumed randomness of the grafting of OSA at the molecular level or determine the MW, monomolecular size and affinity for the solvent of the OSA-HA derivatives.

I. Introduction

Previously in this chapter, the grafting of octenyl succinic anhydride (OSA) onto hyaluronic acid (HA) was represented as potentially occurring on any of the four hydroxyl groups of the HA repeating disaccharide unit (see section A of this chapter,

Figure III.A.6). However, this had not analytically been confirmed. Likewise, the macromolecular distribution of the octenyl succinate (OS) chains along the HA backbone had not been investigated. Knowledge of the substitution pattern of OSA-HA would yet be useful in order to understand the reaction mechanism between HA and OSA and could potentially be exploited to describe some aspects of the solution and physicochemical behaviour of OSA-HA.

Also reported earlier, the molecular weight (MW) of the OSA-HA derivatives could not be determined by size exclusion chromatography–multi-angle laser light scattering (SEC-MALLS) due to their strong retention on the stationary phase of the fractionation column (see section A of this chapter, § III.2). Knowledge of the MW of the OSA-HA derivatives would yet be valuable in order to assess MW degradation during their preparation and could be used to both evidence the modification of HA with OSA and cross-validate the degree of substitution (DS) values determined by proton nuclear magnetic resonance spectroscopy (^{1}H NMR).

The introduction of OSA onto HA is expected to alter the solution properties of the native polymer and in particular the compactedness of its conformation in aqueous media, in the dilute regime, due to the intramolecular hydrophobic interactions between the grafted OS chains of the same OSA-HA molecule and the lower affinity of OSA-HA for aqueous solvents. It is important to evidence these new solutions properties and put them into perspective with that of semi-dilute and concentrated OSA-HA solutions (see Chapter IV) in order to get a continuous understanding of the polymers' behaviour in aqueous media.

In view of the above-mentioned unknowns, the objectives of this work were to study the substitution pattern of OSA-HA and determine the MW, monomolecular size and affinity for aqueous solvents of the OSA-HA derivatives.

Focus was drawn on uncovering which type of HA hydroxyl groups are involved in the reaction with OSA and how the OS chains are distributed along the HA backbone. It was also attempted to develop a method allowing the measurement of intrinsic properties such as MW, root mean square radius (R_{rms}) and osmotic second virial coefficient (A_2) but avoiding the use of the SEC-MALLS fractionation column.

The structural study at the molecular level was performed by master student, Sara Sparre Kofoed, co-supervised by associate professor Charlotte Held Gotfredsen (Technical University of Denmark, Department of Chemistry, Lyngby, Denmark) and Ph.D. student Corinne Eenschooten. The reader is referred to the master thesis [1] for the extensive study and only a few illustrative elements and the main conclusions of the work will be presented hereafter.

II. Materials and methods

A detailed *Materials and methods* section is available from [1] and only the materials and methods used for the SEC-MALLS study are described hereafter.

II.1. Materials

The 20,000-Da HA (HA20) and the OSA-HA derivatives (OSA-HA6, -18 and -44) used were prepared as described in section B of this chapter, § II.2.1 and II.2.2. Sodium chloride (NaCl), potassium chloride (KCl), disodium hydrogen phosphate (Na_2HPO_4) and potassium dihydrogen phosphate (KH_2PO_4) were used as purchased without further purification. The water used for the sample preparation and analysis was distilled and purified to a resistivity of 18.2 MΩ.cm in a milli-Q apparatus (Millipore, Billerica, Massachusetts, United States).

II.2. Methods

The MW, R_{rms} and A_2 of HA20 and of the OSA-HA derivatives were determined in a phosphate buffer saline (PBS, pH = 7.4) which was prepared as followed: NaCl (8.0 g), KCl (0.2 g), Na_2HPO_4 (1.4 g) and KH_2PO_4 (0.2 g) were first dissolved in milli-Q water (1 L) for 1 hour, at room temperature. The pH of the mixture was then measured and, if necessary, adjusted to 7.4 with HCl (0.2 M) or NaOH (0.2 M). The resulting buffer was finally filtered through glass microfiber filters (GF/F 1825 110, porosity 0.7 µm; Whatman, Maidstone, United Kingdom). HA20 was dissolved in PBS for 16 hours (overnight) at the following concentrations: 0.5, 1, 1.5, 2, 3 and 4 g/L. OSA-HA was dissolved in PBS for 16 hours (overnight) at concentrations between 0.001 and 1 g/L. The OSA-HA solutions with a concentration superior or equal to 0.1 g/L were prepared from the 1-g/L solution. Each of the remaining solutions was prepared from the 10-fold more concentrated solution by mixing 1 g of the latter with 9 g of PBS. The dilutions of each HA and OSA-HA sample were injected in a queue directly in the MALLS cell (DAWN EOS; Wyatt Technology Corporation, Santa Barbara, California, United States) using a 5-mL plastic syringe mounted on a filter (Minisart®plus, porosity 0.45 µm; Sartorius, Göttingen, Germany). During each injection, the flow rate was maintained at 25 mL/h using a syringe pump (A-99; Razel Scientific Instruments, Stanford, Connecticut, United States). After injection of about 2 mL of the dilution to be tested, the flow was then stopped and measurements were allowed to take place for 2 min or until voltage plateaus were stable over 2 consecutive minutes. Experiments were repeated 3 times per sample. The variation of the polymer solution refractive index n as a function of the polymer concentration c (dn/dc) was set to 0.153 mL/g for HA. As a first approximation, the same dn/dc value was used for OSA-HA. The MALLS instrument was piloted by the software ASTRA 5.3.1.4 (Wyatt Technology Corporation, Santa Barbara, California, United States). The MW, R_{rms} and A_2 of HA20 and of the OSA-HA derivatives were calculated from Equation III.C.1 by extrapolation at a low scattering angle and concentration [2]:

$$\frac{Kc}{R(\theta,c)} = \frac{1}{MW_w P(\theta)} + 2A_2 c \qquad \text{Equation III.C.1}$$

where:

(i) K is the constant $\frac{4\pi^2\left(\frac{dn}{dc}\right)^2 n_o^{\,2}}{N_A \lambda_0^{\,4}}$ Equation III.C.2

for which n is the refractive index of the polymer solution, c the polymer concentration, n_0 the refractive index of the solvent, N_A Avogadro's number and λ_0 the wavelength of the laser light in vacuum,

(ii) R(θ,c) is the excess Rayleigh ratio of the solution as a function of the scattering angle θ and the polymer concentration c,

(iii) MW_w is the weight-averaged molecular weight,

(iv) P(θ) is the angular dependence of the scattered intensity as a function of the particle size. The expansion of P(θ) to the first order gives:

$$P(\theta) = 1 - \frac{16\pi^2 n_0^{\,2}}{3\lambda_0^{\,2}} \sin^2\left(\frac{\theta}{2}\right)\left\langle R_{rms}^{\,2}\right\rangle \qquad \text{Equation III.C.3}$$

for which R_{rms} is the root mean square radius of the particles,

(v) A_2 is the osmotic second virial coefficient.

III. Results and discussion

III.1. Structural study

The substitution pattern of OSA-HA is twofold; first the type of HA hydroxyl groups involved in the reaction with OSA (molecular level) and secondly the distribution of the OS chains along the HA backbone (macromolecular level).

III.1.1. Molecular level

It is usually assumed that the primary hydroxyl groups of saccharides are appreciably more reactive than the secondary ones [3]. This suggests that the grafting of OSA preferentially occurs at the HA primary hydroxyl groups. However, the grafting of OSA onto starch has been reported to occur both at the starch primary and secondary hydroxyl groups [4,5]. Therefore, it was judged relevant to investigate which HA hydroxyl groups are involved in the reaction with OSA in order to improve the understanding of the reaction mechanism between HA and OSA and the properties of the OSA-HA derivatives.

The grafting of OSA onto HA was investigated by various NMR techniques. Indeed, the replacement of HA hydroxyl protons with OSA is expected to alter the chemical shifts of the axial and hydroxymethylene protons and those of the sugar ring carbon atoms on HA. However, these shift differences cannot be identified on the spectra of the ~20,000-Da OSA-HA derivatives due the broad and overlapping resonances yielded by these macromolecules. Therefore, the NMR study was conducted on OSA-HA oligosaccharides. These were obtained by either reacting HA oligosaccharides and OSA or enzymatically digesting OSA-HA into oligosaccharides. Prior to the NMR study, the various OSA-HA fractions were characterised by high performance liquid chromatography (HPLC) and matrix-assisted laser desorption/ionisation–time-of-flight–mass spectrometry (MALDI-TOF-MS).

In order to obtain HA oligosaccharides on which OSA would be grafted, medium MW HA (MW~650,000 Da) was enzymatically digested with *Streptomyces hyaluronlyticus* hyaluronidase in a sodium acetate (NaOAc) buffer, at pH 6.0 and 50 degrees, for 8 hours. The digestion mixture was sampled after 4, 6 and 8 hours of digestion and analysed by HPLC (Figure III.C.1).

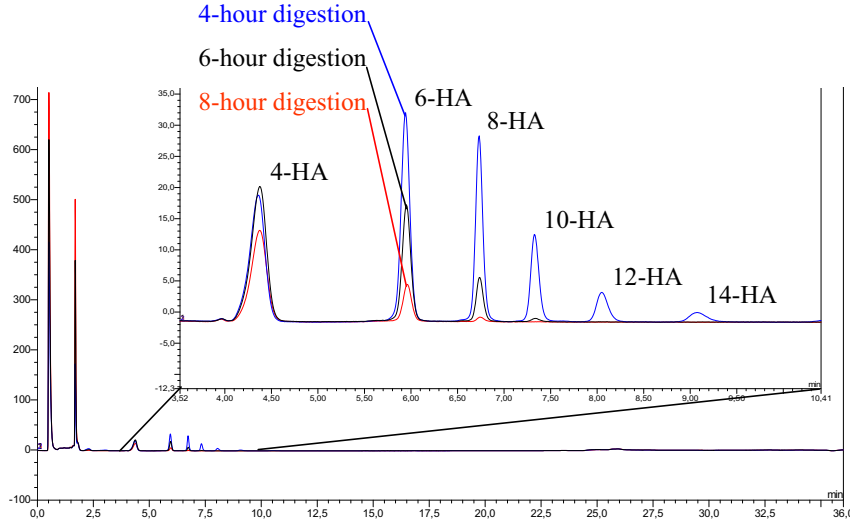

Figure III.C.1: HPLC chromatograms of the digestion mixture.

4-, 6-, 8-, 10-, 12-, 14-HA stand for HA tetra-, hexa-, octa-, deca-, dodeca- and tetradecasaccharide, respectively.

An analysis of a mixture of the NaOAc buffer and deactivated enzyme showed that the peaks between 0 and 3.5 min could be attributed to the digestion system. Those between 3.5 and 9.5 min most probably corresponded to the elution of the HA oligosaccharides in the order 4-, 6-, 8-, 10-, 12- and 14-HA. Indeed, it has been shown that the shortest HA oligosaccharide produced by *Streptomyces hyaluronlyticus* hyaluronidase consist of four sugar units [6]. The expanded portion of the superimposed chromatograms showed that the proportion of the oligosaccharides larger than 4-HA decreased over time and that almost only 4- and 6-HA were left in the digestion mixture after 8 hours which evidenced that the digestion method used was fairly selective.

The composition of the digestion mixture after 8 hours was confirmed by MALDI-TOF-MS in positive reflective mode using a desalted sample. The HA oligosaccharides were mainly detected as their sodium salts (Table III.C.1).

Table III.C.1: MALDI-TOF-MS analysis of the digestion mixture after 8 hours.

HA oligosaccharide	Expected mass (Da)		Experimental mass (m/z)	
	$[M + Na]^+$	$[M - H + 2Na]^+$	$[M + Na]^+$	$[M - H + 2Na]^+$
4-HA	781.62	803.60	781.15	803.43
6-HA	1160.94	1182.92	1160.26	1182.25
8-HA	1540.25	1562.24	1539.37	1561.36

The experimental masses of the HA oligosaccharides were in very good agreement with their expected masses. This confirmed the presence of 4-, 6- and 8-HA in the digestion mixture (see Figure III.C.1).

A separation of the HA oligosaccharides using low pressure gas chromatography (LPGC) was attempted in order to isolate 4-HA on which the reaction with OSA would be performed. However, given the large quantity of material involved compared to the capacity of the LPGC column, this process was fastidious and due to time limitation during the master's project, the grafting of OSA was eventually performed on a desalted mixture of 4-, 6- and 8-HA.

After reaction of the HA oligosaccharides with OSA in a $NaHCO_3$ buffer, at pH 9.0 and room temperature, for 16 hours (overnight), the resulting desalted product was again analysed by MALDI-TOF-MS (Figure III.C.2)

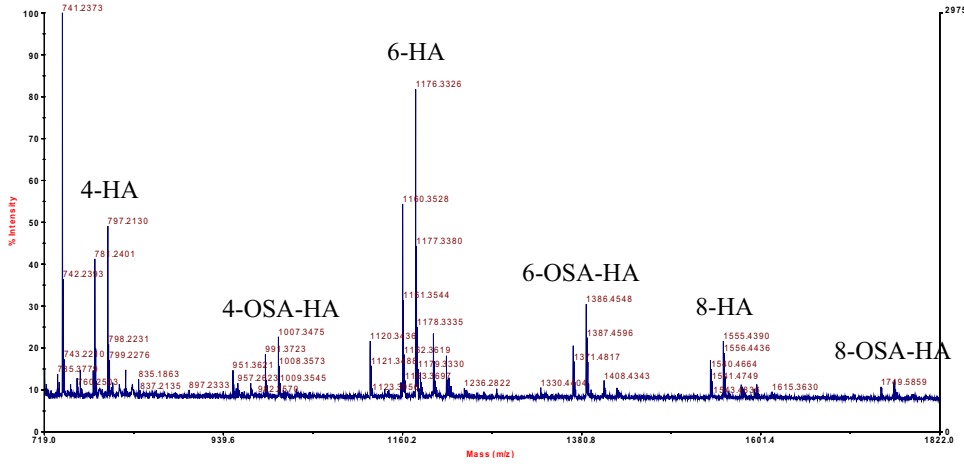

Figure III.C.2: MALDI-TOF-MS spectrum of the product of the reaction between the HA oligosaccharides and OSA.

The spectrum displayed in Figure III.C.2 was detailedly assigned in [1] and only key elements are summarized hereafter. The product of the reaction between the HA oligosaccharides and OSA was a mixture of non-modified and modified HA oligosaccharides. The various HA and OSA-HA oligosaccharides were detected as alkali salts such as $[M + Na]^+$, $[M + K]^+$, $[M – H + 2Na]^+$, $[M –H + Na + K]^+$, $[M – H + 2K]^+$ and $[M – H + Na + 2K]^+$ which explains the numerous peaks observed for each of the oligosaccharides.

The spectrum indicated that only one OS chain was grafted on each of the modified oligosaccharides. This was surprising as a large excess of OSA was used and should have resulted in a larger number of grafted OS substituents per oligosaccharide. Several explanations for this are possible: either the extent of the reaction between the HA oligosaccharides and OSA was actually low evidencing a poor reaction efficiency or it may not have been possible to ionise, with the matrix used, and thus detect by MALDI-TOF-MS OSA-HA oligosaccharides bearing more than one OS substituent. The first explanation could be consistent with the fact that solutions of HA

oligosaccharides are much less viscous than those of several thousand-Da HA leaving OSA much more sensitive to competitive hydration. However, a comparison between the intensity of protons H-4 of the terminal glucuronate and H-4 on grafted OS (see section A of this chapter, Figure III.A.8 for the definition of the notation H-4) in the NMR spectrum of the product of the reaction between the HA oligosaccharides and OSA revealed that there were almost as much of these two protons. Given the presence of unmodified HA oligosaccharides in the mixture analysed, this means that some OSA-HA oligosaccharides must have had more than one OS substituent. Therefore, it is more likely that OSA-HA oligosaccharides with more than one OS substituent cannot be ionised with the matrix used which rules out the first hypothesis.

The various HA and OSA-HA oligosaccharides were finally analysed by 7 different NMR techniques (1D ^{1}H, DQF-COSY, TOCSY, NOESY, gHSQC and gHMBC) at 500 and 800 MHz.

Interestingly, a combination of these techniques uncovered structural alterations such as the change in configuration of the terminal *N*-acetylglucosamine, which for some oligosaccharides had shifted from a *beta* to an *alpha* configuration and the creation of an unsaturation between protons 4 and 5 of the terminal glucuronate. These changes were attributed to the enzymatic action [7,8].

Although it could be expected that the substitution of HA hydroxyl protons with –COR groups would result in adjacent proton shifts of about 0.5 ppm downfield, alterations in neither the proton nor the carbon resonances of the OSA-HA oligosaccharides could be observed.

For comparison a ~20,000-Da OSA-HA derivative (with a DS of approximately 16 % per disaccharide unit) was digested into oligosaccharides and characterised as described before. However, as for the OSA-HA oligosaccharides prepared by reaction between HA oligosaccharides and OSA, the NMR spectra did not

display any shift differences. As a result, it was not possible to determine which type of HA hydroxyl groups bore the OS substituents.

A combination of the following reasons can be put forward to explain the lack of difference between the chemical shifts of the HA and OSA-HA oligosaccharides:
(i) despite the low polymerisation degree of the fractions analysed, there was still a heavy overlap of the carbohydrate resonances,
(ii) the NMR analysis was conducted on a mixture of oligosaccharides. Therefore, multiple similar spin systems were present and had a broadening effect on the resonances,
(iii) the extent of modification of the oligosaccharides was low and it is likely that the HA resonances dominated in the NMR spectra,
(iv) the grafting of OSA was probably random and many different OSA-HA oligosaccharides were most likely obtained. The low abundance of single species resulted, as in point (ii), in resonance broadening.
In the absence of determining proofs, there were however more indications that the grafting of OSA onto HA was more random than otherwise. It is therefore believed that all HA hydroxyl groups are potential targets for the grafting of OSA.

III.1.2. Macromolecular level

The reaction between HA and OSA is not homogeneous since it occurs between an aqueous phase containing HA and a dispersed oil phase consisting of OSA. The grafting of OSA is therefore believed to occur at the surface of the OSA oil droplets which size diminishes as OSA is consumed in the esterification and hydrolysis reactions.
Each time an OSA molecule is grafted onto HA, an anchoring site is most likely created which maintains the modified polymer adsorbed at the surface of the OSA droplet like a surfactant due to hydrophobic interactions between grafted OS and free

OSA. The polymer eventually desorbs when the OSA molecules in the droplets have completely been consumed. Adsorbed HA at the surface of the OSA droplets probably adopts *tail-train-loop* configurations such as those described by Kawaguchi *et al.* at the surface of soybean oil droplets [9] (Figure III.C.3).

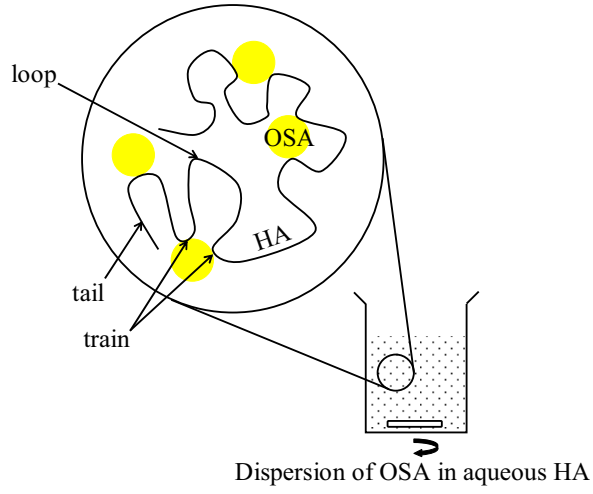

Figure III.C.3: Putative reaction mechanism between HA and OSA.

As a result, it is possible that the degree of freedom of the polymer be reduced and that certain polymer regions be excluded for reaction.

This putative reaction mechanism implies that the distribution of OS on HA is most likely non-homogenous at the macromolecular level and that the distribution of the DS of the OSA-HA derivatives is probably fairly broad. This could explains the size polydispersity of the OSA-HA polymeric micelles (see Chapter IV, § III.2 and III.3).

III.2. Molecular weight and conformation study

Due to the strong retention of the OSA-HA derivatives on the stationary phase of the SEC-MALLS fractionation column, their MW, R_{rms} and A_2 in PBS were determined directly by MALLS (batch mode). Sample dilutions with increasing concentrations were simply injected in the MALLS cells and light scattering measurements were taken on unfractionated samples.

Provided that the preparation of OSA-HA is not accompanied by a significant HA MW decrease, the introduction of OSA chains onto HA is expected to increase the MW of the native polymer. According to the DS values determined by ^{1}H NMR, the MW of OSA-HA6, -18 and -44 should approach 19,600, 20,800 and 23,400 Da, respectively since the MW of the starting HA (HA20) was about 19,000 Da (see section B of this chapter, § II.2.1).

Due to the presence of hydrophobic groups on OSA-HA, the aqueous solubility of HA and of the OSA-HA derivatives should be different and the conformation, in the dilute regime, of OSA-HA should be all the more compact that the DS of OSA-HA is high.

Taglienti *et al.* [10] for example showed that the higher the DS of methylprednisolone-modified HA (45 and 60 % of grafted substituents, respectively), the lower the values of intrinsic viscosity ([η]) of these modified polymers in water (~8.0 and 4.8 L/g, respectively). Considering that the MW of the two polymers is almost the same and that the quantity MW[η] is proportional to the hydrodynamic radius (R_H), these results suggested that the higher the DS of methylprednisolone-modified HA, the lower its R_H and the more compact its conformation due to the increasing hydrophobic interactions between the grafted substituents.

Similarly, Pelletier *et al.* [11] observed that the introduction of dodecyl (5 %) and octadecyl (1 %) chains onto HA (HA-C_{12} and HA-C_{18}, respectively) resulted in a

decrease of [η] from 0.93 L/g (unmodified HA, MW~480,000 Da) to 0.27 L/g (HA-C_{12}) or 0.17 L/g (HA-C_{18}) in 0.15 M NaCl. In this case, the longer the hydrophobic chains, the more compact the conformation of modified HA due to the stronger interactions between the longer alkyl chains.

Pravata *et al.* [12] demonstrated, using SEC-MALLS and the Mark-Houwink-Kunh-Sakurada (MHKS) relationship, a change in the conformation of HA modified with DL-lactic acid oligomers. The conformation of the native polymer was a random coil while that of the modified polymer was a sphere. This was again attributed to the hydrophobic interactions between the grafted substituents.

In this work, the conformation of HA and of the OSA-HA derivatives was assessed by means of two physical quantities, namely R_{rms} and A_2. Based on the studies above, it was expected that R_{rms} and A_2 would decrease with increasing the DS of OSA-HA. Indeed, the higher the DS of OSA-HA, the greater the possibility for hydrophobic interactions and thus the lower the R_{rms} and the affinity of OSA-HA for aqueous solvents. The values of MW, R_{rms} and A_2 obtained are presented in Table III.C.2.

Table III.C.2: Molecular weight, root mean square radius and osmotic second virial coefficient of HA20 and of the OSA-HA derivatives.

Sample	MW (Da)	R_{rms} (nm)	$A_2 \times 10^3$(mol.mL/g^2)
HA20	19,100 ± 200 (± 1.0 %)	28.9 ± 1.5 (± 5.2 %)	-3.836 ± 0.164 (± 4.2 %)
OSA-HA6	27,300 ± 500 (± 1.8 %)	47.8 ± 1.8 (± 3.8 %)	-35.990 ± 0.790 (± 2.2 %)
OSA-HA18	244,100 ± 15,300 (± 6.3 %)	83.8 ± 4.8 (± 5.7 %)	-3.638 ± 0.328 (± 9.0 %)
OSA-HA44	15,830,000 ± 170,000 (± 1.1 %)	60.9 ± 1.0 (± 1.6 %)	-3.503 ± 0.123 (± 3.5 %)

The MW of HA20 was 19,100 ± 200 Da which was very close to the value determined by SEC-MALLS (19,090 ± 191 Da, see section B of this chapter, § II.2.1). The MW values of the OSA-HA derivatives were higher than that of HA20 and increased with increasing the DS of OSA-HA. However, the MW values of OSA-HA18 and OSA-

HA44 were far much larger than expected. This suggested that OSA-HA18 and OSA-HA44 were aggregated and that the MALLS measurements were not performed in the dilute regime of these polymers. However, due to the low intensity of light scattered by lower polymer concentrations, it was not possible to acquire further measurements (see below).

R_{rms} increased as a function of DS except for OSA-HA44 and A_2 was relatively constant except for OSA-HA6. The negativity of A_2 meant that PBS was a poor solvent for both HA20 and the OSA-HA derivatives. In general, these results were in disagreement with our predictions and with the known good affinity between HA and aqueous solvents.

The inconsistency observed between the expected and experimental results most likely arose from the technical difficulties encountered when performing the MALLS experiments. These difficulties were related to both the nature of the derivatives and to experimental limitations.

It is noteworthy that the OSA-HA concentration window in which light scattering measurements were possible was very narrow and varied with the DS of the OSA-HA derivatives. The light scattering signal (voltage) was characterised for each OSA-HA sample by three phases from the injection of the most diluted solution (0.001 g/L) to the most concentrated solution (1 g/L):

(i) for each sample, up to a certain OSA-HA concentration which was dependent on the DS of the derivative, no light scattering different from that of the control (PBS) was observed,

(ii) then, an increasing value of the voltage was detected with increasing the OSA-HA concentration (narrow concentration window),

(iii) finally, high voltage values above the detection limit of the equipment were observed for more concentrated OSA-HA solutions.

The first phase was due to the dilution of the solutions injected which was too high for the objects present in solution to scatter enough detectable light. In the second phase,

the presence of a sufficient amount of objects yielded a measurable signal which intensity was a continuous and increasing function of the OSA-HA concentration. The third phase was related to an important transition occurring in concentrated OSA-HA solutions, most likely the creation of macromolecular OSA-HA structures scattering large amounts of light which saturated the MALLS detectors.

As a consequence, light scattering measurements were performed in the second phase of each sample. The concentration window of this second phase was dependent on the DS of the OSA-HA derivatives: the higher the DS, the less concentrated the OSA-HA solutions at which measurements were possible. This was due to the fact the higher the DS, the lower the concentration range at which the transition occurred. Accordingly, measurements were recorded from 0.005 to 0.008 g/L for OSA-HA44, 0.01 to 0.04 g/L for OSA-HA18 and 0.05 to 0.08 g/L for OSA-HA6.

However, in the optimal concentration windows, the voltage intensity was quite low (< 4 V) due to the low molecular weight of the OSA-HA derivatives. Moreover, the difference in intensity between the voltage plateaus corresponding to the various concentrations tested was equally small.

Finally, by-passing the fractionation column resulted in a rather unstable signal due to the polydispersity of the OSA-HA MW fractions present in each sample and it was difficult to obtain a stable signal.

All the above-mentioned aspects, which are also illustrated Figure III.C.4, affected the quality of the raw data used to determine the MW, R_{rms} and A_2 of the OSA-HA derivatives and it is likely that the experimental error was important.

Obviously, the conditions in which the MW and conformation study were performed were not optimal and it was not possible to draw conclusions with respect to the MW degradation during the preparation of OSA-HA and the solution properties of OSA-HA in the dilute regime since the measurements were not performed in the same conditions of concentration.

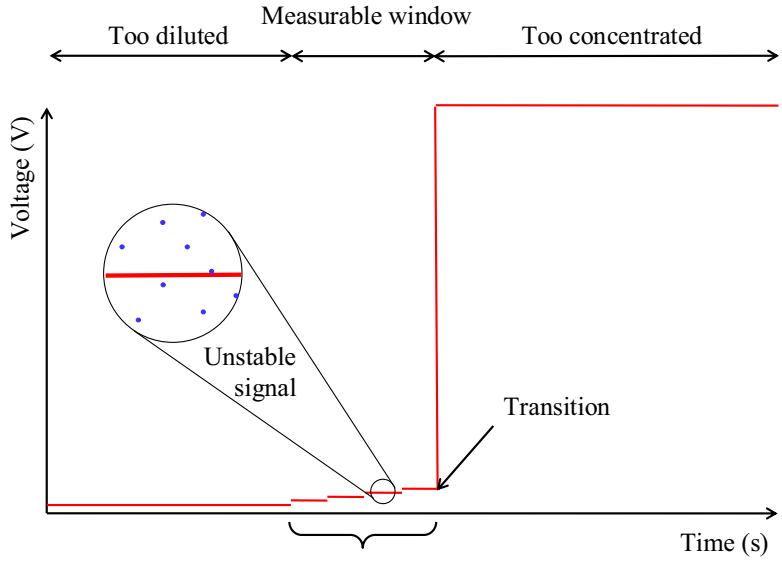

Figure III.C.4: Illustration of the experimental difficulties encountered when performing MALLS.

The computer interface is sketched for a given OSA-HA sample and MALLS detector.

However, a positive outcome was that the concentration ranges at which the sharp increases in the intensity of light scattered occurred were consistent with the values of critical aggregation concentration later found for the OSA-HA derivatives (see Chapter IV, § III.1).

IV. Conclusion

The substitution pattern, molecular weight and conformation in aqueous media of octenyl succinic anhydride-modified hyaluronic acid were investigated by HPLC, MALDI-TOF-MS, NMR and MALLS.

Although these studies were not not performed under optimal conditions due to experimental difficulties related to the purification and/or intrinsic nature of the samples, the results suggested that the substitution pattern of OSA-HA was most likely (i) random at the molecular level, *i.e.* all HA hydroxyl groups were potential targets for the grafting of OSA, and (ii) heterogeneous at the macromolecular level due to the biphasic nature of the reaction between HA and OSA. It was also shown that OSA-HA underwent a major conformation change in aqueous media at a concentration which was dependent on its degree of substitution. However, it was not possible to unequivocally evidence the presumed randomness of the grafting of OSA at the molecular level or determine the MW, monomolecular size and affinity for the solvent of the OSA-HA derivatives.

In order to improve the conditions for the determination of the substitution pattern of OSA-HA at the molecular level, it would be advisable to perform the structural study on a unique oligosaccharide length, for example on OSA-modified tetrasaccharides in order to avoid resonance broadening. This supposes separating the HA oligosaccharides using a preparative technique such as high performance anion-exchange chromatography (HPAEC) [13]. A higher degree of modification and separation of the unmodified HA oligosaccharides from the product would improve the proportion of neighbouring protons to the octenyl succinate grafts and thus the detection of chemical shift differences. Finally, the performance of edited H2BC experiments could allow determining the shifts of methylene protons H-6 and H-6’ on the glucuronate moieties. This would bring additional valuable information.

As for the MW and conformation study by MALLS, a higher MW of the OSA-HA derivatives would increase the intensity of light scattered and the voltage span between consecutive dilutions. It could also be advantageous to precisely determine the boundaries of the polymers' dilute regimes, for example using intrinsic viscosity measurements in order to work under the critical overlap concentration (provided that the latter can be evidenced), *i.e.* when monomolecular coils occur in solution.

Ideally, one should perform experiments on a range of OSA-HA derivatives with different MW values but the same DS and derivatives with the same MW but different DS values and apply the MHKS relationship in order to determine the monomolecular shape of the OSA-HA derivatives [12]. In this way, more reliable information about the conformation of the OSA-HA derivatives could be obtained.

The major conformation change of the OSA-HA derivatives suspected during the MALLS experiments (see above) and the physicochemical properties of the derivatives were subsequently studied. This work is reported in the following chapter.

References

[1] Sparre Kofoed, S. Structural characterization of a novel amphiphilic derivative of hyaluronic acid. Master thesis, Technical University of Denmark, Lyngby, Denmark, March 2008.

[2] Wyatt, P. J. Light scattering and the absolute characterization of macromolecules. *Anal. Chim. Acta* **1993**, *272*, l-40.

[3] Collins, P. M.; Ferrier, R. J. Monosaccharides. Their chemistry and their roles in natural products; Wiley: Chichester, 1995.

[4] Shih, F. F.; Daigle, K. W. Gelatinization and pasting properties of rice starch modified with 2-octen-1-ylsuccinic anhydride. *Nahrung* **2003**, *47*, 64-67.

[5] Nilsson, L.; Bergenstahl, B. Adsorption of hydrophobically modified anionic starch at oppositely charged oil/water interfaces. *J. Colloid Interface Sci.* **2007**, *308*, 508-513.

[6] Ohya, T.; Kaneko, Y. Novel hyaluronidase from Streptomyces. *Biochim. Biophys. Acta* **1970**, *198*, 607-609.

[7] Tawada, A.; Masa, T.; Oonuki, Y.; Watanabe, A.; Matsuzaki, Y.; Asari, A. Large-scale preparation, purification, an characterization of hyaluronan oligosaccharides from 4-mers to 52-mers. *Glycobiology* **2002**, *12*, 421-426.

[8] Blundell, C. D.; Reed, M. A. C.; Almond, A. Complete assignment of hyaluronan oligosaccharides up to hexasaccharides. *Carbohydr. Res.* **2006**, *341*, 2803-2815.

[9] Kawaguchi, Y.; Matsukawa, K.; Ishigami, Y. Conformational changes of hyaluronates with partial palmitoylation and the adsorption structures on the surface of oil droplets. *Carbohydr. Polym.* **1993**, *20*, 183-187.

[10] Taglienti, A.; Valentini, M.; Sequi, P.; Crescenzi, V. Characterization of methylprednisolone esters of hyaluronan in aqueous solution: conformation and aggregation behavior. *Biomacromolecules* **2005**, *6*, 1648-1653.

[11] Pelletier, S.; Hubert, P.; Lapicque, F.; Payan, E.; Dellacherie, E. Amphiphilic derivatives of sodium alginate and hyaluronate: synthesis and physico-chemical properties of aqueous dilute solutions. *Carbohydr. Polym.* **2000**, *43*, 343-349.

[12] Pravata, L.; Braud, C.; Boustta, M.; El Ghzaoui, A.; Tømmeraas, K.; Guillaumie, F.; Schwach-Abdellaoui, K.; Vert, M. New amphiphilic lactic acid oligomer-hyaluronan conjugates: synthesis and physicochemical characterization. *Biomacromolecules* **2008**, *9*, 340-348.

[13] Guillaumie, F.; Justesen, S. F. L.; Mutenda, K. E.; Roepstorff, P.; Jensen, K. J.; Thomas, O. R. T. Fractionation, solid-phase immobilization and chemical degradation of long pectin oligogalacturonides. Initial steps towards sequencing of oligosaccharides. *Carbohydr. Res.* **2006**, *341*, 118-129.

CHAPTER IV

Physicochemical characterisation of amphiphilic hyaluronic acid derivatives

Novel self-associative multi-phase nanostructured soft carriers based on amphiphilic hyaluronic acid derivatives

Corinne Eenschooten[1,2], Andrea Vaccaro[3], Florence Delie[4], Fanny Guillaumie[1], Kristoffer Tømmeraas[1], Georgios M. Kontogeorgis[2], Khadija Schwach-Abdellaoui[1], Michal Borkovec[3], Robert Gurny[4]

[1]Novozymes Biopolymer A/S, Krogshøjvej 36, 2880 Bagsværd, Denmark

[2]Technical University of Denmark, Department of Chemical and Biochemical Engineering, Centre for Phase Equilibria and Separation Processes (IVC-SEP), Building 229, 2800 Lyngby, Denmark

[3]University of Geneva, University of Lausanne, Department of Inorganic Analytical and Applied Chemistry, 30 quai Ernest-Ansermet, 1211 Geneva 4, Switzerland

[4]University of Geneva, University of Lausanne, School of Pharmaceutical Sciences, Department of Pharmaceutics and Biopharmaceutics, 30 quai Ernest-Ansermet, 1211 Geneva 4, Switzerland

Abstract

The physicochemical properties of water soluble amphiphilic octenyl succinic anhydride-modified hyaluronic acid (OSA-HA) were evaluated in aqueous media. The self-associative properties of OSA-HA were studied by fluorescence spectroscopy using Nile Red as fluorophore. The morphology, size and surface charge of the OSA-HA assemblies were determined by transmission electron microscopy, dynamic light scattering and by means of measuring their electrophoretic mobility, respectively. OSA-HA was shown to self-associate in aqueous media into negatively charged multi-phasic spherical nanostructures with a hydrodynamic diameter between 170 and 230 nm and to solubilise hydrophobic compounds such as Nile Red. This is a good indication that OSA-HA could be used as building blocks for the formulation of soft

nanocarriers towards the encapsulation and controlled delivery of hydrophobic active ingredients or drugs.

Keywords amphiphilic hyaluronic acid derivative, octenyl succinic anhydride, self-associative polysaccharide, critical aggregation concentration, polymeric micelle, colloidal size distribution

I. Introduction

Hyaluronic acid (HA) is a natural linear polysaccharide consisting of D-glucuronic acid and *N*-acetyl-D-glucosamine linked through *β*-1,3 glycosidic bonds while consecutive disaccharide units are linked through *β*-1,4 glycosidic bonds [1] (Figure IV.1).

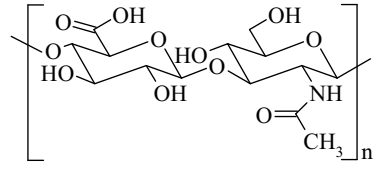

Figure IV.1: Molecular structure of the HA repeating unit.

HA is found in all mammalian tissues and is particularly abundant in the vitreous humor of the eye, the synovial fluid and the skin [2].

Due to its biocompatibility and resorbability, HA constitutes an interesting building block for applications in drug delivery [3]. However, the development of HA carriers is impeded by the high hydrophilicity and the poor biomechanical properties of the native molecule [4]. A variety of chemical modifications have been devised to provide HA with new improved physicochemical properties [4]. In particular, the

introduction of alkyl chains onto the HA backbone has shown that the resulting HA derivatives exhibit significantly different physicochemical properties compared to the native polymer and that new associative systems can be created [5,6].

We previously developed a novel, simple and easily upscalable modification method for the preparation of amphiphilic HA derivatives based on the reaction between HA and octenyl succinic anhydride (OSA) in aqueous mild alkaline media [7].

The objective of this study was to evaluate the physicochemical properties of a selection of OSA-HA derivatives. This investigation was conducted in the perspective of using these derivatives to formulate nanocarriers towards the encapsulation and controlled delivery of hydrophobic active ingredients or drugs.

II. Materials and methods

II.1. Materials

The OSA-HA derivatives with a degree of substitution (DS) of 6, 18 and 44 % (OSA-HA6, OSA-HA18 and OSA-HA44) were prepared as described in Chapter III, B. Sodium chloride (NaCl), potassium chloride (KCl), disodium hydrogen phosphate (Na_2HPO_4), potassium dihydrogen phosphate (KH_2PO_4), tetrahydrofurane (THF), acetone, Nile Red and uranyl acetate were used as purchased without further purification. The water used for sample preparation or analysis was distilled and purified to a resistivity of 18.2 MΩ.cm in a milli-Q apparatus. The physicochemical properties of the OSA-HA derivatives were investigated in a phosphate buffer saline (PBS, pH = 7.4) which was prepared as followed: NaCl (8.0 g), KCl (0.2 g), Na_2HPO_4 (1.4 g) and KH_2PO_4 (0.2 g) were first dissolved in milli-Q water (1 L) for 1 hour, at room temperature. The pH of the resulting mixture was then measured and, if

necessary, adjusted to 7.4 with HCl (0.2 M) or NaOH (0.2 M). The resulting buffer was finally filtered through glass microfiber filters (GF/F 1825 110, porosity 0.7 µm; Whatman, Maidstone, United Kingdom). The uranyl acetate solution used to stain the OSA-HA polymeric micelles was a distilled water/saturated uranyl acetate mixture (60:40 v/v).

II.2. Methods

II.2.1. Critical aggregation concentration of the OSA-HA derivatives

The critical aggregation concentration (CAC) of the OSA-HA derivatives was determined in PBS (pH = 7.4) at 25 °C by fluorescence spectroscopy (FluoroMax; HORIBA Jobin Yvon Inc, Edison, New Jersey, United States) using Nile Red as fluorophore. OSA-HA was dissolved in PBS at the following concentrations: 0.001, 0.002, 0.004, 0.006, 0.008, 0.01, 0.02, 0.04, 0.06, 0.08, 0.1, 0.2, 0.4, 0.6, 0.8 and 1 g/L. The 0.2, 0.4, 0.6 and 0.8-g/L OSA-HA solutions were prepared from the 1-g/L OSA-HA solution by mixing 2, 4, 6 and 8 g of the latter into 8, 6, 4 and 2 g of PBS. Each of the remaining OSA-HA solutions was prepared from the 10-fold more concentrated OSA-HA solution by mixing 1 g of the solution into 9 g of PBS. Nile Red (3.184 mg) was dissolved in a THF/acetone mixture (50:50 v/v, 10 mL). A fraction of the resulting solution (0.01 mL) was added to each OSA-HA sample (10 mL) so that the final concentration of Nile Red in each sample was 1 µmol/L. The OSA-HA samples were stirred overnight, at room temperature and in the dark. Cuvettes were rinsed prior to use with 0.5 mL of the sample to be tested. Nile Red was excited at 543 nm and emission spectra were recorded from 580 to 700 nm. Three consecutive fluorescence spectra per sample were recorded. The emission spectra were fitted with a polynomial function (order 6) to determine the wavelength corresponding to the maximum intensity of the fluorescence emission. The averaged wavelengths were plotted as a

function of the OSA-HA concentration and the CAC was derived at the abscissa of the inflexion point of the plot.

II.2.2. Morphology of the OSA-HA polymeric micelles

The morphology of the OSA-HA polymeric micelles was studied in PBS (pH = 7.4), at room temperature, by transmission electron microscopy (TEM, EM 410; Philips Electronic Instruments, Eindhoven, The Netherlands) using ionized carbon-coated copper grids and a uranyl acetate negative staining. OSA-HA (10 mg) was dissolved in PBS (10 mL) at room temperature, overnight. The carbon-coated copper grids were ionized for 20 s, under a pressure of 0.3 Torr and a voltage of 400 V and then deposited onto a 30-µL drop of the OSA-HA micellar solution for 30 s. Excess of the solution was drained from the grid which was then deposited onto a first 100-µL drop of uranyl acetate solution for a few seconds and immediately after onto a second 100-µL drop of uranyl acetate for 30 s. Excess of the solution was drained and the grid was dried prior to observation. Three grids per OSA-HA micellar solution were prepared and a minimum of four micrographs per grid were acquired at an accelerating voltage of 60 kV.

II.2.3. Size distribution of the OSA-HA polymeric micelles

The size distribution of the OSA-HA polymeric micelles was determined by extracting micelle diameters on TEM micrographs. The diameters of more than 600 micelles were individually and manually measured using the software ImageJ (United States National Institutes of Health, Bethesda, Massachusetts, United States). The size distribution obtained was fitted with the Schulz [8] and log-normal [9] distributions. The hydrodynamic diameter of the OSA-HA polymeric micelles was determined in PBS (pH = 7.4), at room temperature, by dynamic light scattering (DLS, ALV-CGS-8, equipped with eight-fibre optic detectors and a 532 nm solid-state laser as light source,

ALV, Langen, Germany). OSA-HA (10 mg) was first dissolved in PBS (10 mL), at room temperature, overnight. The resulting solution was then filtered to remove dust particles. Four consecutive measurements of the diffusion coefficient per scattering angle were recorded from 20 to 120 degrees.

The hydrodynamic diameter of the OSA-HA polymeric micelles was also simulated, based on the size distribution obtained by TEM, by applying the Rayleigh-Gans-Debye (RGD) theory of dynamic light scattering [10] which most relevant relationship is presented in Equation IV.1.

$$d_H(\theta) = \frac{\sum_i d_i^6 P\left(\frac{d_i}{2} q\right) f_i}{\sum_i d_i^5 P\left(\frac{d_i}{2} q\right) f_i} \qquad \text{Equation IV.1}$$

In Equation IV.1, d_H, θ, d_i, and f_i represent the average hydrodynamic diameter of the micelles (nm), the scattering angle (degrees), the diameter of the micelle class i (nm) and the probability density of the micelle class i (nm^{-1}), respectively. P is a function defined in Equation IV.2 and the relationship between the modulus of the scattering vector q (nm^{-1}) and the scattering angle θ is presented in Equation IV.3.

$$P(u) = \frac{9}{u^6}(\sin u - u\cos u)^2 \qquad \text{Equation IV.2}$$

$$q = \frac{4\pi n}{\lambda}\sin\frac{\theta}{2} \qquad \text{Equation IV.3}$$

In Equation IV.3, n and λ represent the refractive index of the dispersion medium and the wavelength of light in vacuum (nm), respectively.

The diameter values of the micelle classes on the size distribution obtained by TEM were adjusted so as to take into account micelle swelling. Micelle swelling was characterised by means of a swelling coefficient α which was defined as the ratio between the volume of water and the volume of OSA-HA making up the fully

hydrated micelles. The diameter values of the micelle classes on the size distribution obtained by TEM were accordingly multiplied by the constant $\sqrt[3]{\alpha+1}$.

II.2.4. Zeta potential of the OSA-HA polymeric micelles

The zeta potential of the OSA-HA polymeric micelles (1 g/L) was determined in a diluted NaCl solution (0.001 mol/L), at 25 °C, by means of measuring their electrophoretic mobility (Zetasizer 3000 HS, Malvern, Worcestershire, United Kingdom). Three consecutive measurements of the zeta potential were recorded per OSA-HA micellar solution.

III. Results and discussion

III.1. Critical aggregation concentration of the OSA-HA derivatives

The introduction of OSA chains onto HA is expected to alter the physicochemical properties of the native HA and in particular the intra- and intermacromolecular interactions between the HA chains.
The CAC of OSA-HA was determined in PBS (pH = 7.4) at 25 °C by fluorescence spectroscopy using Nile Red as fluorophore.

The fluorescence of Nile Red and more specifically its maximum fluorescence emission wavelength is dependent on the polarity of its surrounding environment. This wavelength is lower in non-polar environments than in polar environments [11]. Due to this intrinsic property, Nile Red can be used to determine the CAC of associative amphiphilic polymers in aqueous media. Indeed, this physical transition typically involves the formation of segregated non-polar colloidal domains where Nile Red can readily be incorporated.

Nile Red was dissolved in a range of OSA-HA PBS-buffered solutions with increasing OSA-HA concentration from 0.001 to 1 g/L. The PBS was used to buffer both ionic strength and acidity variations among the different OSA-HA samples. The maximum fluorescence emission wavelength of Nile Red was followed as a function of the OSA-HA concentration for OSA-HA derivatives with a DS of 6, 18 and 44 % (Figure IV.2).

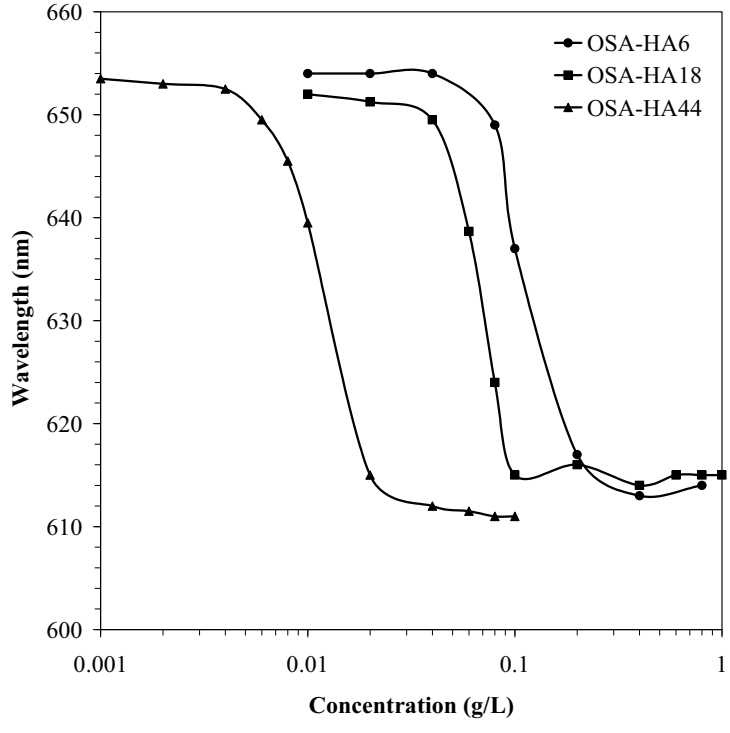

Figure IV.2: Maximum fluorescence emission wavelength of Nile Red as a function of the OSA-HA concentration.

On Figure IV.2, the maximum fluorescence emission wavelength of Nile Red suddenly decreases from about 650 to 610 nm when the OSA-HA concentration increases.

This abrupt wavelength change indicates that the immediate environment of the dye changes from polar to less polar owing to the interactions between Nile Red and the octenyl succinate (OS) chains upon formation of OSA-HA polymeric micelles. Furthermore, the concentration at which this rapid transition is observed depends on the DS of the OSA-HA derivative. A plot of the CAC as a function of the DS of the OSA-HA derivatives indicated that the CAC linearly decreased with increasing DS (Figure IV.3).

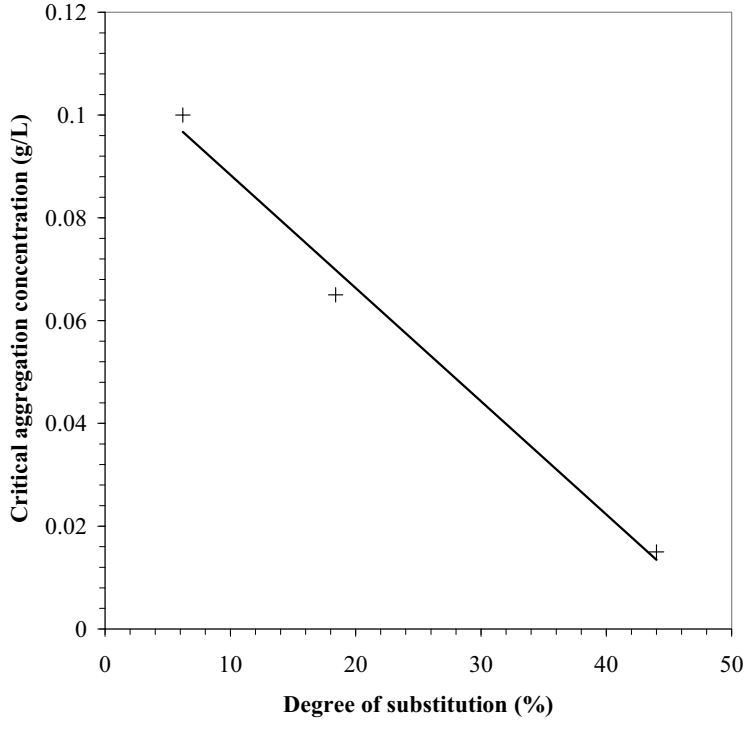

Figure IV.3: Critical aggregation concentration as a function of the degree of substitution of OSA-HA. CAC = -0.0022DS + 0.1104; R^2 = 0.99.

Indeed, the increased attraction between the OS chains at high DS resulted in the formation of OSA-HA polymeric micelles at lower concentrations.
Interestingly, the trend observed between the CAC and the DS of the OSA-HA derivatives validated the determination of DS by proton nuclear magnetic resonance spectroscopy in Chapter III, B.

The polymer concentration values corresponding to the formation of hydrophobic domains found in the present work (0.015-0.1 g/L) were of the same order of magnitude than those previously reported for alkylated HA derivatives. For instance, Pelletier *et al*. [5] have shown using fluorescence spectroscopy and pyrene as probe that 480,000-Da HA modified with alkyl chains containing 12 carbon atoms (C_{12}, DS = 5 %) and 18 carbon atoms (C_{18}, DS = 2 %) self-associated and formed hydrophobic domains in which pyrene was solubilised at polymer concentrations of 0.05 g/L (HA-C_{12}) and 0.01 g/L (HA-C_{18}). Likewise Creuzet *et al*. [6] have shown using a similar experimental procedure that 300,000-Da HA modified with alkyl chains containing 10 carbon atoms (C_{10}, DS = 5 %) and 12 carbon atoms (C_{12}, DS = 4 %) rearranged into polymeric aggregates at polymer concentrations between 0.01 and 0.1 g/L. Although a direct comparison between these results and those of the present study is made difficult by the differences in HA molecular weight (MW), modification chemistry, nature of the hydrophobic pendant groups and DS, the order of magnitude of the OSA-HA concentrations at which self-association occurred indicates a relatively good consistency with the literature.

In summary, OSA-HA was demonstrated to self-associate in aqueous media and solubilise Nile Red above a CAC which was dependent on the DS of the OSA-HA derivative. Micellisation of OSA-HA is therefore a controllable property through the DS of the OSA-HA derivative and can be predicted for derivatives with DS between 6 and 44 %.

Due to its higher hydrophobic character, OSA-HA44 was chosen as a model compound for the detailed study of the morphology, size distribution, surface charge and molecular structure of the polymeric micelles.

III.2. Morphology of the OSA-HA polymeric micelles

The morphology of the OSA-HA polymeric micelles was studied in PBS (pH = 7.4), at room temperature, by transmission electron microscopy using a uranyl acetate negative staining (Figure IV.4).

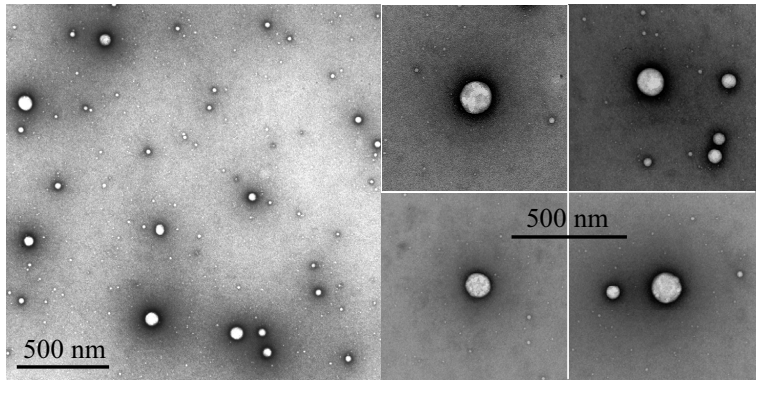

Figure IV.4: Selected TEM micrographs of the OSA-HA polymeric micelles.

The micrograph on the left of Figure IV.4 shows that the OSA-HA polymeric micelles are relatively polydisperse spherical assemblies with a diameter between 10 and 120 nm. The difference in size between the micelles was most likely due to the difference in the number of OSA-HA molecules involved in the micelles and to the potential non-homogenous DS of OSA-HA44 (see Chapter III, C, § III.1.2).

The set of four micrographs on the right of Figure IV.4 shows that the micelle structure is non-homogenous which suggests that the micelles are composed of distinct colloidal

domains which could consist of segregated non-polar poaches embedded into a polar polymeric matrix (also see § III.5. and Figure IV.9).

III.3. Size distribution of the OSA-HA polymeric micelles

In order to determine the size distribution of the OSA-HA polymeric micelles more precisely, a statistical analysis of the micelle diameters on TEM micrographs was conducted in parallel to dynamic light scattering measurements.

Microscopy and light scattering (LS) can both give information about the size of colloids, although in a different manner, as they are based on different physical principles.

When studied by microscopy, the size of the colloids is directly obtained. However, the sample preparation can alter the properties of the colloids and therefore the size observed.

When studied by LS, the size of the colloids is indirectly obtained as it is derived from colloidal diffusion in solution by means of the Stokes-Einstein equation. However, no sample preparation other than suspending the colloids in solution is required and the colloids are analysed as they truly occur in solution.

Given these principles, microscopy and LS were used in combination to obtain statistical and reliable information about the size of the OSA-HA polymeric micelles.

The size distribution of the OSA-HA polymeric micelles obtained by statistically extracting micelle diameters from TEM micrographs with the software ImageJ is presented in Figure IV.5. The size distribution showed that the OSA-HA polymeric micelles were polydisperse objects with an arithmetic average micelle diameter of 26 nm (standard deviation = 15 nm) and a mean diameter between 10 and 20 nm.

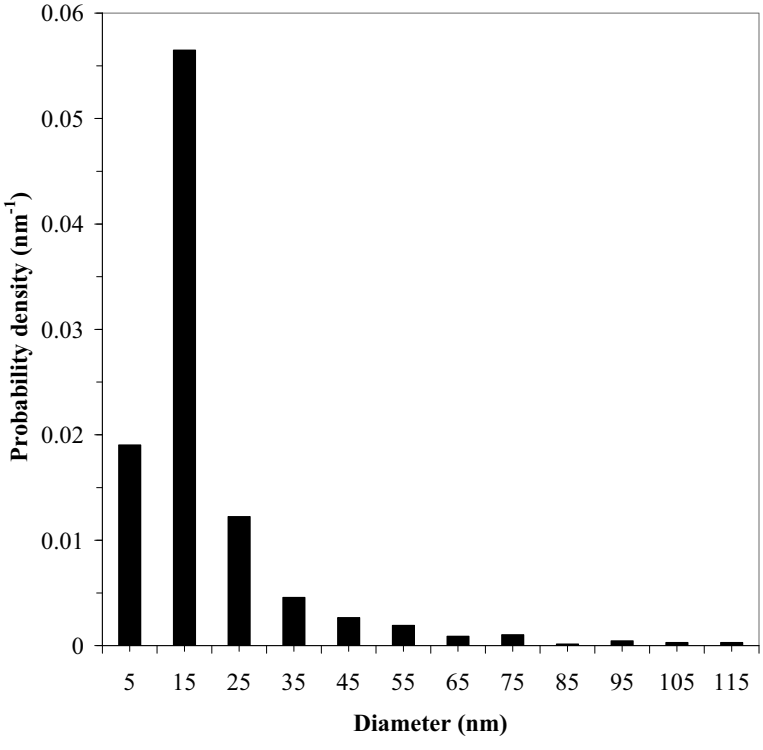

Figure IV.5: Number-weighed size distribution of the OSA-HA polymeric micelles based on micelle diameter extraction from TEM micrographs.

The cumulative size distribution of the OSA-HA polymeric micelles (Figure IV.6) revealed that 80 % of the micelles had a diameter below 25 nm. It was fitted with the Schulz and log-normal models [8,9]. The best fits were obtained with the following parameters: $\sigma = 4.82$ and $\mu = 16.02$ for the Schulz and $\sigma = 0.43$ and $\mu = 2.71$ for the log-normal fit. The experimental data were well fitted up to a cumulative frequence of 0.80. However both models failed to represent the contribution of the larger micelle population due to the relatively high polydispersity of the micelles (see Figure IV.5).

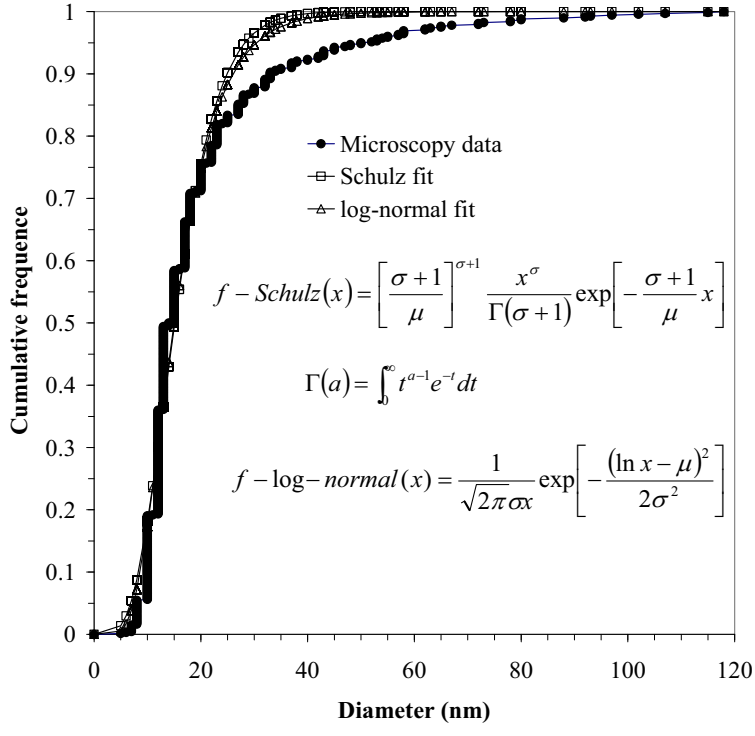

Figure IV.6: Number-weighed cumulative size distribution of the OSA-HA polymeric micelles based on micelle diameter extraction from TEM micrographs.

The hydrodynamic diameter of the OSA-HA polymeric micelles was determined in PBS (pH = 7.4), at room temperature, by DLS and was simulated from the micelle size distribution obtained by TEM. Figure IV.7 presents the variation of the hydrodynamic diameter as a function of the scattering angle as measured by DLS and as simulated from the micelle size distribution obtained by TEM for two different values of the swelling coefficient α (α = 0 for dehydrated micelles and α = 12 for hydrated micelles).

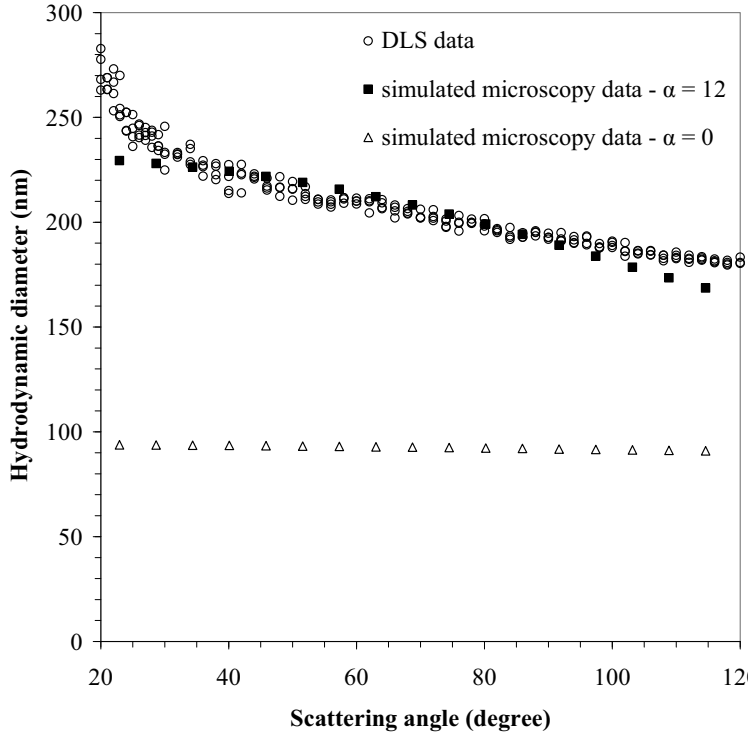

Figure IV.7: Experimental and simulated hydrodynamic diameter of the OSA-HA polymeric micelles as a function of the scattering angle.

The values of the hydrodynamic diameter measured by DLS were considerably higher than those simulated from the crude microscopy data, *i.e.* when $\alpha = 0$. Indeed, the OSA-HA polymeric micelles were hydrated during the DLS analysis, whereas they had lost their water content before the TEM analysis. Taking into account micelle hydration in the simulation ($\alpha = 12$), a better fit between the values of the hydrodynamic diameter obtained by DLS and those obtained by TEM was observed over most of the scattering angles. This indicated that the micelles analysed by DLS contained a volume of water of up to 12 times larger than the volume of OSA-HA making up the fully hydrated micelles.

The swelling coefficient found in this study was of the same order of magnitude as previously reported values of the swelling ratio in chemically cross-linked HA hydrogels.

Srinivas and Ramamurthi [12] have namely reported that the swelling ratio of HA hydrogels obtained by cross-linking with divinyl sulfone (DVS) (HA/DVS weight ratio = 3) could reach values up to 7. In this study, the swelling ratio was defined as the ratio of the difference between the weight of the swollen and the dried gel and the weight of the dried gel when the latter was obtained by freeze-drying. Since TEM micrographs are acquired under vacuum, this degree of dehydration of the hydrogel is comparable to that of the OSA-HA polymeric micelles observed by TEM. It could be demonstrated that the definition of the swelling ratio by Srinivas and Ramamurthi is equivalent to that of the present study if the density of OSA-HA is close to 1.0. Therefore the value of the swelling coefficient found in this study (12) can directly be compared to that found by Srinivas and Ramamurthi (7).

Similarly, Smeds *et al*. [13] observed that HA hydrogels obtained by photocross-linking of methacrylated HA could swell up to 11 times their dry weight when the dried gels were obtained by freeze drying. This swelling ability was dependent on the degree of cross-linking (DS between 3 and 17 %). The gels with the highest degree of cross-linking had the least ability to swell due to their tight polymeric networks. In this study, the swelling coefficient was defined as the ratio of the weight of the swollen gel and that of the dried gel. It could be shown that the relationship between this swelling ratio A and the swelling ratio α defined in the present study is $\alpha = A - 1$ if the density of OSA-HA is close to 1.0. In other words, the value of the swelling coefficient found in the present study (12) is to be compared with an adjusted value of 10 [13].

Interestingly, the OSA-HA polymeric micelles exhibited comparable swelling properties as chemically cross-linking HA but with the difference that they were not stabilised by chemical cross-linking but by hydrophobic interactions. Therefore they can be regarded as physically cross-linked nanogels.

The fairly large deviation of the hydrodynamic diameter measured by DLS from that simulated by microscopy (with $\alpha = 12$) at low scattering angles indicated that a few structures with dimensions superior to the detection range of the DLS instrument were present in solution. These few structures could be micelle aggregates although micelle aggregation could not clearly be identified on the TEM micrographs.

In summary, the data provided by the microscopy and DLS analysis showed that the OSA-HA polymeric micelles were highly hydrated structures in solution with a mean hydrodynamic diameter falling between 170 and 230 nm.

III.4. Zeta potential of the OSA-HA polymeric micelles

The zeta potential of the OSA-HA polymeric micelles was determined in PBS (pH = 7.4), at 25 °C, by means of measuring their electrophoretic mobility. The results showed that the surface of the OSA-HA polymeric micelles was negatively charged with a zeta potential of approximately -28 mV under the applied conditions (pH ~ 3.0-4.0, Figure IV.8). This negative charge was due to the presence of carboxylate groups on OSA-HA, arising from both the native HA backbone and the hemiesters generated during the reaction between HA and OSA.

III.5. Molecular structure of the OSA-HA polymeric micelles

Chen *et al*. [14] have described the structure of polymeric micelles based on hydrophobically modified HA with 2300 Da poly(caprolactone) chains as a spherical HA hydrophilic corona surrounding a poly(caprolactone) hydrophobic core. Given the relatively short length of the OS chains, the aggregation of OSA-HA is unlikely to occur in this fashion.

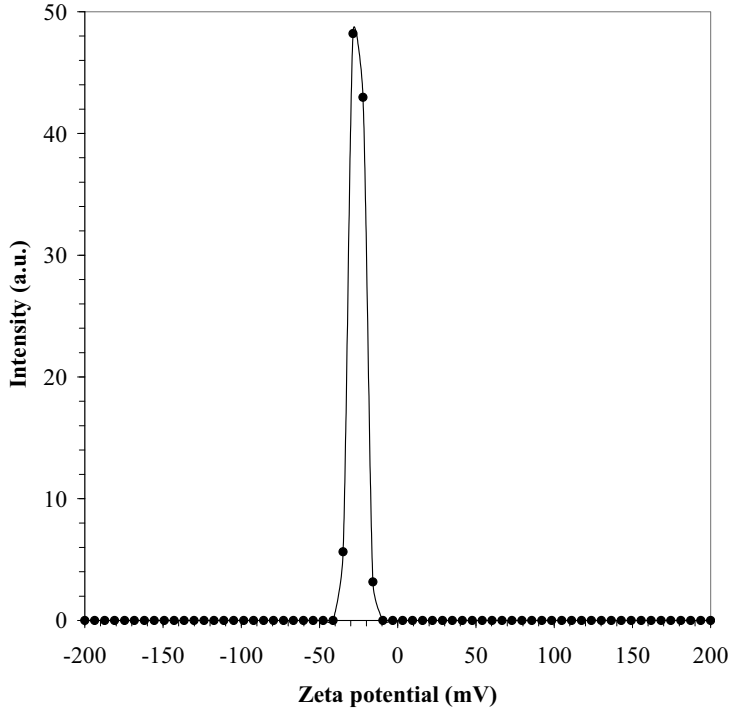

Figure IV.8: Zeta potential of the OSA-HA polymeric micelles.

Substituted disaccharide units on OSA-HA were assumed to behave like monomeric surfactant moieties capable of self-associating into conventional spherical monomeric micellar domains. OSA-HA polymeric micelles were therefore believed to consist of a dispersion of hydrophobic domains formed by the modified HA units in a hydrophilic matrix structured by the remaining unmodified HA units (Figure IV.9). In this multi-vesicular model, the OS chains involved in the hydrophobic domains potentially can originate from the same or different OSA-HA molecules and the micelle structure is believed to be stabilized by a combination of hydrophobic interactions between the OS chains and the three fundamental HA structures in solution discussed in Chapter I.

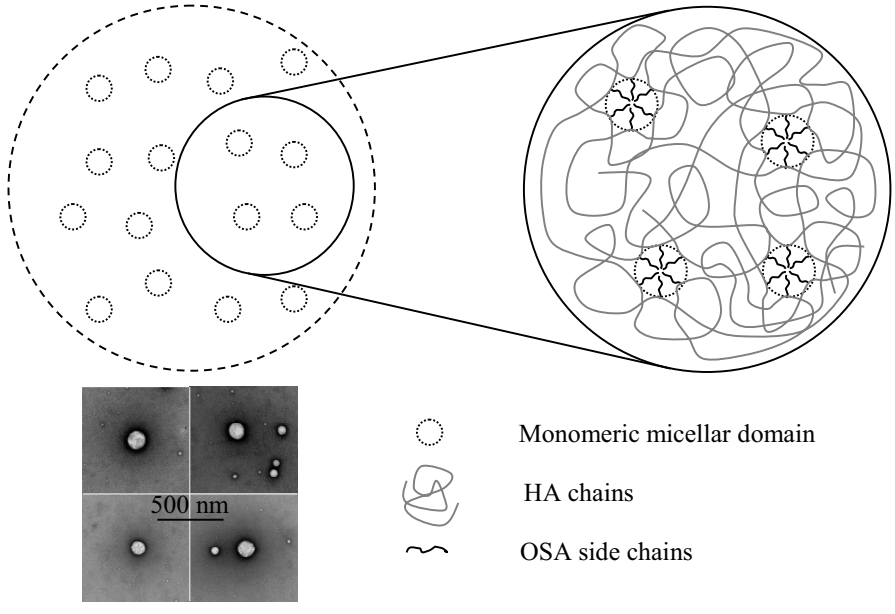

Figure IV.9: Putative representation of the structure of the OSA-HA polymeric micelles.

The number of substituted HA units per hydrophobic domains, of hydrophobic domains per micelle and the average distance between vicinal hydrophobic domains were calculated for the most occurring micelle, *i.e.* a micelle with a radius of approximately 8 nm in the dehydrated state (cf. Figure IV.5) or 19 nm in the hydrated state. The dimensions of the modified disaccharide unit used in the calculations were the following: the length and width of the disaccharide unit were approximated to 1 and 0.5 nm, respectively [15]. The length of the OS chains was approximated to 1 nm as it consists of about 10 carbon-to-carbon bonds. It should be noted that the influence of the geometric isomerism of the OS chains (*cis*/*trans*) on the packing of the hydrophobic domains was disregarded as the distribution of the *cis* and

trans OS moieties on HA is unknown. In the following calculations, the densities of HA and OSA-HA were considered to be close to 10^6 g/m^3.

The number of OSA-HA units per hydrophobic domain was calculated by dividing the volume of one hydrophobic domain by the volume of one OSA-HA unit. The volume of one OSA-HA unit can further be decomposed as the sum of the volume of one HA unit and the volume of the cone deployed by one OS chain. Substitution with more elementary physical quantities led to Equation IV.4:

$$N(OSA-HAu)/domain = \frac{\frac{4}{3}\pi\left(w(HAu)+l(OSA)\right)^3}{\frac{MW(HAu)}{\rho(HA)N_A}+\frac{1}{3}\pi\left(\frac{l(HAu)}{2}\right)^2 l(OSA)} \qquad \text{Equation IV.4}$$

where N(OSA-HAu)/domain, w(HAu), l(OS), MW(HAu), ρ(HA), N_A and l(HAu) represent the number of OSA-HA units per hydrophobic domain, the width of the HA unit, the length of the OS chain, the molecular weight of the HA unit, the density of HA, the Avogadro number and the length of the HA unit, respectively.

The number of hydrophobic domains per micelle was calculated by dividing the number of OSA-HA units per micelle by the number of OSA-HA units per hydrophobic domain. The number of OSA-HA units per micelle corresponds to the number of OSA-HA molecules per micelle multiplied by the number of OSA-HA units per OSA-HA molecule. This number is related to the DS of OSA-HA. The number of OSA-HA molecules per micelle can further be calculated by dividing the volume of one micelle by the volume of one OSA-HA molecule. Subsequent substitutions and rearrangements led to Equation IV.5:

$$N(domains)/micelle = \frac{\frac{4}{3}\pi R(micelle)^3 \rho(OSA-HA)N_A}{\frac{MW(HAu)}{DS}+MW(OSA)} \Big/ N(OSA-HAu)/domain \qquad \text{Equation IV.5}$$

where N(domains)/micelle, R(micelle), ρ(OSA-HA), N_A, MW(HAu), DS, MW(OSA) and N(OSA-HAu)/domain stand for the number of hydrophobic domains per micelle, the average radius of the most occurring micelle, the density of OSA-HA, the Avogadro number, the molecular weight of the HA unit, the degree of substitution of OSA-HA, the molecular weight of OSA and the number of OSA-HA unit per hydrophobic domain, respectively.

Finally, the distance between vicinal hydrophobic domains was calculated by applying the relation shown in Equation IV.6.

$$l(between.domains) = \sqrt[3]{\frac{1}{C(domain)}} \qquad \text{Equation IV.6}$$

In Equation IV.6, l(between.domains) and C(domain) correspond to the distance between vicinal hydrophobic domains and concentration of hydrophobic domains inside the micelle, respectively. The latter can be expressed as the ratio between the number of hydrophobic domains per micelle and the volume of the hydrated micelle (Equation IV.7).

$$l(between.domains) = \sqrt[3]{\frac{\frac{4}{3}\pi\left(\sqrt[3]{\alpha+1}R(micelle)\right)^3}{N(domains)/micelle}} \qquad \text{Equation IV.7}$$

In Equation IV.7, l(between.domains), α, R(micelle) and N(domains)/micelle represent the distance between vicinal hydrophobic domains, the swelling coefficient, the radius of the most occurring micelle and the number of hydrophobic domains per micelle, respectively.

According to our calculations, the most occurring OSA-HA micelle consisted of about 72 hydrophobic domains separated by a distance of 6-9 nm, with a diameter of 3 nm, each involving 16 OSA-HA units. Although approximate, this model is believed to provide a rough but realistic picture of the internal structure of the micelles.

IV. Conclusion

The physicochemical properties of water soluble amphiphilic octenyl succinic anhydride-modified hyaluronic acid were investigated in aqueous media. OSA-HA was shown to self-associate and solubilise Nile Red into the hydrophobic domains formed by the OS chains above a critical aggregation concentration which was dependent on the degree of substitution of the derivatives. The CAC of OSA-HA was a linear decreasing function of the derivatives' DS between 6 and 44 % per disaccharide unit and can be predicted for OSA-HA derivatives with a DS in this range.

The OSA-HA polymeric micelles were negatively charged polydisperse spherical physically cross-linked nanogels characterised by a high degree of hydration (typically 12 g of water per g of polymer) and a hydrodynamic diameter between 170 and 230 nm.
The molecular structure of the OSA-HA polymeric micelles is most probably a distribution of OS-rich hydrophobic monomeric micellar nanodomains into a HA-rich hydrophilic polymeric matrix.

The nanoengineered structures of the OSA-HA polymeric nanogels constitute biocompatible and resorbable multi-functional systems which could be used to solubilise and carry poorly soluble active ingredients in aqueous media. It is believed that the presence of multiple hydrophobic nanodomains in the nanogels could be useful for the controlled release of hydrophobic active ingredients or drugs.
The formulation of stabilised OSA-HA nanoparticles insensitive to dilution and study of the release of model hydrophobic substances *in vitro* and *in vivo* will be the subject of future investigations.

References

[1] Weissman, B.; Meyer, K. The structure of hyalobiuronic acid and of hyaluronic acid from umbilical cord. *J. Am. Chem. Soc.* **1954**, *76*, 1753-1757.

[2] Baier Leach, J.; Schmidt, C. E. Hyaluronan. In Encyclopedia of biomaterials and biomedical engineering; Wnek, G. E.; Bowlin G. L., Eds.; Marcel Dekker: New York, 2004; pp 779-789.

[3] Gustafson, S. Hyaluronan in drug delivery. In *The chemistry, biology and medical applications of hyaluronan and its derivatives*; Laurent, T. C., Ed.; Portland Press: London, 1998; pp 291-304.

[4] Prestwich, G. P.; Marecek, D. M.; Marecek, J. F.; Vercruysse, K. P.; Ziebell, M. R. Chemical modification of hyaluronic acid for drug delivery, biomaterials and biochemical probes. In *The chemistry, biology and medical applications of hyaluronan and its derivatives*; Laurent, T. C., Ed.; Portland Press: London, 1998.

[5] Pelletier, S.; Hubert, P.; Lapicque, F.; Payan, E.; Dellacherie, E. Amphiphilic derivatives of sodium alginate and hyaluronate: synthesis and physico-chemical properties of aqueous dilute solutions. *Carbohydr. Polym.* **2000**, *43*, 343-349.

[6] Creuzet, C.; Kadi, S.; Rinaudo, M.; Auzley-Velty, R. New associative systems based on alkylated hyaluronic acid. Synthesis and aqueous solution properties. *Polymer* **2006**, *47*, 2706-2713.

[7] Tømmeraas, K.; Eenschooten, C. Aryl/alkyl succinic anhydride hyaluronan derivatives. WO 2007/033677 A1, March 29, 2007.

[8] Schulz, G. V. The kinetics of chain polymerisation V. The influence of various types of reactions on the poly-molecularity. *Z. Phys. Chem. Abt. B* **1939**, *43*, 25-46.

[9] Limpert, E.; Stahel, W.; Abbt, M. Log-normal distributions across the sciences: keys and clues. *Bioscience* **2001**, *51*, 341-352.

[10] Berne, B. J.; Pecora, R. Dynamic Light Scattering; Dover Publications: Mineola, New York, 2000.

[11] Dutt, G. B.; Doriswami, S. Picosecond reorientational dynamics of polar dye probes in binary aqueous mixtures. *J. Chem. Phys.* **1992**, *96*, 2475-2491.

[12] Srinivas, A.; Ramamurthi, A. Effects of gamma-irradiation on physical and biologic properties of cross-linked hyaluronan tissue engineering scaffolds. *Tissue Eng.* **2007**, *13*, 447-459.

[13] Smeds, K. A.; Pfister-Serres, A.; Miki, D.; Dastgheib, M.; Inoue, M.; Hatchell, D. L.; Grinstaff, M. W. Photocrosslinkable polysaccharides for *in situ* hydrogel formation. *J. Biomed. Mater. Res.* **2001**, *55*, 254-255.

[14] Chen, J. H.; Tsai, B. H.; Chang, H. T.; Chen, M. L.; Chen, Y. H.; Jan, S. H.; Liu, M. J. Biodegradable hyaluronic acid derivative and biodegradable polymeric micelle composition. US 2005/0123505 A1, June 9, 2005.

[15] Ionov, R.; El-Abed, A.; Goldmann, M.; Peretti, P. Interactions of lipid monolayers with the natural biopolymer hyaluronic acid**.** *Biochim. Biophys. Acta* **2004**, *1667*, 200-207.

CHAPTER V
Conclusion and future work

I. Summary

This project was initiated in the perspective of providing biocompatible and resorbable nanocarriers based on hyaluronic acid (HA) towards drug delivery and in particular dermal drug delivery (see Chapter I).

A literature review (see Chapter II) about polymeric nanoparticle-mediated (trans)dermal drug delivery reaffirmed the high potential of using the skin as an administration route and identified new approaches to better understand the fate of particulate systems in this tissue. It also took inventory of the current hypothesis with regards to how polymeric nanoparticles can enhance drug uptake and/or sustain drug release and spotted the challenges faced by this branch of research. Interestingly, the studies reported mostly concern synthetic polymeric nanoparticles which by nature are not truly biocompatible. For this reason, systems based on the naturally occurring glycosaminoglycan hyaluronic acid were developed in this project.

Whereas most of the currently available methods for the preparation of HA nanoparticles rely on random collisions in the medium to create structures, a novel molecular technique was here developed which relies on the controlled self-assembly of amphiphilic HA leading to multiphasic nanoarchitectured HA templates.

Such properties of HA were obtained by modifying the biopolymer's hydrophilic/lipophilic balance via the covalent grafting of hydrophobic groups onto the HA backbone. After a preliminary evaluation of two novel proprietary methods to hydrophobically modify HA, octenyl succinic anhydride-modified HA (OSA-HA) was chosen as starting material for the preparation of the HA-based nanostructures (see Chapter III, A). Its preparation process was optimised so as to develop a reproducible and robust technique for the routine laboratory production of OSA-HA. With the reaction conditions tested, HA derivatives with a maximum degree of substitution (DS) of 44 % per disaccharide unit according to proton nuclear magnetic resonance spectroscopy were prepared (see Chapter III, B).

Although it was not possible to precisely determine the substitution pattern and measure the molecular weight and monomolecular size of the OSA-HA derivatives, there were some indications that the substitution pattern of OSA-HA was most likely random at the molecular level and heterogeneous at the macromolecular level and that OSA-HA undergoes a major conformation change in aqueous media at a concentration which is dependent on its degree of substitution (see Chapter III, C).
The self-assembly in aqueous media of OSA-HA was due to hydrophobic interactions between the grafted octenyl succinate (OS) chains on HA and was controlled by the DS of the derivatives. The critical aggregation concentration (CAC) of OSA-HA was indeed all the more low that its DS was high. Self-assembling of OSA-HA was therefore a controllable and predictable property for derivatives with a DS up to 44 %. In addition, it was demonstrated that OSA-HA could solubilise the model hydrophobic compound Nile Red. Above the CAC, the OSA-HA assemblies were rather polydisperse spherical and negatively charged polymeric micelles with a hydrodynamic diameter between 170 and 230 nm. They were characterised by a high degree of hydration (on averaged 12 g of water per g of polymer). This suggested that the fundamental mechanism of their stabilisation was a physical cross-linking mediated by the hydrophobic interactions between the grafted OS chains. The internal structure of the OSA-HA nanogels was believed to consist of a dispersion of hydrophobic monomeric micellar domains formed by the OS chains embedded in a hydrophilic polymeric matrix composed of the unmodified HA segments (see Chapter IV).

The development of OSA-HA nanogels described herein is believed to constitute a valuable first step towards formulating HA-based nanoparticles with more complex configurations than single ingredient or core-shell structures. In particular, the presence of multiple vesicle-like substructures inside the nanogels could be an interesting feature for sustaining drug delivery as these could delay drug release in biological environments.

Moreover, it should be emphasised that the methods underlying the OSA-HA nanogels are simple, aqueous and easily upscalable thus potentially valuable for the industry. The modification with OSA preserves and even increases the distribution of negative charges along the modified polymer at neutral pH which could constitutes an advantageous property for the electrostatic stabilisation of future nanoparticles from OSA-HA.

II. Future work

As for now, the OSA-HA nanogels only exist above their CAC. This sets the lower limit of their concentration when incorporated into formulations. In addition, it is unlikely that they maintain their shape when administered and/or exhibit higher *in vivo* residence times compared to native HA unless they are stabilised. The next main challenge therefore concerns the preparation of stable OSA-HA nanoparticles.

For an application such as dermal drug delivery, it could be necessary to reduce the size of the OSA-HA nanogels down to several tens of nanometres and better control their polydispersity (see Chapter II).

In the perspective of using the stabilised OSA-HA nanogels for concrete applications, it is foreseeable that future work will also involve biocompatibility tests and release studies *in vitro* and *in vivo*. Incorporation and stability in final formulations will also constitute an important challenge.

Appendices

Educational activities

I. Training

I.1. Courses

- Chemical and Biochemical Product Design, Technical University of Denmark, Lyngby, Denmark, autumn 2003 (10 ECTS).

- Patents and patent search, Novozymes A/S, Bagsværd, Denmark, June 17, 2005 (0.6 ECTS).

- Design of experiment, Umetrics, Bagsværd, Denmark, September 1, 2005 (2.2 ECTS).

- Intensive course in dermato-cosmetic sciences, Faculty of Medicine and Pharmacy, Brussels, Belgium, September 12-16, 2005 (3.6 ECTS).

- Polymeric surfactants, Institute for Surface Chemistry, Stockholm, Sweden, December 12-14, 2005 (3 ECTS).

- Fundamentals of percutaneous penetration, pre-conference course of the 10^{th} International Conference in Perspectives in Percutaneous Penetration, La Grande Motte, France, April 18, 2006 (0.6 ECTS).

- Spectroscopy of organic compounds, Technical University of Denmark, Lyngby, Denmark, spring 2006 (5 ECTS).

- Business course, Danish Ministry of Science, Technology and Innovation through mandated Copenhagen Business School and Haslund & Alsted, Pharmakon, Hillerød,

Denmark, October 16-17, 2006, February 12-13, 2007, September 11-12, 2007 (5 ECTS).

I.2. Conferences

- Kick-off meeting Nano-DTU/Nano-Science Centre, Hørsholm, Denmark, March 2, 2006.

- 6th European Workshop on Particulate Systems, Geneva, Switzerland, March 23-24, 2006.

- 10th International Conference in Perspectives in Percutaneous Penetration, La Grande Motte, France, April 18-22, 2006.

- Skin and Formulation 2nd Symposium, Versailles, France, October 8-10, 2006.

- 8th Annual Meeting of Skin Forum, London, United Kingdom, March 3-4, 2007.

- 7th International Conference on Hyaluronan, Charleston, South Carolina, United State, April 22-27, 2007.

- 21st Conference of the European Colloid and Interface Society, Geneva, Switzerland, September 10-14, 2007.

I.3. External study trips

The external study trips were carried out at the University of Geneva, University of Lausanne, School of Pharmaceutical Sciences, Department of Pharmaceutics and Biopharmaceutics, 30 quai Ernest-Ansermet, CH-1211 Geneva 4, Switzerland under

the supervision of Professor Robert Gurny and Associate Professor Florence Delie in the periods July 3-August 31, 2006 and March 12-June 29, 2007.

II. Dissemination of knowledge

II.1. Publications

II.1.1. Posters

- Eenschooten, C.; Guillaumie-Longin, F.; Kontogeorgis, G. M.; Schwach-Abdellaoui, K. Synthesis and formulation of modified hyaluronic acid (HA) for cosmetic applications. Annual discussion meeting 2005 of the Centre for Phase Equilibria and Separation Processes, Roskilde, Denmark, May 25-27, 2005.

- Eenschooten, C.; Guillaumie-Longin, F.; Gurny, R.; Kontogeorgis, G. M.; Schwach-Abdellaoui, K.; Stenby E. H. Development and formulation of hyaluronic acid-based nanoparticles for cosmetic applications. Kick-off meeting Nano-DTU/Nano-Science Centre, Hørsholm, Denmark, March 2, 2006.

- Eenschooten, C.; Delie, F.; Guillaumie-Longin, F.; Gurny, R.; Kontogeorgis, G. M.; Schwach-Abdellaoui, K.; Stenby, E. H. Development of colloidal carriers from modified hyaluronic acid. Skin and Formulation 2nd Symposium, Versailles, France, October 8-10, 2006.

- Eenschooten, C.; Delie, F.; Guillaumie-Longin, F.; Kontogeorgis, G. M.; Stenby, E. H.; Schwach-Abdellaoui, K.; Gurny, R. Development of colloidal carriers from modified hyaluronic acid. 8th Annual Meeting of the Skin Forum, London, United Kingdom, March 3-4, 2007.

- Eenschooten, C.; Delie, F.; Guillaumie-Longin, F.; Kontogeorgis, G. M.; Stenby, E. H.; Schwach-Abdellaoui, K.; Gurny, R. Development of colloidal carriers from modified hyaluronic acid. 7th International Conference on Hyaluronan, Charleston, South Carolina, United State, April 22-27, 2007.

- Eenschooten, C.; Vaccaro, A.; Delie, F.; Guillaumie-Longin, F.; Kontogeorgis, G. M.; Stenby, E. H.; Schwach-Abdellaoui, K.; Borkovec, M.; Gurny, R. Development of colloidal carriers from a novel amphiphilic hyaluronic acid. 21st Conference of the European Colloid and Interface Society, Geneva, Switzerland, September 10-14, 2007.

II.1.2. Oral presentations

Seminars of the Centre for Phase Equilibria and Separation Processes

- Eenschooten, C. Development of derivatized hyaluronic acid and formulation of nanoparticles for the delivery of cosmetic actives and drugs. Centre for Phase Equilibria and Separation Processes, Department of Chemical and Biochemical Engineering, Technical University of Denmark, Lyngby, Denmark, May 18, 2006.

- Eenschooten, C. Development of colloidal carriers from modified hyaluronic acid. Centre for Phase Equilibria and Separation Processes, Department of Chemical and Biochemical Engineering, Technical University of Denmark, Lyngby, Denmark, February 15, 2007.

Annual discussion meetings of the Centre for Phase Equilibria and Separation Processes

- Eenschooten, C. Development of derivatized hyaluronic acid and formulation of nanoparticles for the delivery of cosmetic actives and drugs. Annual discussion

meeting 2006 of the Centre for Phase Equilibria and Separation Processes, Elsinore, Denmark, June 26-28, 2006.

- Eenschooten, C. Development of novel colloidal carriers from chemically modified hyaluronic acid. Annual discussion meeting 2007 of the Centre for Phase Equilibria and Separation Processes, Elsinore, Denmark, May 30-June 1, 2007.

- Eenschooten, C. Development of soft nanocarriers from novel amphiphilic hyaluronic acid derivatives towards topical drug delivery. Annual discussion meeting 2008 of the Centre for Phase Equilibria and Separation Processes, Værløse, Denmark, June 16-18, 2008.

II.1.3. Manuscript contributions

- Eenschooten, C.; Guillaumie, F.; Kontogeorgis, G. M.; Stenby, E. H.; Schwach-Abdellaoui, K. Development of hyaluronic acid-based nanoparticles for topical delivery of cosmetic actives. In *Department of Chemical Engineering, Technical University of Denmark, Graduate schools yearbook*; Dam-Johansen K.; Bøjer, M., Eds.; BookPartner, Nørhaven Digital: Copenhagen, 2006.

- Eenschooten, C.; Guillaumie, F.; Kontogeorgis, G. M.; Stenby, E. H.; Schwach-Abdellaoui, K. Development of hyaluronic acid-based nanocarriers towards the topical delivery of cosmetic active ingredients or pharmaceutical drugs. In *Department of Chemical Engineering, Technical University of Denmark, Graduate schools yearbook*; Dam-Johansen K.; Bøjer, M., Eds.; BookPartner, Nørhaven Digital: Copenhagen, 2007.

II.1.4. Patents

- Tømmeraas, K.; Eenschooten, C. Aryl/alkyl succinic anhydride hyaluronan derivatives. WO2007/033677 A1, March 29, 2007.

- Eenschooten, C.; Christensen, M. W. Aryl/Alkyl vinyl sulfone hyaluronic acid derivatives. WO2007/098770 A1, September 7, 2007.

II.1.5. Articles in preparation

- Eenschooten, C.; Guillaumie, F.; Delie, F.; Kontogeorgis, G. M.; Schwach-Abdellaoui, K. Towards an understanding of the mechanisms underlying polymeric nanoparticle-mediated (trans)dermal drug delivery (based on Chapter II).

- Eenschooten, C.; Guillaumie, F.; Kontogeorgis, G. M.; Stenby, E. H.; Schwach-Abdellaoui, K. Preparation and structural characterization of novel and versatile amphiphilic hyaluronic acid derivatives (based on Chapter III, section B).

- Eenschooten, C.; Vaccaro, A.; Delie, F.; Guillaumie, F.; Tømmeraas, K.; Kontogeorgis, G. M.; Schwach-Abdellaoui, K.; Borkovec, M.; Gurny, R. Novel self-associative multi-phase nanostructured soft carriers based on amphiphilic hyaluronic acid derivatives (based on Chapter IV).

II.2. Teaching

II.2.1. Assistantship in master's courses

- Soft Nanotechnology in Colloid and Surface Chemistry, master's course, Technical University of Denmark, DTU Department of Chemical and Biochemical Engineering, Autumn 2005 and 2006.

II.2.2. Co-supervision

- Structural characterization of a novel amphiphilic derivative of hyaluronic acid, master's project, Technical University of Denmark, Department of Chemistry, Autumn 2007.

NOTES

NOTES

NOTES

NOTES

NOTES

Department of Chemical
and Biochemical Engineering
DTU Building 229
Søltofts Plads
DK-2800 Kgs. Lyngby
www.kt.dtu.dk